LAYERWISE THEORY FOR DISCRETELY STIFFENED LAMINATED CYLINDRICAL SHELLS

by

Samuel Kinde Kassegne

Dissertation submitted to the Faculty of the

Virginia Polytechnic Institute and State University

in partial fulfillment of the requirements for the degree of

DOCTOR OF PHILOSOPHY

in

Engineering Mechanics

APPROVED:

J. N. Reddy, Chairman

R. Plaut

L. Librescu

S. Hendricks

D. Telionis

December, 1992

Blacksburg, Virginia

LAYERWISE THEORY FOR DISCRETELY STIFFENED LAMINATED CYLINDRICAL SHELLS

by

Samuel Kinde Kassegne

J.N. Reddy, Chairman

Engineering Mechanics

(ABSTRACT)

The Layerwise Shell Theory is used to model discretely stiffened laminated composite cylindrical shells for stress, vibration, pre-buckling and post-buckling analysis. The layerwise theory reduces a three-dimensional problem to a two-dimensional problem by expanding the three-dimensional displacement field as a function of a surface-wise two-dimensional displacement field and a one-dimensional interpolation through the shell thickness. Any required degree of accuracy can be obtained by an appropriate, independent selection of the one-dimensional interpolation functions through the thickness and the two-dimensional interpolation of the variables on the surface.

Using a layerwise format, discrete axial and circumferential stiffeners are modeled as two-dimensional beam elements. Similar displacement fields are prescribed for both the stiffener and shell elements. The contribution of the stiffeners to the membrane stretching, bending and twisting stiffnesses of the laminated shell is accounted for by forcing compatibility of strains and equilibrium of forces between the stiffeners and the shell skin. The layerwise theory is also used to model initial imperfections of the unstressed configuration. A finite element scheme of the layerwise model is developed and applied here to investigate the effect of imperfections on the response of laminated cylindrical shells.

Using a finite element model of the layerwise theory for shells and shell stiffener elements, the accuracy and reliability of the elements is investigated through a wide variety of examples. The examples include laminated stiffened and unstiffened plates and shells and stand-alone beams under different types of external destabilizing loads. Finally, the study identifies the particular types of problems where the layerwise elements possess a clear advantage and superiority over the conventional equivalent single-layer models.

ACKNOWLEDGMENTS

This modest work, by no means a culmination of an academic odyssey that began way back in time and space, is nevertheless a conclusion to that stage of life where everything else before seems artificial and too simplistic and everything else after heralds the setting of reality. But the line that separates these stages often looks so fine that one might be tempted to overlook it or even perhaps down play its importance. But while it lasts, I would like to take the opportunity to recognize the many, many people who helped me experience what is only just one alternative path of life-the academic path. In the midst of this, I have learned that the course of History of mankind or, at the very personal level, one's life wouldn't change much - maybe marginally - by works of this calibre. But still, coming this far was not easy. And people made it possible for me.

Prof. J.N. Reddy, my doctoral advisor whom I had earlier known through books and papers only, has given me an important opportunity to work under him in the infinite world of finite element theory. The financial assistance he provided me towards the end of this study could not have come at a better time. The advisory committee members, Drs. S. Hendricks, L. Librescu, R. Plaut and D. Telionis, have been patient with me through the endless hurdles of preliminary exams, proposal defense and the final defense. My thanks go for their patience and interest in this work. I would also like to thank Dr. Y.S.N. Reddy for proof reading the manuscript.

My father, Dr. Kinde, and my uncle, Ambassador Zemene, had over the years persistently maintained a huge trust in me which at times, I must admit, I was afraid to shoulder. My mother and sisters have been patient with me as the demands of this academic venture drove me selfish. My younger sister Etseguenet deserves a special recognition. She was the one who consistently supported me financially and morally when the things that bothered me most were not only post-buckling, snap-through and discrete stiffeners but very basic things like finance and summer jobs.

My friend, the Rev. Rick Swindel, a very gentle and godly man and his loving wife, Arlene, have helped me financially and morally and offered me a pure and beautiful friendship. A lot more people have made living in Blacksburg a rewarding experience. My home town

school-mate Eskinder Sahle encouraged me on many occasions to complete this endeavor and has been a constant companion in building a microcosm of the St. Joseph high school days in Ethiopia. Mouin Nasseredine (Nesro) is a very warm person who made sure that there was more to friendship even after graduation. I also want to pause here and recognize the two decades of friendship I have enjoyed with my friend Teodros Kidane. Yonael, a friend with a lot of sense of humor, has been a good source of fun and light hearted jokes. Ahmed Bouzid, Rajesh Ramachandra, Joe Obidigeou and many others have given me friendship and hours of "hanging out", that was in many instances a very welcome change from the hectic routine of a graduate student's life. And when computer funds were no more "funny money", Rajesh, Eskinder and Sultana helped me raise "funds". Most of the plots and tables reported here would have remained just as data files somewhere on the VM1, if it were not for their help.

Sultana, my very close friend, has been immensely patient with me in these last two years as I immersed myself into the details of this work. I owe her a lot for her patience and love.

Last but not least, I thank the Almighty LORD, who has always reminded me to keep things in perspective. I am grateful for his love and free gift so far and count on his blessing for all the things that I always wanted to do and postponed thus far.

Table of Contents

List of Figures

List of Tables

CHAPTER 1

INTRODUCTION

1.1 Motivation

Stiffened cylindrical shells are frequently used as structural components for aerospace and underwater vehicles. Because of their inherent high stiffness and strength to weight ratio, advanced fiber reinforced composites have been widely used in the construction of such structures. The efficient use of these materials requires a good understanding of the system response characteristics to external causes such as mechanical and environmental loads. Good analytical models are required to assess the response of shell-type structures both at the global and local levels. In the past five or six decades, a very significant amount of research work has gone to the formulation of the kinematics and stability analysis of shells made out of steel, aluminum and advanced composite materials.

Laminated shells have often been modeled as equivalent single-layer shells using the classical shell theory. The Love-Kirchhoff classical shell theory [1] assumes that straight lines normal to the undeformed middle surface remain straight, inextensible and normal to the deformed middle surface. As a result, transverse normal and shear deformations are neglected. It has long been recognized that classical two-dimensional shell theories yield good results only when these structures are thin, the dynamic excitations are within the low-frequency range, and the material anisotropy is not severe. The classical shell theory

could give errors in the order of 30% for deflections, stresses, and natural frequencies when used for laminated anisotropic shells [2].

The quantitative assessment of the effects of stiffeners on the local and global behavior of stiffened shells is crucial to the clear understanding of the response and reliability of such structures. A significant amount of research in stiffened shells dealt with cases where the stiffener spacing is small compared to the dimensions of the shell. In such shells, the behavior of the closely spaced stiffeners is averaged out or "smeared" over the shell surface. However, most researchers ignored the eccentricity of the stiffeners. Such models resulted in higher buckling loads [3]. The post-buckling behavior of stiffened laminated composite cylindrical shells has not received much attention. Small-deflection classical shell theories have given erroneous results compared to experimental results. The major drawback in all the theories is the lack of shear deformation capabilities in the buckling and post-buckling analysis of stiffened laminated composite shells.

The proposed model for cylindrical shells with discrete stiffeners, typical of aircraft fuselage structures and rocket cases, is intended to carry out a vibration, buckling, stress and post-buckling analysis of such structures using Reddy's [4] layerwise theory. Discrete axial and circumferential stiffeners are modeled as two-dimensional beam elements and their contribution to the axial, bending and twisting stiffnesses of the laminated shell is accounted for by forcing compatibility of strains and equivalence of energy between the stiffeners and the shell skin at their common nodes. The layerwise theory of Reddy has effectively been employed in developing a two-dimensional model for laminated plates, which is capable of determining the in-plane and interlaminar stresses [5]. This theory gives an accurate description of the three-dimensional displacement field. In this model, the displacements are approximated linearly through each layer. This accounts for any

discontinuities in the derivatives of the displacements at the interfaces of the lamina. The von Kárman type geometric nonlinearities are also considered with an additional provision for imperfection sensitivity analysis. Previous investigations lack a generalized treatment with shear deformation capability valid for linear and nonlinear post-buckling analyses. The present study is intended to fill in the gap that exists in the analysis of discretely stiffened laminated cylindrical shells with initial geometric imperfections. The study also focuses on the local behavior of stiffened shells and plates. This includes determining the state of stress and strain near the skin-stiffener interface. Unlike the equivalent single-layer two-dimensional shell theories, the layerwise theory of shells has the capacity to accurately determine the through-the-thickness variation of stresses and strains at discontinuities such as free-edges and stiffener attachment areas. The literature reviewed in the next section forms a background for the present work.

1.2 LITERATURE REVIEW

In this section, a review of previous research work in the areas of theory of shells, kinematics and modeling of stiffened shells and the stability of shells is given.

1.2.1 Shell Theories

The first publication in the theory of shells was by Love [1] in 1888. He assumed small strains and small thickness to radius ratios, in addition to the assumptions that the normals to the reference surface remain straight and normal during the deformation, and that the transverse normal stress is negligibly small. Within the framework of a linear first-order theory, modifications of Love's theory have been presented in order to remove some of the inconsistencies. Budiansky and Sanders' [6] and Koiter's [7] works are some of the examples. Donnell [8] presented a simple set of nonlinear equations for cylindrical shells. Vlasov [9] extended Love's theory to shallow shells of general geometry in a form commonly known as Donnel-Mushatari-Vlasov (DMV) equations for quasi-shallow shells. Novozhilov [10] presented nonlinear equations for shells of general shapes. One of the earliest analyses of homogeneous orthotropic cylindrical shells was published by March et al. [11] in 1945. Subsequently, several theoretical analyses limited to orthotropic shell configurations were performed by Schnell and Bush [12], Thielmann et al. [13], and Hess [14]. The general linear theoretical solutions to anisotropic cylinders were presented by Cheng and Ho [15], Jones and Morgan [16], Jones [17] and Hennemann and Hirano [18]. Several papers compared the efficiency and accuracy of Flügge's [19] linear shell theory, which was employed by Cheng and Ho [15], and other shell theories such as the work of

Tasi et al. [20], Martin and Drew [21], whose theory was based on Donnell's equations, and the work done by Chao [22] whose analysis was based on Timoshenko's buckling equations. All the theories discussed above are based on the classical shell theory where the Love-Kirchhoff assumptions are used. The Love-Kirchhoff assumptions amount to treating shells as infinitely rigid in the transverse direction by neglecting transverse strains. The theory underestimates deflections and stresses and overestimates natural frequencies and buckling loads. Since the transverse shear moduli of advanced composite materials are usually very low compared to the in-plane moduli, the transverse shearing strains must be taken into account for an accurate representation of the response of laminated plates and shells. Numerous plate and shell theories which account for transverse shear deformations are documented in the literature.

The shear deformation plate and shell theories can be classified into two groups as displacement-based and stress-based theories. The first stress based shear deformation shell theory is that of Reissner [23]. The theory assumes a linear distribution of the inplane normal and shear stresses through the thickness of the plate. The transverse stresses are obtained by integrating the equilibrium equations of the three-dimensional elasticity theory. Gol'denveizer [24] generalized Reissner's theory by replacing the linear variation of stresses through the thickness by a general function of the thickness coordinate. Kromm [25] developed a shear deformation theory that is a special case of Gol'denveizer's theory. Basset's [26] theory was perhaps the pioneering displacement-based shell shear deformation theory. According to his formulation, the displacement components are expanded in a series of powers of the thickness coordinate z. Following Basset's work, Hildeband, Reissner and Thomas [27] presented a first-order shear deformation theory for shells. The first order shear deformation theory was extended to anisotropic laminated

plates by Yang, Norris and Stavsky [28]. Higher order displacement-based shear deformation theories, where the components of the displacements are expanded in power series of the thickness coordinate and unknown generalized displacement functions, were later formulated by Librescu and Khdeir [29], Reddy [30], Schmidt [31], Levinson [32], and Murthy [33]. Librescu [34] developed a refined geometrically nonlinear theory for anisotropic laminated shells, based on the expansion of the displacement field with respect to the thickness coordinate. Vlasov [35] was the first investigator to develop a higher-order displacement field that satisfies stress-free boundary conditions on the top and bottom planes of a plate. Krishna Murthy [36] introduced a modification to the displacement field by splitting the transverse deflection into bending and shear terms.

The above discussed theories all fall under the equivalent single layer two-dimensional theories. These theories give accurate results for global responses such as maximum deflections, fundamental vibration frequencies, and critical buckling loads and the finite element models of these theories are computationally less expensive as compared to those based on three-dimensional elasticity solutions. However, the single-layer theories are usually inadequate in describing the stress field at the ply level. The major deficiency of the single-layer theories in modeling composite laminated shells and plates is that the transverse strain components are continuous across interfaces between disimilar materials; therefore, the transverse stress components are discontinuous at the layer interfaces.

Recently, Reddy [4] developed a generalized laminate theory called Layerwise Laminate Theory that provides a framework upon which any of the displacement-based, two-dimensional laminate theories can be derived. Based on this work, a layerwise shell theory that is capable of modeling three-dimensional kinematics in shells has been developed by Reddy [37]. The Layerwise Shell Theory of Reddy (LWST) gives an accurate description

of the displacement field. The three-dimensional displacement field is expanded as a function of a surface-wise two-dimensional displacement field and a one-dimensional interpolation function through the thickness. The use of higher order polynomial interpolation functions or more sub-divisions through the thickness improves the degree of accuracy in expanding the three-dimensional displacement field. The resulting transverse strains are discontinuous at the layer interfaces if a piece-wise continuous polynomial interpolation of the displacements through the thickness is used. As a result, continuous transverse stresses can be obtained at the ply interfaces.

1.2.2 Stiffened Shells

The first work in the area of stability of eccentrically stiffened shell was carried out by van der Neut [3] in 1940. By including stiffener centroid eccentricity in his model, van der Nuet showed that placing the centroid at the shell wall middle surface in the theoretical analysis could result in large errors in the buckling load if the centroid of the stiffeners in the actual structure was offset from the middle surface. However, his conclusion that the buckling load under axial compression of an externally stiffened shell could be as high as twice or three times that of an internally stiffened shell went essentially unnoticed. Wilson [38] had arrived at similar conclusions for cylinders under external pressure. Baruch and Singer [39] studied the instability of stiffened simply supported cylindrical shells under hydrostatic pressure. They used the "average stiffness" approach. The influence of discrete ring stiffeners was investigated by Hedgepeth and Hall [40], who ignored prebuckling deformations, and by Block [41], who took the prebuckling deformation into account. Jones [17] was probably among the earliest to investigate laminated composite shells with stiffeners. He assumed the laminae to have orthotropic material properties with the principal axes of orthotropy coincident with the shell coordinate direction. The stiffeners were treated as one-dimensional isotropic beam elements and their property averaged or "smeared" over the stiffener spacing.

The finite element method has been used to solve the problem of shells with stiffeners by formulating a beam element whose displacement pattern is compatible with that of the shell. Kohnke et al. [42] proposed a 16 degree of freedom isotropic beam finite element, which has displacements compatible with the cylindrical shell element from which the beam element is reduced. However, its application is limited to isotropic cylindrical shells. A

laminated anisotropic curved stiffener element with 16 degrees of freedom was generated from a laminated anisotropic rectangular shallow thin shell element with 48 degrees of freedom by Venkatesh and Rao [43]. This compatible curved stiffener element and the rectangular shell element [44] have been used by Venkatesh and Rao [45] to solve problems of laminated anisotropic shells stiffened by laminated anisotropic stiffeners. Rao and Venkatesh [46] later presented a 48 degree of freedom doubly curved quadrilateral shell of revolution element where the stiffness of the stiffener elements again is superimposed after a suitable transformation. In these methods, no additional degrees of freedom are introduced.

Carr and Clough [47] and Schmit [48] used an alternative approach where axial stiffeners (stringers) and radial stiffeners (rings) were approximated by the same element type as the shell. The main disadvantage of their approach was that a substantial number of additional nodes and nodal displacements are introduced as unknowns. Ferguson and Clark [49] developed a variable thickness curved beam and shell stiffener element with transverse shear deformation capabilities. Here, a family of two-dimensional and three-dimensional beam elements are developed as double degenerates of a fully three-dimensional isoparametric continuum element. There is a displacement compatibility with Ahmad's thick shell element [50] transverse shear and variable thickness properties. Liao [51] introduced a shear deformable degenerated curved element which has nonlinear and post-buckling analysis capability.

1.2.3 Stability of Shells

Stability of shells has been a research topic for a very long time. However, early researchers were only involved with the linear buckling theory. In most cases, the determination of the buckling load is considered to be an adequate stability solution for a structure. Buckling, however, does not always result in the collapse of the structure [52]. Therefore, determining the post-buckling displacement pattern of the structure is essential to have a clear understanding of the dangers of instability.

The fundamental theory of buckling of orthotropic cylinders was developed by Flügge [19]. Bodner [53] worked out solutions to Flügge's orthotropic theory. Batdorf [54] reviewed the early test data available for buckling of cylinders. Ho and Cheng [55] studied the stability of heterogeneous cylindrical shells under combined loading and arbitrary boundary conditions. Their theory is based on small displacements and the Love-Kirchhoff hypothesis. Donnell [8] was the first researcher to propose that imperfections in the shape of the shell play a significant role in the buckling phenomenon. Von Kárman and Tsien [56] included nonlinear terms in the strain-displacement relations. Their approximate solution to the nonlinear problem showed that, in addition to the pre-buckling membrane state of stress, other equilibrium states exist for loads lower than the buckling load. Jones [17] presented the exact solutions for buckling of cross-ply, simply supported circular cylindrical shells for both symmetrical and unsymmetrical lamination schemes. Not much work has been done in the study of the post-buckling behavior of stiffened and unstiffened shells. Shell theories based on small displacements are not applicable to post-buckling analysis of shells [52]. A finite displacement theory of shells must be used as the basis of post-buckling analysis. Naghdi developed such a theory [57]. A review of the early

historical developments in the field of general instability of orthotropic cylinders is found in [58]. Koiter [59] published a general theory of post-buckling behavior of structures. His theory is based on the expansion of the potential energy about solutions of the equilibrium equations at bifurcation points. Limit points are treated accurately only if they occur near the bifurcation points. Koiter's theory has been applied by Hutchinson [60], Budiansky and Hutchinson [61], and others [62] to measure imperfection sensitivity near bifurcation points of perfect structures. Koiter's theory predicts that even for very small magnitudes of imperfections, the buckling load can be substantially reduced.

Shell stability analysis is a highly nonlinear problem where the finite element method possesses a special advantage. Numerous researchers have investigated the stability problem of shells using the finite element method [63]. Sharifi and Popov [64], Walker [65], and Noor and Peters [66] have used the finite element procedure to analyze arch and shell instability problems. Near the limit point and the post-buckling region, special numerical techniques must be adopted to trace the path of the load-deflection curve. This is due to the fact that the stiffness matrix is singular at the limit point and not positive definite in the post-buckling region. A number of algorithms have been proposed to overcome this numerical difficulty. Bergan et al. [67,68] proposed a simple method of suppressing equilibrium iteration. Popov et al. [64] suggested the use of an "artificial spring" for the post-buckling analysis of arches. Argyris [69] and Batoz and Dhatt [70] used the displacement control method to navigate through the post-buckling path, whereas Riks and Wempner [71] used the "constant-arc-length method". Ramm [72] and Crisfield [73] gave good reviews of the algorithms commonly used for shell stability analysis. The modified Riks-Wempner method is the most convenient algorithm for finite element applications.

1.3 Present Study

The present study focuses on developing laminated composite cylindrical shell and shell stiffener elements based on the Layerwise Theory of Reddy. The elements are used to model unstiffened and stiffened laminated plates and shells for global and local analyses. The accuracy and reliability of the elements are investigated by solving a wide variety of laminated stiffened and unstiffened plates and shells and stand-alone beams under different types of external destabilizing loads. The study identifies the particular types of problems where the layerwise elements possess a clear advantage and superiority over the conventional equivalent single-layer methods. The stability of shells that exhibit bifurcation and snap-through is investigated and reported. The influence of stiffeners on the global responses, like critical load and load-deflection curve, and local effects, such as through-the-thickness distribution of stresses and strains, is studied.

Following this introduction, the layerwise theory for cylindrical shells and stiffener elements is developed in Chapters 2 and 3 respectively. Both discrete and "smeared" models are developed for the stiffener elements. In Chapter 4, the theory is extended to cylinders containing initial imperfections. The effect of imperfections on the stability of cylindrical shells is discussed. Chapter 5 focuses on the solution techniques used for the models developed. A comprehensive overview of the application of the finite element method in the present study for solving natural vibration, linearized buckling, linear stress and post-buckling problems is given. Chapter 6 features an extensive verification and demonstration of the analysis of a wide variety of plate, shell and shell type structures. A global analysis and local analysis for discontinuities in plates and cylindrical panels with

stiffeners is included to demonstrate the power of the layerwise theory in capturing local effects. A discussion of the convergence characteristics of the elements and the effects of the order of integration is also included, wherever appropriate. The effect of stiffeners on the global and local response of plates and shells, their stability and state of stress and strain in particular, is investigated in the same chapter. The conclusions from this study and identification of areas which require further investigation are included in Chapter 7. In Appendix A, the algorithm for deriving the tangent stiffness matrix from the direct stiffness matrix is given. The nonlinear tangent element stiffness matrices for cylindrical shell and stiffener elements are given in Appendices B and C respectively. The components of the element stiffness matrix for a stiffener element using the "average stiffness" or "smearing" approach are given in Appendix D. Appendix E gives the additional nonlinear terms for the stiffness matrices of a cylindrical shell with imperfections.

CHAPTER 2

LAYERWISE SHELL THEORY FOR CYLINDRICAL SHELLS

2.1 Introduction

In this chapter, the formulation of a general two-dimensional model for cylindrical shells based on Reddy's layerwise laminate theory will be reviewed. The layerwise theory of Reddy reduces a three-dimensional problem into a two-dimensional one by expanding the displacement field through the thickness. Any desired degree of displacement variation through the thickness is easily obtained by using higher order interpolation polynomials or by subscribing more subdivisions through the thickness. The resulting transverse strains are discontinuous at the boundaries of the subdivisions if the variation of the displacements through the thickness is defined by piece-wise continuous polynomials. This allows the possibility of introducing continuous transverse stresses at the interface of two dissimilar lamina.

Unlike the equivalent single-layer theories such as the shear deformation and classical shell theories, the layerwise theory explicitly prescribes the displacement field, strain field and stress at each interface through the thickness. The expansion of the w-component of the displacement field through the thickness relaxes the condition of the inextensibility of normals imposed on the conventional single-layer theories. As a result, the layerwise model developed is essentially a three-dimensional model in a two-dimensional format.

2.1.1 Displacement Fields

Consider a laminated cylindrical shell made up of N orthotropic lamina oriented arbitrarily with respect to the shell (x, y, z) coordinates as shown in Figure 1. The cylindrical shell has a length of L, thickness t and undeformed mid-surface of radius R, with $t << R$. The displacements (u, v, w) at a generic point (x, y, z) in the laminate are assumed to be of the form:

$$u(x,y,z) = \sum_{j=1}^{N+1} u_j(x,y)\,\Phi^j(z)$$

$$v(x,y,z) = \sum_{j=1}^{N+1} v_j(x,y)\,\Phi^j(z) \qquad (2.1)$$

$$w(x,y,z) = \sum_{j=1}^{N+1} w_j(x,y)\,\Phi^j(z)$$

where u_j, v_j, and w_j are the nodal interface displacement values in x, y and z directions of each layer and Φ^j is a linear Lagrangian interpolation function through the thickness of the laminate. N is the number of mathematical layers in the laminate. This may be equal to or less than the number of physical layers. For laminates containing plies of the same geometrical and material properties, it is often convenient to group identical plies together (i.e., a sublaminate concept) to reduce the computational effort. As a result, the number of "mathematical" layers will be less than the number of physical layers. In equation (2.1) and all subsequent equations, summation is used on repeated indices. The Φ^j are assumed

to be linear approximation functions with local support that assume a value equal to unity at the j-th interface and zero at the k-th interface where k is different from j. The expansion of w through the thickness relaxes the condition for the inextensibility of the normals to the mid-surface as stipulated by the classical lamination theory and the shear deformation theories. This allows a non-zero transverse normal strain as in the three-dimensional models. The transverse normal stresses assume a very significant value (when compared to the allowable stress) in laminates with localized effects, like cut-outs and free edges.

The global linear approximation functions are defined as below:

$$\Phi^j(z) = \left\{ \begin{array}{l} \psi_2^{(j-1)}(z) = \dfrac{z - z_{j-1}}{t_{j-1}},\ z_{j-1} \le z \le z_j \\ \\ \psi_1^{(j)}(z) = \dfrac{z_j - z}{t_j},\ z_j \le z \le z_{j+1} \end{array} \right\} \quad (j = 1,2, \ldots N) \qquad (2.2)$$

where ψ_i^j (i = 1,2) is the local or layer Lagrange interpolation function associated with the i-th node of the j-th layer and t_j is the thickness of the j-th layer as shown in Figure 2. Here, it could be recognized that each layer is in effect a one dimensional finite element through the thickness. The ψ_i^j are the interpolation functions of the j-th element (i = 1, 2 for linear elements and i = 1, 2, 3 for quadratic elements).

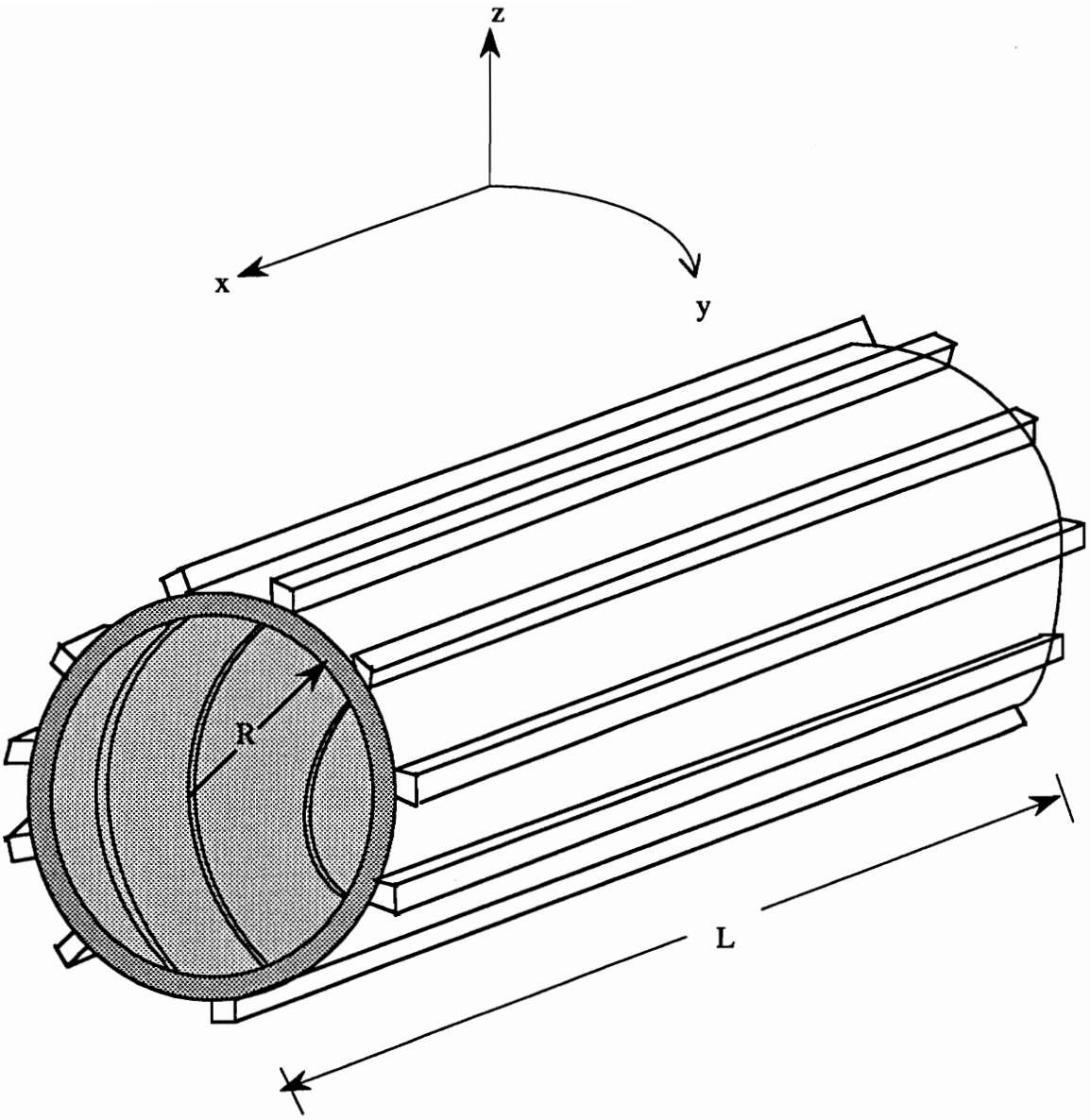

Figure 1. Geometry and coordinate system of a stiffened cylindrical shell.

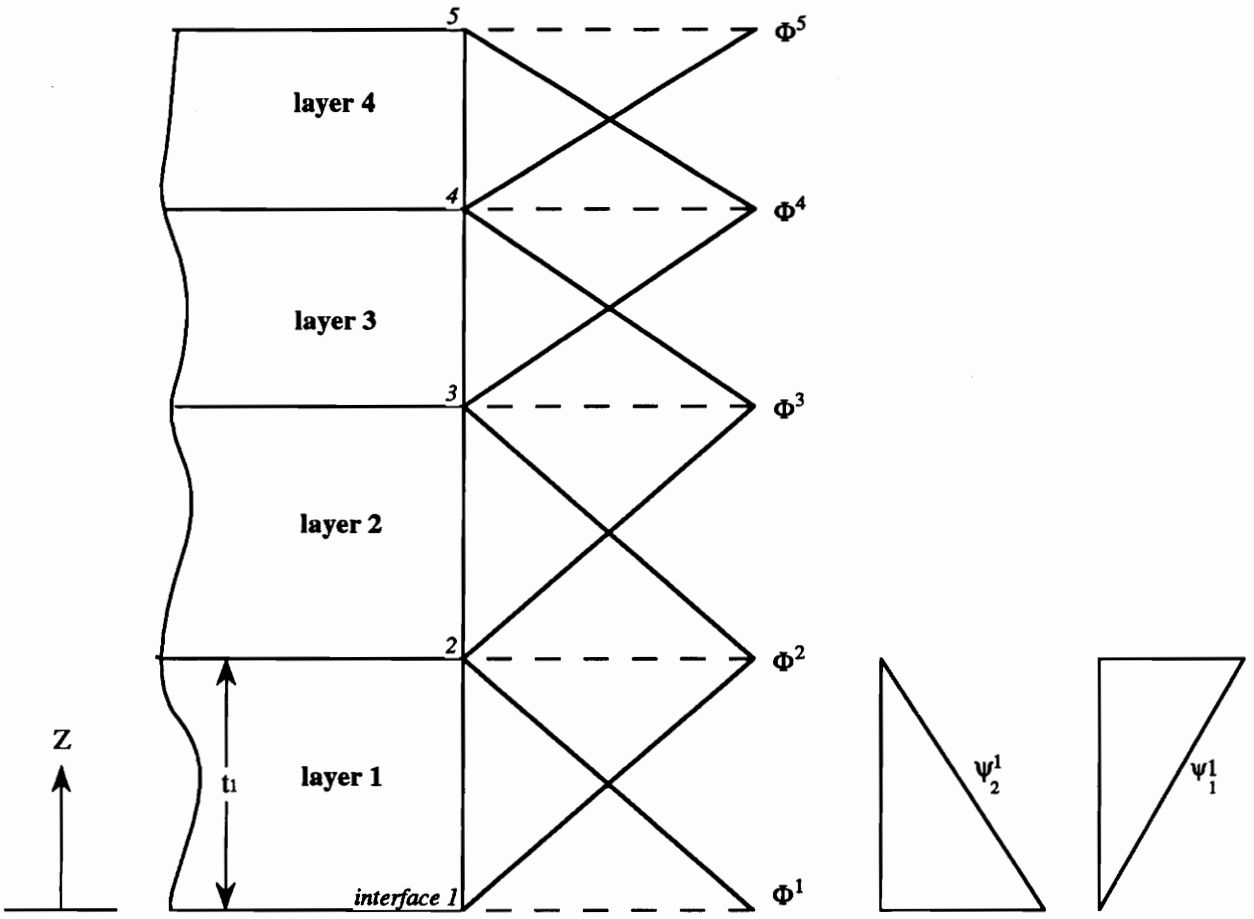

Figure 2. One-dimensional approximation functions through the thickness.

2.1.2 Strains

The von Kárman type of nonlinear strains are considered, where small strains and moderate rotations with respect to the shell reference surface are assumed. Rotations about the normals to the shell reference surface are considered to be negligible for cylinders where the ratio t/R is considerably less than unity, where t is the thickness and R is the radius of the cylindrical shell. The Donnell type strain-displacement equations in an orthogonal cylindrical coordinate system are:

$$\varepsilon_{xx} = \frac{\partial u}{\partial x} + \frac{1}{2}\left(\frac{\partial w}{\partial x}\right)^2 = \frac{\partial u_i}{\partial x}\Phi^i + \frac{1}{2}\frac{\partial w_i}{\partial x}\frac{\partial w_j}{\partial x}\Phi^i\Phi^j$$

$$\varepsilon_{yy} = \frac{\partial v}{\partial y} + \frac{w}{R} + \frac{1}{2}\left(\frac{\partial w}{\partial y}\right)^2 = \left(\frac{\partial v_i}{\partial y} + \frac{w_i}{R}\right)\Phi^i + \frac{1}{2}\frac{\partial w_i}{\partial y}\frac{\partial w_j}{\partial y}\Phi^i\Phi^j$$

$$\gamma_{xy} = \frac{\partial u}{\partial y} + \frac{\partial v}{\partial x} + \frac{\partial w \partial w}{\partial x \partial y} = \left(\frac{\partial u_i}{\partial y} + \frac{\partial v_i}{\partial x}\right)\Phi^i + \frac{\partial w_i}{\partial y}\frac{\partial w_j}{\partial x}\Phi^i\Phi^j \qquad (2.3)$$

$$\gamma_{yz} = \frac{\partial v}{\partial z} + \frac{\partial w}{\partial y} - \frac{v}{R} = v_i\frac{d\Phi^i}{dz} + \left(\frac{\partial w_i}{\partial y} - \frac{v_i}{R}\right)\Phi^i$$

$$\gamma_{xz} = \frac{\partial u}{\partial z} + \frac{\partial w}{\partial x} = u_i\frac{d\Phi^i}{dz} + \frac{\partial w_i}{\partial x}\Phi^i$$

$$\varepsilon_{zz} = \frac{\partial w}{\partial z} = w_i\frac{d\Phi^i}{dz}$$

2.1.3 Virtual Work Statement

The virtual work statement can be written using Hamilton's principle. The stationary total potential energy principle dictates that $\delta\Pi = 0$, where $\delta\Pi$ is the first variation of the total potential energy,

$$\delta\Pi = \delta U + \delta V \tag{2.4}$$

The virtual strain energy of the shell due to internal stresses is δU and is given as:

$$\delta U = \int_{\Omega} \int_{-\frac{h}{2}}^{\frac{h}{2}} (\sigma_{xx}\delta\varepsilon_{xx} + \sigma_{yy}\delta\varepsilon_{yy} + \sigma_{zz}\delta\varepsilon_{zz} + \sigma_{yz}\delta\gamma_{yz} + \sigma_{xz}\delta\gamma_{xz} + \sigma_{xy}\delta\gamma_{xy}) \, dz \, dA \tag{2.5}$$

Here Ω is the reference surface of the shell. The work done by the specified pre-buckling stresses $\bar{\sigma}_i$ is of the form:

$$\delta V = \int_{\Omega} \int_{-\frac{h}{2}}^{\frac{h}{2}} (\bar{\sigma}_i \, \delta\varepsilon_i) \, dz \, dA \tag{2.6}$$

Substituting the strain-displacement relations (2.3) into the total potential energy given by equations (2.4) and (2.6) gives the following weak form of the virtual work statement:

$$
\begin{aligned}
0 = \int_{\Omega} \{ & N_x^i \frac{\partial \delta u_i}{\partial x} + N_y^i \left(\frac{\partial \delta v_i}{\partial y} + \frac{\delta w_i}{R}\right) + N_{xy}^i \left(\frac{\partial \delta u_i}{\partial y} + \frac{\delta \delta v_i}{R}\right) + M_x^{ij} \frac{\partial \delta w_i}{\partial x} \frac{\partial w_j}{\partial x} \\
& + M_y^{ij} \frac{\partial \delta w_i}{\partial y} \frac{\partial w_j}{\partial y} + M_{xy}^{ij} \left[\frac{\partial \delta w_i}{\partial x} \frac{\partial w_j}{\partial y} + \frac{\partial \delta w_i}{\partial y} \frac{\partial w_j}{\partial x}\right] + Q_{xz}^i \delta u_i + Q_{yz}^i \delta v_i \\
& + Q_{zz}^i \delta w_i + K_{xz}^i \frac{\partial \delta w_i}{\partial x} + K_{yz}^i \left(\frac{\partial \delta w_i}{\partial y} + \frac{\delta v_i}{R}\right) + \overline{M}_x^{ij} \frac{\partial \delta w_i}{\partial x} \frac{\partial w_j}{\partial x} \\
& + \overline{M}_y^{ij} \frac{\partial \delta w_i}{\partial y} \frac{\partial w_j}{\partial y} + M_{xy}^{ij} \left[\frac{\partial \delta w_i}{\partial x} \frac{\partial w_j}{\partial y} + \frac{\partial \delta w_i}{\partial y} \frac{\partial w_j}{\partial x}\right] + p_i \delta w_i \} \, dA
\end{aligned}
\tag{2.7}
$$

where the laminate resultants are given as:

$$
(N_x^i, N_y^i, N_{xy}^i) = \int_{-\frac{h}{2}}^{\frac{h}{2}} (\sigma_{xx}, \sigma_{yy}, \sigma_{xy}) \, \Phi^i \, dz
$$

$$
(M_x^{ij}, M_y^{ij}, M_{xy}^{ij}) = \int_{-\frac{h}{2}}^{\frac{h}{2}} (\sigma_{xx}, \sigma_{yy}, \sigma_{xy}) \, \Phi^i \, \Phi^j dz
$$

$$
(Q_{xz}^i, Q_{yz}^i, Q_{zz}^i) = \int_{-\frac{h}{2}}^{\frac{h}{2}} (\sigma_{xz}, \sigma_{yz}, \sigma_{zz}) \frac{d\Phi^i}{dz} \, dz \tag{2.8}
$$

$$
(K_{xz}^i, K_{yz}^i) = \int_{-\frac{h}{2}}^{\frac{h}{2}} (\sigma_{xz}, \sigma_{yz}) \, \Phi^i dz
$$

$$
(\overline{M}_x^{ij}, \overline{M}_y^{ij}, \overline{M}_{xy}^{ij}) = \int_{-\frac{h}{2}}^{\frac{h}{2}} (\overline{\sigma}_{xx}, \overline{\sigma}_{yy}, \overline{\sigma}_{xy}) \, \Phi^i \, \Phi^j dz
$$

2.1.4 Equations of Motion

The Euler-Lagrange equations of the layerwise shell theory are obtained by integrating by parts the derivatives of the various quantities of the weak form given by equation (2.7) and collecting the coefficients of δu, δv, and δw. The equations of motion are:

$$0 = \frac{\partial N_x^i}{\partial x} + \frac{\partial N_{xy}^i}{\partial y} - Q_{xz}^i$$

$$0 = \frac{\partial N_{xy}^i}{\partial x} + \frac{\partial N_y^i}{\partial y} - Q_{yz}^i + \frac{1}{R} K_{yz}^i \qquad (2.9)$$

$$q_i = \frac{\partial K_{xz}^i}{\partial x} + \frac{\partial K_{yz}^i}{\partial y} - \left(\frac{1}{R} N_y^i + Q_{zz}^i\right) + \frac{\partial}{\partial x}\left(\overline{M}_x^{ij} \frac{\partial w_j}{\partial x} + \overline{M}_x^{ij} \frac{\partial w_j}{\partial y}\right) + \frac{\partial}{\partial y}\left(\overline{M}_{xy}^{ij} \frac{\partial w_j}{\partial x} + \overline{M}_y^{ij} \frac{\partial w_j}{\partial y}\right)$$

The equations of motion (2.9) consist of 3(N+1) differential equations in 3(N+1) unknowns (u_i, v_i, w_i).

2.1.5 Boundary Conditions

The essential and natural boundary conditions for this theory are given as:

Geometric (Essential)		Force(Natural)
u_i		$N_x^i n_x + N_{xy}^i n_y$
v_i	or	$N_{xy}^i n_x + N_y^i n_y$
w_i		$K_{xz}^i n_x + K_{yz}^i n_y$

(2.10)

where (n_x, n_y) denote the components of the unit outward normal vector on the boundary.

2.1.6 Constitutive Equations

The three-dimensional constitutive equations of an arbitrarily oriented orthotropic laminae in the laminate coordinate system are:

$$\begin{bmatrix} \sigma_{xx} \\ \sigma_{yy} \\ \sigma_{zz} \\ \sigma_{xy} \end{bmatrix} = \begin{bmatrix} C_{11} & C_{12} & C_{13} & C_{16} \\ C_{12} & C_{22} & C_{23} & C_{26} \\ C_{13} & C_{23} & C_{33} & C_{36} \\ C_{16} & C_{26} & C_{36} & C_{66} \end{bmatrix} \begin{bmatrix} \varepsilon_{xx} \\ \varepsilon_{yy} \\ \varepsilon_{zz} \\ \gamma_{xy} \end{bmatrix} \qquad (2.11.a)$$

$$\begin{bmatrix} \sigma_{yz} \\ \sigma_{xz} \end{bmatrix} = \begin{bmatrix} C_{44} & C_{45} \\ C_{45} & C_{55} \end{bmatrix} \begin{bmatrix} \gamma_{yz} \\ \gamma_{xz} \end{bmatrix} \qquad (2.11.b)$$

2.1.7 Laminate Force Resultants

Substituting the constitutive relations given by equation (2.11) into the force resultants of equation (2.8) gives an expression for the laminate force resultants in terms of the displacements:

$$N_x^i = A_{11}^{ij} \frac{\partial u_j}{\partial x} + A_{12}^{ij} \left(\frac{\partial v_j}{\partial y} + \frac{w_j}{R}\right) + \overline{A}_{13}^{ij} w_j + A_{16}^{ij} \left(\frac{\partial u_j}{\partial y} + \frac{\partial v_j}{\partial x}\right) + \frac{1}{2} D_{11}^{ijk} \frac{\partial w_j}{\partial x} \frac{\partial w_k}{\partial x} + \frac{1}{2} D_{12}^{ijk} \frac{\partial w_j}{\partial y} \frac{\partial w_k}{\partial y} + D_{16}^{ijk} \frac{\partial w_j}{\partial x} \frac{\partial w_k}{\partial y}$$

$$N_y^i = A_{12}^{ij} \frac{\partial u_j}{\partial x} + A_{22}^{ij} \left(\frac{\partial v_j}{\partial y} + \frac{w_j}{R}\right) + \overline{A}_{23}^{ij} w_j + A_{26}^{ij} \left(\frac{\partial u_j}{\partial y} + \frac{\partial v_j}{\partial x}\right) + \frac{1}{2} D_{12}^{ijk} \frac{\partial w_j}{\partial x} \frac{\partial w_k}{\partial x} + \frac{1}{2} D_{22}^{ijk} \frac{\partial w_j}{\partial y} \frac{\partial w_k}{\partial y} + D_{26}^{ijk} \frac{\partial w_j}{\partial x} \frac{\partial w_k}{\partial y}$$

$$N^{i}_{xy} = A^{ij}_{16}\frac{\partial u_j}{\partial x} + A^{ij}_{26}\left(\frac{\partial v_j}{\partial y} + \frac{w_j}{R}\right) + \overline{A}^{ij}_{36} w_j + A^{ij}_{66}\left(\frac{\partial u_j}{\partial y} + \frac{\partial v_j}{\partial x}\right) + \frac{1}{2} D^{ijk}_{16}\frac{\partial w_j}{\partial x}\frac{\partial w_k}{\partial x} + \frac{1}{2} D^{ijk}_{26}\frac{\partial w_j}{\partial y}\frac{\partial w_k}{\partial y} + D^{ijk}_{66}\frac{\partial w_j}{\partial x}\frac{\partial w_k}{\partial y}$$

$$Q^{i}_{zz} = \overline{A}^{ji}_{13}\frac{\partial u_j}{\partial x} + \overline{A}^{ji}_{23}\left(\frac{\partial v_j}{\partial y} + \frac{w_j}{R}\right) + \overline{\overline{A}}^{ji}_{33} w_j + \overline{A}^{ji}_{36}\left(\frac{\partial u_j}{\partial y} + \frac{\partial v_j}{\partial x}\right) + \frac{1}{2}\overline{D}^{jki}_{13}\frac{\partial w_j}{\partial x}\frac{\partial w_k}{\partial x} + \frac{1}{2}\overline{D}^{jki}_{23}\frac{\partial w_j}{\partial y}\frac{\partial w_k}{\partial y} + \overline{D}^{jki}_{36}\frac{\partial w_j}{\partial x}\frac{\partial w_k}{\partial y}$$

$$Q^{i}_{xz} = \overline{\overline{A}}^{ij}_{55} u_j + \overline{A}^{ji}_{55}\frac{\partial w_j}{\partial x} + \overline{\overline{A}}^{ij}_{45} v_j + \overline{A}^{ji}_{45}\left(\frac{\partial w_j}{\partial y} - \frac{v_j}{R}\right)$$

$$Q^{i}_{yz} = \overline{\overline{A}}^{ij}_{45} u_j + \overline{A}^{ji}_{45}\frac{\partial w_j}{\partial x} + \overline{\overline{A}}^{ij}_{44} v_j + \overline{A}^{ji}_{44}\left(\frac{\partial w_j}{\partial y} - \frac{v_j}{R}\right)$$

$$K^{i}_{xz} = \overline{A}^{ij}_{55} u_j + A^{ji}_{55}\frac{\partial w_j}{\partial x} + \overline{A}^{ij}_{54} v_j + A^{ij}_{45}\left(\frac{\partial w_j}{\partial y} - \frac{v_j}{R}\right) \qquad (2.12)$$

$$K^{i}_{yz} = \overline{A}^{ij}_{45} u_j + A^{ji}_{45}\frac{\partial w_j}{\partial x} + \overline{A}^{ij}_{44} v_j + A^{ij}_{44}\left(\frac{\partial w_j}{\partial y} - \frac{v_j}{R}\right)$$

$$M^{ij}_{x} = D^{ijk}_{11}\frac{\partial u_k}{\partial x} + D^{ijk}_{12}\left(\frac{\partial v_k}{\partial y} + \frac{w_k}{R}\right) + \overline{D}^{ijk}_{13} w_k + D^{ijk}_{16}\left(\frac{\partial u_k}{\partial y} + \frac{\partial v_k}{\partial x}\right) + \frac{1}{2} F^{ijkl}_{11}\frac{\partial w_k}{\partial x}\frac{\partial w_l}{\partial x} + \frac{1}{2} F^{ijkl}_{12}\frac{\partial w_k}{\partial y}\frac{\partial w_l}{\partial y} + F^{ijkl}_{16}\frac{\partial w_k}{\partial x}\frac{\partial w_l}{\partial y}$$

$$M^{ij}_{y} = D^{ijk}_{12}\frac{\partial u_k}{\partial x} + D^{ijk}_{22}\left(\frac{\partial v_k}{\partial y} + \frac{w_k}{R}\right) + \overline{D}^{ijk}_{23} w_k + D^{ijk}_{26}\left(\frac{\partial u_k}{\partial y} + \frac{\partial v_k}{\partial x}\right) + \frac{1}{2} F^{ijkl}_{12}\frac{\partial w_k}{\partial x}\frac{\partial w_l}{\partial x} + \frac{1}{2} F^{ijkl}_{22}\frac{\partial w_k}{\partial y}\frac{\partial w_l}{\partial y} + F^{ijkl}_{26}\frac{\partial w_k}{\partial x}\frac{\partial w_l}{\partial y}$$

$$M^{ij}_{xy} = D^{ijk}_{16}\frac{\partial u_k}{\partial x} + D^{ijk}_{26}\left(\frac{\partial v_k}{\partial y} + \frac{w_k}{R}\right) + \overline{D}^{ijk}_{36} w_k + D^{ijk}_{66}\left(\frac{\partial u_k}{\partial y} + \frac{\partial v_k}{\partial x}\right) + \frac{1}{2} F^{ijkl}_{16}\frac{\partial w_k}{\partial x}\frac{\partial w_l}{\partial x} + \frac{1}{2} F^{ijkl}_{26}\frac{\partial w_k}{\partial y}\frac{\partial w_l}{\partial y} + F^{ijkl}_{66}\frac{\partial w_k}{\partial x}\frac{\partial w_l}{\partial y}$$

The laminate stiffness coefficients used in equations (2.12) are given as:

$$A_{mn}^{ij} = \int_{-\frac{h}{2}}^{\frac{h}{2}} C_{mn}\, \Phi^i\, \Phi^j\, dz$$

$$\bar{A}_{mn}^{ij} = \int_{-\frac{h}{2}}^{\frac{h}{2}} C_{mn}\, \Phi^i\, \frac{d\Phi^j}{dz}\, dz$$

$$\bar{\bar{A}}_{mn}^{ij} = \int_{-\frac{h}{2}}^{\frac{h}{2}} C_{mn}\, \frac{d\Phi^i}{dz}\, \frac{d\Phi^j}{dz}\, dz \qquad (2.13)$$

$$D_{mn}^{ijk} = \int_{-\frac{h}{2}}^{\frac{h}{2}} C_{mn}\, \Phi^i\, \Phi^j\, \Phi^k dz$$

$$\bar{D}_{mn}^{ijk} = \int_{-\frac{h}{2}}^{\frac{h}{2}} C_{mn}\, \Phi^i\, \Phi^j\, \frac{d\Phi^k}{dz}\, dz$$

$$F_{mn}^{ijkl} = \int_{-\frac{h}{2}}^{\frac{h}{2}} C_{mn}\, \Phi^i\, \Phi^j\, \Phi^k\, \Phi^l\, dz$$

Here i, j, k, l = 1, 2, ..., N+1 and m, n = 1, 2, ..., 6. Note that the laminate stiffness matrices with single bars on them are not symmetric with respect to the superscripts, whereas all the other matrices are symmetric with respect to both the superscripts and subscripts.

2.2 Buckling Analysis

Even though for generally anisotropic shells the coupling between the different displacement modes introduces a significant pre-buckling deformation, it is however important to carry out a linearized buckling analysis to have an estimate of the critical or the limit load. For orthotropic and cross-ply laminated shells, however, the pre-buckling deformations are non-existent and the buckling analysis could give realistic results. Moreover, for post-buckling and imperfection sensitivity analysis, a linearized buckling analysis is needed to determine the critical load and buckling modes of the shell. These are very important in determining the kind of symmetry, if any, to be used for analysis. Symmetry should be exploited as much as possible in full nonlinear analysis to reduce the computational expense and effort.

Reddy [37] has shown that the pre-buckling stress state specified below corresponds to a pure membrane state for which the end effects could be ignored:

$$\sigma_{xx} = - q_o$$
$$\sigma_{yy} = (P_1 + P_{n+1})\, R/h$$
$$\sigma_{xz} = \sigma_{yz} = \sigma_{xy} = \sigma_{zz} = 0 \qquad (2.14)$$

The work done by these pre-buckling stresses can be written as:

$$\delta W = \int_{\Omega} \left(M_x^{ij} \frac{\partial w_i}{\partial x} \frac{\partial \delta w_j}{\partial x} + M_y^{ij} \frac{\partial w_i}{\partial y} \frac{\partial \delta w_j}{\partial y} \right) dx\, dy \qquad (2.15)$$

where

$$M_x^{ij} = - q_o G^{ij} \tag{2.16a}$$

$$M_y^{ij} = - (P_{n+1} + P_1) \frac{R}{h} G^{ij} \tag{2.16b}$$

and

$$G^{ij} = \int_{-\frac{h}{2}}^{\frac{h}{2}} \Phi^i \Phi^j \, dz \tag{2.16c}$$

Note that i and j vary from 1 to N+1, where N is the number of layers in the shell.

2.3 Natural Vibration Analysis

It is often desired to determine the fundamental vibration mode and frequency of a cylindrical shell through an eigenvalue analysis. The principle of virtual displacements dictates that the time integral of the total potential energy and the kinetic energy vanishes:

$$0 = \int_0^T (\delta U - \delta K) \, dt \tag{2.17}$$

The total potential energy, δU, is as defined in equation (2.5). The kinetic part, δK, is given by:

$$\int_0^T \delta K \, dt = \rho \int_0^T \int_{-\frac{h}{2}}^{\frac{h}{2}} \int_\Omega \left\{ (\dot{u}_i \Phi^i)(\delta\dot{u}_j \Phi^j) + (\dot{v}_i \Phi^i)(\delta\dot{v}_j \Phi^j) + (\dot{w}_i \Phi^i)(\delta\dot{w}_j \Phi^j) \right\} dz \, dA \, dt \tag{2.18}$$

2.4 Finite Element Model

The finite element model is developed by expanding the interface displacements (u_i, v_i, w_i) over each element as a linear combination of the two-dimensional Lagrange interpolation functions φ^j and the nodal values (u_i^j, v_i^j, w_i^j) as follows:

$$(u_i, v_i, w_i) = \sum_{j=1}^{p} (u_i^j, v_i^j, w_i^j)\, \varphi^j \tag{2.19}$$

where p is the number of nodes in each element. Substitution of equation (2.19) into the virtual work statement , equation (2.7), gives the finite element model of a typical element as:

$$\begin{bmatrix} {}^{11}K_{ij}^{\alpha\beta} & {}^{12}K_{ij}^{\alpha\beta} & {}^{13}K_{ij}^{\alpha\beta} \\ {}^{21}K_{ij}^{\alpha\beta} & {}^{22}K_{ij}^{\alpha\beta} & {}^{23}K_{ij}^{\alpha\beta} \\ {}^{31}K_{ij}^{\alpha\beta} & {}^{32}K_{ij}^{\alpha\beta} & {}^{33}K_{ij}^{\alpha\beta} \end{bmatrix} \begin{Bmatrix} \{u\} \\ \{v\} \\ \{w\} \end{Bmatrix} = \begin{Bmatrix} \{q_u\} \\ \{q_v\} \\ \{q_w\} \end{Bmatrix} \tag{2.20}$$

where i, j = 1, 2, ..., p and $\alpha, \beta = 1, 2, ..., N+1$. The displacements vectors are given by $\{u\}$, $\{v\}$ and $\{w\}$, whereas the corresponding load vectors are $\{q_u\}$, $\{q_v\}$ and $\{q_w\}$.

For eigenvalue analysis, the finite element model takes the form:

$$\begin{bmatrix} {}^{11}K_{ij}^{\alpha\beta} & {}^{12}K_{ij}^{\alpha\beta} & {}^{13}K_{ij}^{\alpha\beta} \\ {}^{21}K_{ij}^{\alpha\beta} & {}^{22}K_{ij}^{\alpha\beta} & {}^{23}K_{ij}^{\alpha\beta} \\ {}^{31}K_{ij}^{\alpha\beta} & {}^{32}K_{ij}^{\alpha\beta} & {}^{33}K_{ij}^{\alpha\beta} \end{bmatrix} - \lambda \begin{bmatrix} {}^{11}S_{ij}^{\alpha\beta} & 0 & 0 \\ 0 & {}^{22}S_{ij}^{\alpha\beta} & 0 \\ 0 & 0 & {}^{33}S_{ij}^{\alpha\beta} \end{bmatrix} = \begin{Bmatrix} \{0\} \\ \{0\} \\ \{0\} \end{Bmatrix} \tag{2.21}$$

For linearized buckling analysis, we have

$$ {}^{11}S_{ij}^{\alpha\beta} = {}^{22}S_{ij}^{\alpha\beta} = 0 \tag{2.22} $$

$$ {}^{33}S_{ij}^{\alpha\beta} = \int_{\Omega} (G^{\alpha\beta} \frac{\partial \varphi_i}{\partial x} \frac{\partial \varphi_j}{\partial x} + G^{\alpha\beta} \frac{\partial \varphi_i}{\partial y} \frac{\partial \varphi_j}{\partial y}) \, dx \, dy \tag{2.23} $$

For natural vibration analysis, we have

$$ {}^{11}S_{ij}^{\alpha\beta} = {}^{22}S_{ij}^{\alpha\beta} = {}^{33}S_{ij}^{\alpha\beta} = \int_{\Omega} \rho^{\alpha} (G^{\alpha\beta} \varphi_i \varphi_j) \, dx \, dy \tag{2.24} $$

where ρ^{α} is the density of the composite material of layer-α.

Note that the solution of the eigenvalue problem defined by equation (2.21) gives the eigenvalues λ_i^{α}. The minimum eigenvalue is the critical buckling load for the case of buckling analysis, and the square of the fundamental frequency for the case of natural vibration analysis.

The elements of the tangent stiffness matrix for a cylindrical shell element are given in Appendix B. Note that for eigenvalue analysis, only the linear part of the tangent stiffness matrix is used.

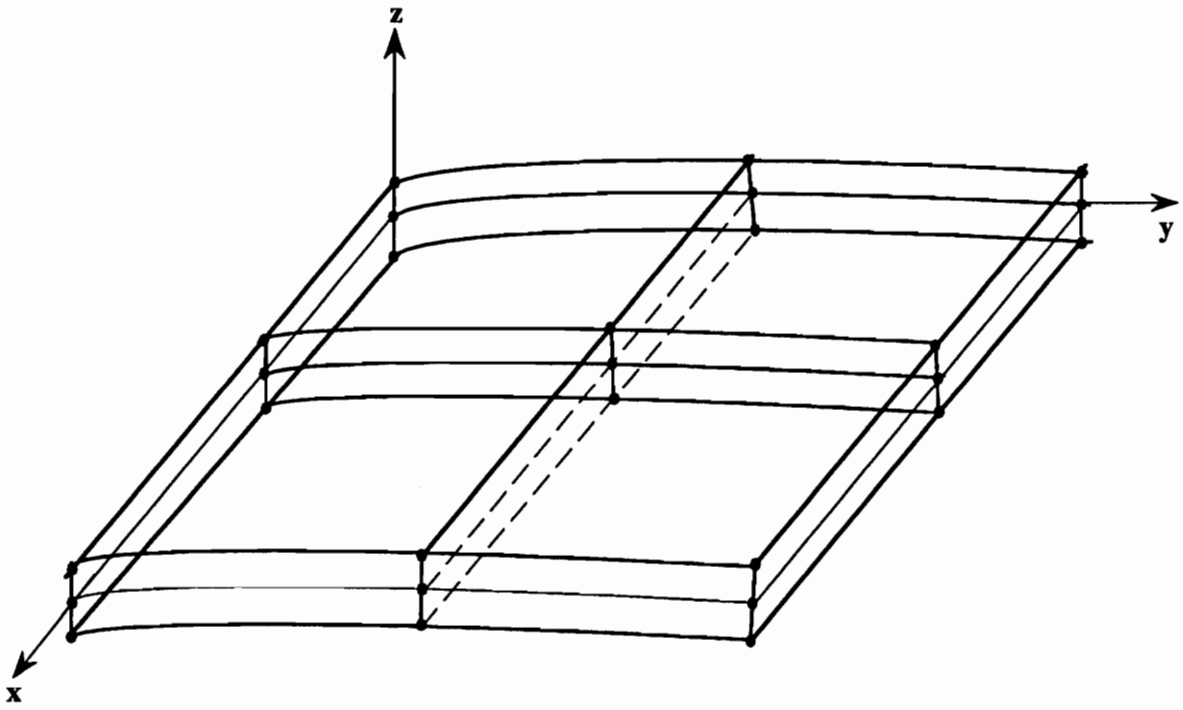

Figure 3. A typical layerwise finite element discretization.

CHAPTER 3

LAYERWISE THEORY FOR SHELL STIFFENER ELEMENTS

3.1 Introduction

Stiffeners are used to efficiently increase the load carrying capacity of shells. Stiffened shells have higher critical loads, lower frequencies and less deflections and strains. For the analysis of stiffened laminated shells, a compatible displacement field has to be prescribed for both the shell and the stiffener element. In light of this, a new layerwise shell and plate stiffener element is developed here. The element is assumed to exhibit a two-dimensional behavior. The normal and shear stresses in the width direction (σ_{xx}, σ_{xy} and σ_{xz}) are neglected due to their small magnitude. The transverse normal stress σ_{zz} is kept to maintain compatibility with the skin material. For stiffeners and stand-alone beams made out of composite laminates, the transverse shear stresses assume a significant magnitude because of the large differences in the inplane and shear moduli of the laminate material. Hence, any refined model should have the capacity to model the transverse shear stress for accurately describing the kinematics and state of stress.

In reducing the three-dimensional constitutive equations for a generally anisotropic laminate to that of a two-dimensional beam element, emphasis is placed on eliminating the stress components (σ_{xx}, σ_{xy} and σ_{xz}) only and not the corresponding strain components (ε_{xx}, γ_{xy} and γ_{xz}). The finite element model of the layerwise stiffener element is also developed in this chapter. The scheme for adopting this element to stiffened shells is discussed in detail.

3.2.1 Displacement Fields

Consider a laminated curved beam element of length L, thickness t, and undeformed middle surface of radius R, with $t << R$ as shown in Figure 4. The derivations shown here are for the general case of a circumferential stiffener, commonly called ring, oriented in the global y-z plane. The choice of the global coordinate plane as y-z is arbitrary. For straight beam elements and longitudinal stiffeners, the radius of curvature is taken as infinity.

The displacements (v, w) at a generic point (x, y, z) in the stiffener element are assumed to be of the form:

$$v(x,y,z) = \sum_{j=1}^{N+1} v_j(x,y)\,\Phi^j(z) \qquad (3.1)$$

$$w(x,y,z) = \sum_{j=1}^{N+1} w_j(x,y)\,\Phi^j(z)$$

where N is the number of mathematical layers in the stiffener, v_j and w_j are the nodal values of displacements of each interface, and Φ^j is a linear Lagrangian interpolation function through the thickness. In equation (3.1) and all subsequent equations, summation is used on repeated subscripts and superscripts. The global interpolation functions have the same definition as discussed in section 2.1.1.

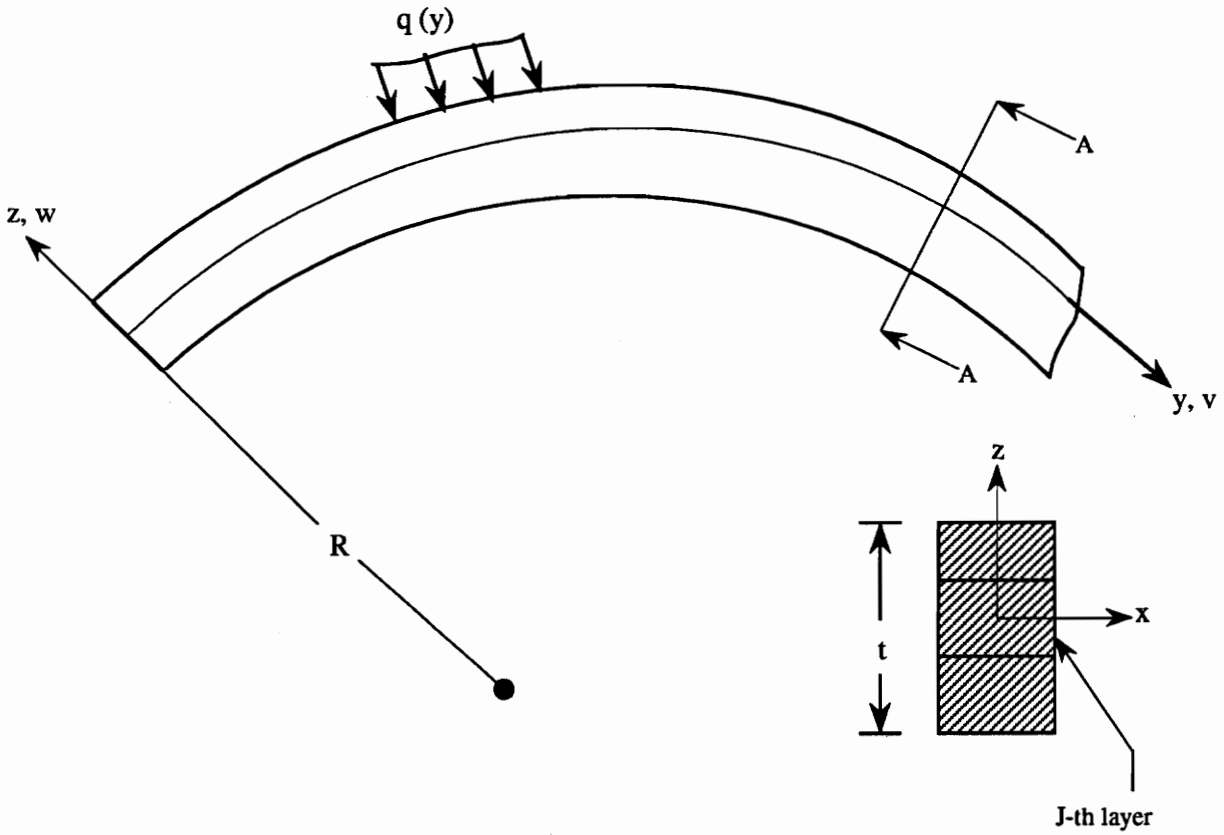

Figure 4. A laminated curved shell stiffener element.

3.2.2 Strains

The von Kárman type non-linear strains are considered, where small strains and moderate rotations with respect to the curved beam reference surface are assumed. Transverse normal strains are also included in the formulation:

$$\varepsilon_{yy} = \frac{\partial v}{\partial y} + \frac{w}{R} + \frac{1}{2}\left(\frac{\partial w}{\partial y}\right)^2 = \left(\frac{\partial v_i}{\partial y} + \frac{w_i}{R}\right)\Phi^i + \frac{1}{2}\frac{\partial w_i}{\partial y}\frac{\partial w_j}{\partial y}\Phi^i\Phi^j$$

$$\gamma_{yz} = \frac{\partial v}{\partial z} + \frac{\partial w}{\partial y} - \frac{v}{R} = v_i\frac{d\Phi^i}{dz} + \left(\frac{\partial w_i}{\partial y} - \frac{v_i}{R}\right)\Phi^i \qquad (3.2)$$

$$\varepsilon_{zz} = \frac{\partial w}{\partial z} = w_i\frac{d\Phi^i}{dz}$$

3.2.3 Virtual Strain Energy

The virtual work due to the internal stresses in the stiffener element can be written as:

$$\delta U = \int_{\Omega}\int_{-\frac{h}{2}}^{\frac{h}{2}} \left(\sigma_{yy}\delta\varepsilon_{yy} + \sigma_{zz}\delta\varepsilon_{zz} + \sigma_{yz}\delta\gamma_{yz}\right) dz\, dA \qquad (3.3)$$

where σ_{yy}, σ_{yz}, and σ_{zz} are the stresses, V is the total volume of the stiffener element, and Ω is the area of the reference surface.

Substituting the strain-displacement relations given by equations (3.2) into the virtual work statement, equation (3.3), gives an expression for the virtual strain energy in terms of the displacements as given below:

$$\delta U = \int_{\Omega} [\, N_y^i \left(\frac{\partial \delta v_i}{\partial y} + \frac{\delta w_i}{R}\right) + \frac{1}{2} M_y^{ij} \frac{\partial \delta w_i}{\partial y} \frac{\partial w_i}{\partial y} + Q_{zz}^i \delta w_i + Q_{yz}^i \delta v_i + K_{yz}^i \frac{\partial \delta w_i}{\partial y} - \frac{1}{R} K_{yz}^i \delta v_i \,] \, dA \tag{3.4}$$

where the laminate force resultants used in equation (3.4) are defined as:

$$N_y^i = \int_{-\frac{h}{2}}^{\frac{h}{2}} \sigma_{yy} \Phi^i \, dz$$

$$M_y^{ij} = \int_{-\frac{h}{2}}^{\frac{h}{2}} \sigma_{yy} \Phi^i \Phi^j dz \tag{3.5}$$

$$K_{yz}^i = \int_{-\frac{h}{2}}^{\frac{h}{2}} \sigma_{yz} \Phi^i \, dz$$

$$(Q_{yz}^i, Q_{zz}^i) = \int_{-\frac{h}{2}}^{\frac{h}{2}} (\sigma_{yz}, \sigma_{zz}) \frac{d\Phi^i}{dz} \, dz$$

3.2.4 Constitutive Equations for Laminated Beams

The three-dimensional constitutive equations of an anisotropic body are reduced to a two-dimensional form by eliminating the normal stress σ_{xx}, the shear stress σ_{xy}, and the transverse shear stress σ_{xz} in the width and depth directions. Here, it should be borne in mind that it is only certain stresses which are ignored and not the strains. Thus for a beam element, the constitutive equations reduce to the form:

$$\begin{bmatrix} \sigma_{yy} \\ \sigma_{zz} \\ \sigma_{yz} \end{bmatrix} = \begin{bmatrix} C^*_{11} & C^*_{13} & 0 \\ C^*_{13} & C^*_{33} & 0 \\ 0 & 0 & C^*_{44} \end{bmatrix} \begin{bmatrix} \varepsilon_{yy} \\ \varepsilon_{zz} \\ \gamma_{yz} \end{bmatrix} \tag{3.6}$$

where the modified elastic constants C^*_{ij} are given as:

$$C^*_{11} = C_{11} + \frac{C_{13}C_{23} - C_{12}C_{33}}{C_{22}C_{33} - C_{23}C_{23}} C_{12} + \frac{C_{12}C_{23} - C_{13}C_{22}}{C_{22}C_{33} - C_{23}C_{23}} C_{13}$$

$$C^*_{13} = C_{13} + \frac{C_{33}C_{23} - C_{23}C_{33}}{C_{22}C_{33} - C_{23}C_{23}} C_{12} + \frac{C_{23}C_{23} - C_{33}C_{22}}{C_{22}C_{33} - C_{23}C_{23}} C_{13} \tag{3.7}$$

$$C^*_{33} = C_{33} + \frac{C_{33}C_{23} - C_{23}C_{33}}{C_{22}C_{33} - C_{23}C_{23}} C_{23} + \frac{C_{23}C_{23} - C_{33}C_{22}}{C_{22}C_{33} - C_{23}C_{23}} C_{33}$$

$$C^*_{44} = C_{44} - \frac{C_{45}C_{45}}{C_{55}}$$

Substituting the constitutive relations given by equations (3.6) into the laminate force resultants, equation (3.5), gives an expression for the laminate force resultants in terms of the displacements as:

$$N_y^i = A_{11}^{ij}\left(\frac{\partial v_j}{\partial y} + \frac{w_j}{R}\right) + \overline{A}_{13}^{ij}\, w_j + \frac{1}{2} D_{11}^{ijk} \frac{\partial w_j}{\partial y}\frac{\partial w_k}{\partial y}$$

$$Q_{zz}^j = \overline{A}_{13}^{ji}\left(\frac{\partial v_j}{\partial y} + \frac{w_j}{R}\right) + \overline{\overline{A}}_{33}^{ij}\, w_j + \frac{1}{2} \overline{D}_{13}^{jki} \frac{\partial w_j}{\partial y}\frac{\partial w_k}{\partial y}$$

$$Q_{yz}^j = \overline{A}_{44}^{ji}\left(\frac{\partial w_j}{\partial y} - \frac{v_j}{R}\right) + \overline{\overline{A}}_{44}^{ij}\, v_j \qquad (3.8)$$

$$K_{yz}^j = A_{44}^{ij}\left(\frac{\partial w_j}{\partial y} - \frac{v_j}{R}\right) + \overline{A}_{44}^{ij}\, v_j$$

$$M_y^{ij} = D_{11}^{ijk}\left(\frac{\partial v_k}{\partial y} + \frac{w_k}{R}\right) + \frac{1}{2} F_{11}^{ijkl} \frac{\partial w_j}{\partial y}\frac{\partial w_k}{\partial y}$$

The laminate stiffness coefficients are given in terms of the modified elastic constants as follows:

$$A_{mn}^{ij} = \int_{-\frac{h}{2}}^{\frac{h}{2}} C_{mn}^{*}\, \Phi^i\, \Phi^j\, dz$$

$$\overline{A}_{mn}^{ij} = \int_{-\frac{h}{2}}^{\frac{h}{2}} C_{mn}^{*}\, \Phi^i \frac{d\Phi^j}{dz}\, dz$$

$$\overline{\overline{A}}^{ij}_{mn} = \int_{-\frac{h}{2}}^{\frac{h}{2}} C^{*}_{mn} \frac{d\Phi^{i}}{dz} \frac{d\Phi^{j}}{dz} dz$$

$$D^{ijk}_{mn} = \int_{-\frac{h}{2}}^{\frac{h}{2}} C^{*}_{mn} \Phi^{i} \Phi^{j} \Phi^{k} dz$$

(3.9)

$$\overline{D}^{ijk}_{mn} = \int_{-\frac{h}{2}}^{\frac{h}{2}} C^{*}_{mn} \Phi^{i} \Phi^{j} \frac{d\Phi^{k}}{dz} dz$$

$$F^{ijkl}_{mn} = \int_{-\frac{h}{2}}^{\frac{h}{2}} C^{*}_{mn} \Phi^{i} \Phi^{j} \Phi^{k} \Phi^{l} dz$$

Here i, j = 1, 2, ..., N+1 and m, n = 1, 3, 4. N is the number of mathematical layers in the stiffener under consideration.

Note that the ply stiffness coefficients with a single hat are not symmetric with respect to the superscripts. All the other stiffness coefficients are symmetric with respect to both superscripts and subscripts.

3.2.5 Finite Element Model

A displacement finite element model of the stiffener equations defined in the previous sections is developed here. The interface displacements (v_i, w_i) are expressed over each element as a linear combination of the one-dimensional Lagrange interpolation function φ^j and the nodal values v_i^j and w_i^j as follows:

$$(v_i,\ w_i) = \sum_{j=1}^{p} (v_i^j,\ w_i^j)\,\varphi^j \tag{3.10}$$

where p is the number of nodes in a typical element. Substituting equation (3.10) into the virtual work statement of the stiffener element, the finite element model of a typical stiffener element is obtained:

$$\begin{bmatrix} {}^{11}K_{ij}^{\alpha\beta} & {}^{12}K_{ij}^{\alpha\beta} \\ {}^{21}K_{ij}^{\alpha\beta} & {}^{22}K_{ij}^{\alpha\beta} \end{bmatrix} \begin{bmatrix} \{v\} \\ \{w\} \end{bmatrix} = \begin{Bmatrix} \{q_v\} \\ \{q_w\} \end{Bmatrix} \tag{3.11}$$

where [K] is the element stiffness matrix. The displacement vectors are given by {v} and {w}, whereas the corresponding load vectors are {qv} and {qw}. Here i, j = 1, 2, ..., p and α, β = 1, 2, ..., N+1.

For eigenvalue analysis, the finite element model takes the form:

$$\begin{bmatrix} {}^{11}K_{ij}^{\alpha\beta} & {}^{12}K_{ij}^{\alpha\beta} \\ {}^{21}K_{ij}^{\alpha\beta} & {}^{22}K_{ij}^{\alpha\beta} \end{bmatrix} - \lambda \begin{bmatrix} {}^{11}S_{ij}^{\alpha\beta} & 0 \\ 0 & {}^{22}S_{ij}^{\alpha\beta} \end{bmatrix} = \begin{Bmatrix} \{0\} \\ \{0\} \end{Bmatrix} \tag{3.12}$$

For natural vibration analysis, the lowest λ is the square of the fundamental frequency and [S] is the mass matrix. For a linearized stability analysis, the lowest λ is the critical buckling load and [S] is the geometric stiffness matrix. The matrix [S] is defined below.

For linearized buckling analysis, we have

$$ {}^{11}S_{ij}^{\alpha\beta} = 0 \tag{3.13} $$

$$ {}^{22}S_{ij}^{\alpha\beta} = \int_{\Omega} \left(G^{\alpha\beta} \frac{\partial \varphi_i}{\partial y} \frac{\partial \varphi_j}{\partial y} \right) dy \tag{3.14} $$

For natural vibration analysis, we have

$$ {}^{11}S_{ij}^{\alpha\beta} = {}^{22}S_{ij}^{\alpha\beta} = \int_{\Omega} \rho^{\alpha} \left(G^{\alpha\beta} \varphi_i \varphi_j \right) dy \tag{3.15} $$

where ρ^{α} is the density of the composite material of layer-α.

The elements of the tangent stiffness matrix for a shell/plate stiffener element are given in Appendix C.

3.3 Smeared Stiffener Model

When the spacing between the stiffeners is very small and a large number of stiffeners are used, the use of discrete models becomes unjustifiably costly and one should resort to the less costly "smeared" approach. For global responses such as natural vibration, linearized buckling and post-buckling, the "smeared" approach gives quite satisfactory results. In light of this, the formulation of a smeared or "averaged-stiffness" model is included here.

3.3.1 Strains and Displacement Fields

Here the stiffener is again assumed to lie in the y-z plane, and the formulation is presented for circumferential stiffeners. By setting the radius to infinity and using the corresponding material and geometry properties, the same derivation developed here for circumferential stiffeners can be used for the longitudinal stiffeners. The stiffeners are assumed to behave as a one-dimensional Euler-Bernoulli beam element:

$$v = v_n - z\frac{\partial w_n}{\partial y}$$

$$w = w_n \tag{3.16}$$

$$\varepsilon_{yy} = \frac{\partial v_n}{\partial y} + \frac{w_n}{R} + \frac{1}{2}\left(\frac{\partial w_n}{\partial y}\right)^2 - z\frac{\partial^2 w_n}{\partial y^2}$$

The subscript 'n' represents the interface number of the shell skin layer to which the stiffener is attached.

3.3.2 Stresses

Assuming a one-dimensional behavior of the stiffeners, only the normal stress, i.e., σ_{yy}, is considered:

$$\sigma_{yy} = E_{yy}\,\varepsilon_{yy} \tag{3.17}$$

where E_{yy} is the equivalent Young's modulus of the stiffener material in the y direction.

3.3.3 Virtual Strain Energy of Stiffeners

The work done by the internal stresses in the stiffeners is given as:

$$\delta U = \frac{1}{S}\int_{\Omega}\int_{A}\left(\sigma_{yy}\,\delta\varepsilon_{yy} + \frac{GJ}{S}\frac{\partial^2 w_n}{\partial x\partial y}\frac{\partial^2 \delta w_n}{\partial x\partial y}\right) dx\,dy \tag{3.18}$$

$$\begin{aligned}\delta U = \frac{1}{S}\int_{\Omega}\Bigg[& EA\left(\frac{\partial \delta v_n}{\partial y} + \frac{\delta w_n}{R} + \frac{\partial w_n}{\partial y}\frac{\partial \delta w_n}{\partial y}\right)\left(\frac{\partial v_n}{\partial y} + \frac{w_n}{R} + \frac{1}{2}\left(\frac{\partial w_n}{\partial y}\right)^2\right) \\ & + EI\frac{\partial^2 w_n}{\partial y^2}\frac{\partial^2 \delta w_n}{\partial y^2} - \bar{Z}\,AE\frac{\partial^2 w_n}{\partial y^2}\left(\frac{\partial \delta v_n}{\partial y} + \frac{\delta w_n}{R} + \frac{\partial w_n}{\partial y}\frac{\partial \delta w_n}{\partial y}\right) \\ & - \bar{Z}\,AE\frac{\partial^2 w_n}{\partial y^2}\left(\frac{\partial v_n}{\partial y} + \frac{w_n}{R} + \frac{1}{2}\left(\frac{\partial w_n}{\partial y}\right)^2\right) \\ & + GJ\frac{\partial^2 w_n}{\partial x\partial y}\frac{\partial^2 \delta w_n}{\partial x\partial y}\Bigg]\,dx\,dy\end{aligned} \tag{3.19}$$

where

S = the spacing between stiffeners.

= L/N_r for circumferential stiffeners (i.e., rings)

= $2\pi R/N_a$ for axial stiffeners (i.e., stringers)

L = the length of the stiffener

R = radius of the stiffener

E = the Young's modulus of the stiffener material

A = area of cross section of the stiffener

G = shear modulus of the stiffener material

J = polar moment of inertia of the stiffener

I = moment of inertia of the stiffener about the reference surface of the shell

$\overline{Z}$ = eccentricity of the centroid of the stiffener measured from the reference surface.

3.3.4 Equations of Motion

In the presence of stiffeners modeled by the "smearing approach", the Euler-Lagrange equilibrium equations of a cylindrical shell are derived by combining the virtual strain energies of the shell and the stiffeners. The weak forms of the unstiffened shell given by equation (2.7) and that of the stiffener given by (3.19) are integrated by parts and the coefficients of δu, δv, and δw collected to get:

$$0 = \frac{\partial N_x^i}{\partial x} + \frac{\partial N_{xy}^i}{\partial y} - Q_{xz}^i + \left(\frac{E_s A_s}{S_s} \frac{\partial^2 u_n}{\partial x^2} - \frac{\overline{Z}_s E_s A_s}{S_s} \frac{\partial^3 w_n}{\partial x^3} \right) \delta_{in} \qquad (3.20a)$$

$$o = \frac{\partial N^i_{xy}}{\partial x} + \frac{\partial N^i_y}{\partial y} - Q^i_{yz} + \frac{1}{R} K^i_{yz} + \left(\frac{E_r A_r}{S_r} \left(\frac{\partial^2 v_n}{\partial y^2} + \frac{1}{R} \frac{\partial w_i}{\partial y} \right) - \frac{\bar{Z}_r E_r A_r}{S_r} \frac{\partial^3 w_n}{\partial y^3} \right) \delta_{in} \qquad (3.20b)$$

$$\begin{aligned} q_i = {} & \frac{\partial K^i_{xz}}{\partial x} + \frac{\partial K^i_{yz}}{\partial y} - \left(\frac{1}{R} N^i_y + Q^i_{yz} \right) + \left(- \frac{E_s A_s}{S_s} \frac{\partial^4 w_n}{\partial x^4} - \frac{E_r A_r}{S_r} \frac{\partial^4 w_n}{\partial x^4} \right) \\ & - \left(\frac{G_s J_s}{S_s} + \frac{G_r J_r}{S_r} \right) \frac{\partial^4 w_n}{\partial x^2 \partial y^2} + \frac{\bar{Z}_s E_s A_s}{S_s} \frac{\partial^3 u_n}{\partial x^3} \Big) \\ & + \frac{\bar{Z}_r E_r A_r}{S_r} \left(\frac{\partial^3 v_n}{\partial y^3} + \frac{2}{R} \frac{\partial^2 w_n}{\partial y^2} \right) \\ & - \frac{1}{R} \frac{E_r A_r}{S_r} \left(\frac{\partial v_n}{\partial y} + \frac{1}{R} w_n \right) \Big) \Big) \delta_{in} \end{aligned} \qquad (3.20c)$$

where δ_{in} is the Kronecker delta defined below:

$$\delta_{in} = \begin{cases} 1, & i = n \\ 0, & i \neq n \end{cases} \qquad (3.21)$$

3.3.5 Finite Element Model for the Smeared Approach

Along the same lines as the other elements developed so far in this study, the finite element model of the "smeared" approach is formulated. Here, the stiffness matrix does not have a layerwise format through the thickness of the stiffener. Instead, it is added to that of the top or bottom layer of the shell skin depending on the location of the stiffener.

The components of the nonlinear tangent stiffness matrix for the smeared model are given in Appendix D. The components are given for both the longitudinal and circumferential stiffeners.

3.4 Modeling of Stiffened Shells

Since both the shell and stiffener elements have the same displacement patterns, compatibility of strains and equilibrium of forces can be enforced by letting the two elements share the same nodes in the finite element mesh. The linear layerwise stiffener elements share one of the sides of the 2-D surface-wise shell element. Depending on the location of the stiffener, the stiffener element will again share one or more of the through-thickness nodes of the skin element. Apart from enforcing compatibility of strains and equilibrium of forces, the sharing of nodes significantly reduces the size of the equations to be assembled and solved. Figure 5 shows a typical skin-interface model one encounters in stiffened laminated shells. The layerwise format of the stiffener and shell skin element takes care of eccentricity automatically. The effect of the location of the stiffeners is also handled readily by the model developed.

For shells stiffened by closely spaced rings and stringers, the "smeared" approach offers an economical alternative as discussed in section 3.3. In this approach, the stiffeners are treated as one-dimensional beam elements whose equivalent material properties are determined by a laminate analysis. The stiffness of the equivalent beam element is added to that of the shell skin at the common node. This model has no provisions for variation of the displacement field through the thickness of the stiffener. The "average stiffness" method is also used for stiffeners whose plies are normal to the plane of the shell skin. Although there is a certain degree of approximation introduced by this model, global responses like buckling loads, fundamental vibration modes and frequencies can be determined with a reasonable accuracy.

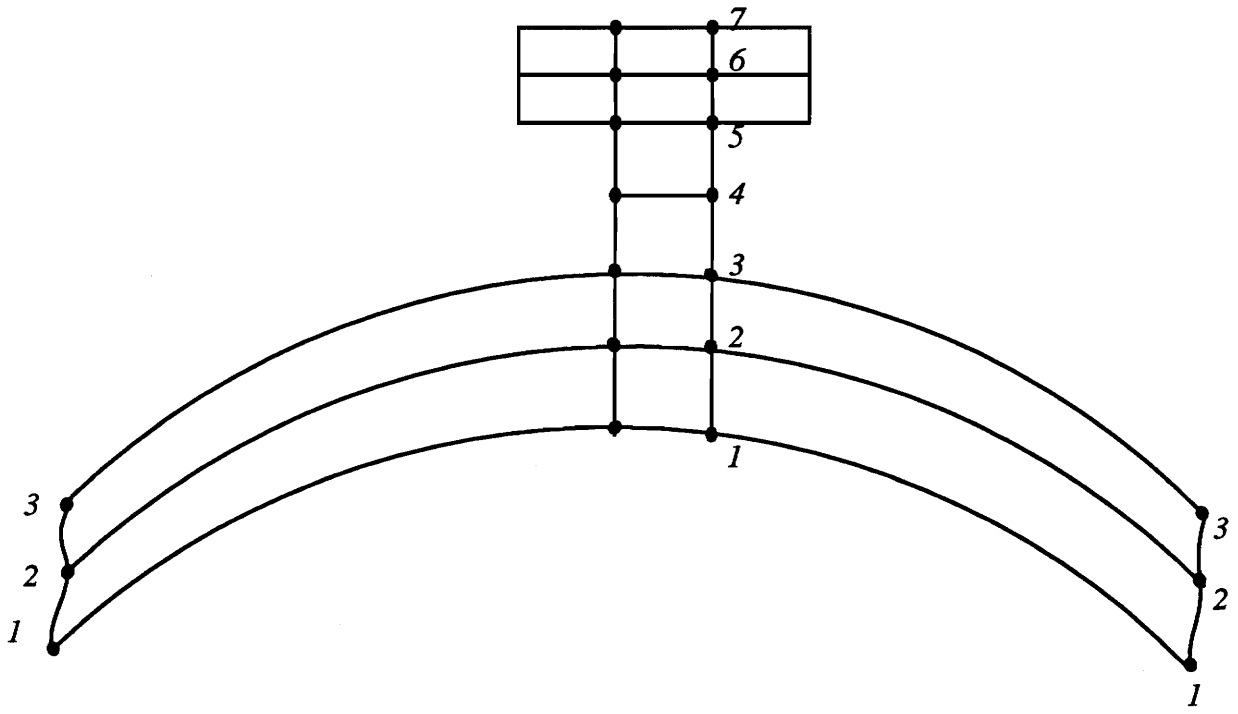

Figure 5. Interface numbering and modelling of a stiffened shell.

CHAPTER 4

IMPERFECTION SENSITIVITY ANALYSIS

4.1 Introduction

Initial imperfections, i.e., small deviations from the initial assumed geometry, reduce the bifurcation-point loads of cylindrical shells significantly. Experiments on axially compressed cylindrical shells have given as low as 10 to 20 percent of the corresponding theoretical values [74]. For very thin shells, the reduction is even more. It has been observed that the post-buckling equilibrium of axially compressed cylindrical shells can drop sharply downward from the bifurcation point as shown in Figure 6.

The shape of the secondary equilibrium path has a very important bearing on the load carrying capacity of the structure beyond buckling. A positive slope of the initial portion of the secondary path indicates that the structure sustains more load in the post-buckling range. On the other hand, for a secondary equilibrium path with a negative slope the imperfections will reduce the buckling load and the stability. Curve B in Figure 6 indicates that initial imperfections can be detrimental for the load carrying capacity of such structures with a secondary equilibrium path having a negative slope. In this chapter, the layerwise theory is extended to generally anisotropic cylinders with imperfections along the same lines as Reference [89]. Unlike Reference [89], which deals with cross-ply laminated shells, the formulations are valid for generally anisotropic cylindrical shells. A finite element model for shells with initial imperfections is also developed here.

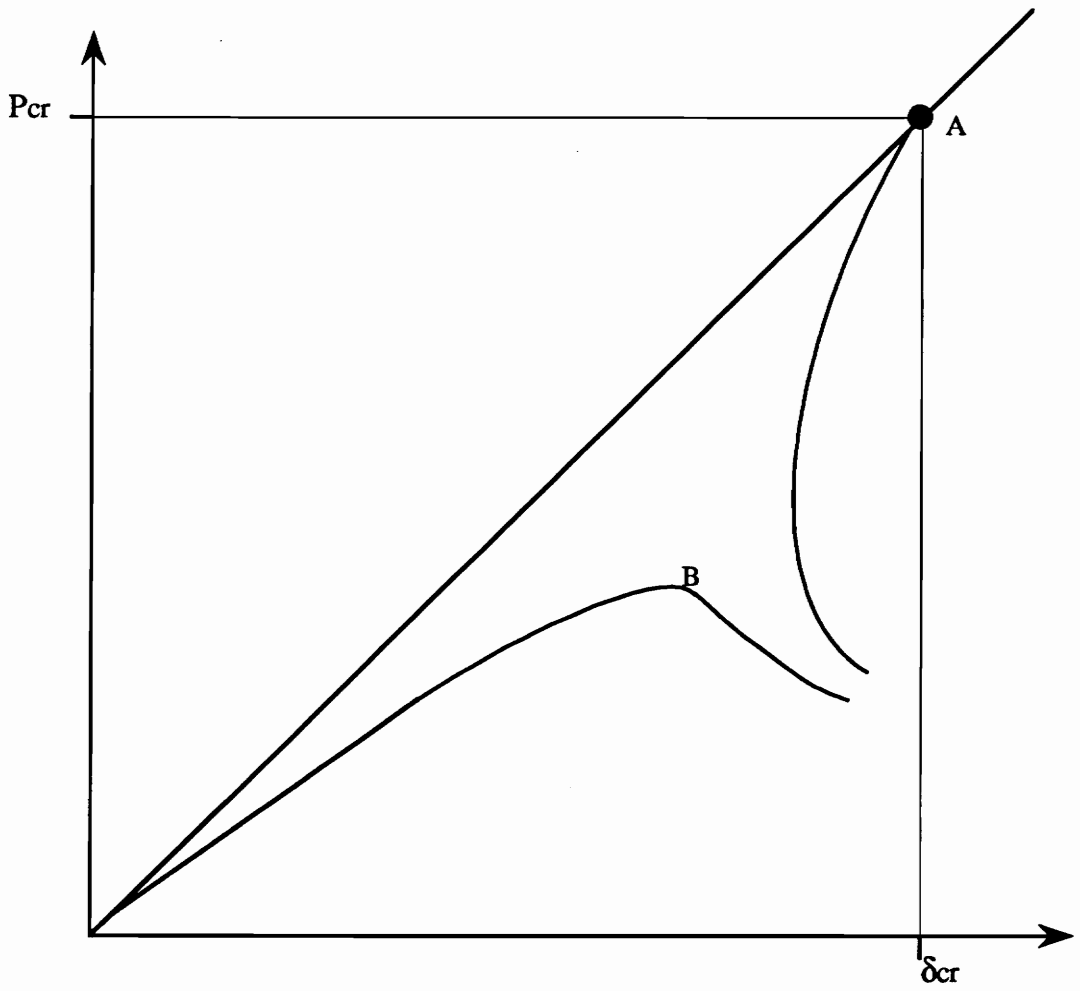

Figure 6. Equilibrium path for axially loaded imperfect cylindrical shell.

4.2 Layerwise Theory for Cylinders with Imperfections

Here, we shall assume that $\hat{w}_j$ is a known small deviation of interface j of a laminate from a perfectly circular cylindrical shape. The unloaded shell with initial imperfections $\hat{w}_j$ is considered to be stress-free.

4.2.1 Displacement Fields

In addition to the expansion of the displacement fields for u, v, and w given in equation (2.1), an additional displacement field is specified for the initial imperfection $\hat{w}_j$.:

$$\hat{w}(x, y, z) = \sum_{j=1}^{N} \hat{w}_j(x, y)\, \Phi^j \tag{4.1}$$

4.2.2 Strain-Displacement Relationships

The angles of rotations, which are assumed to be of small magnitude, take the form $\frac{d}{dx}(w + \overline{w})$ due to the presence of initial imperfections. The strain-displacement relations previously defined in equation (2.3) for the perfect geometry of a cylindrical shell take the following form:

$$\varepsilon_{xx}=\frac{\partial u}{\partial x}+\frac{1}{2}\frac{\partial w}{\partial x}[\frac{\partial w}{\partial x}+2\frac{\partial \hat{w}}{\partial x}]$$

$$\varepsilon_{yy}=\frac{\partial v}{\partial y}+\frac{w}{R}+\frac{1}{2}\frac{\partial w}{\partial y}[\frac{\partial w}{\partial y}+2\frac{\partial \hat{w}}{\partial y}] \qquad (4.2)$$

$$\varepsilon_{xy}=\frac{\partial u}{\partial y}+\frac{\partial v}{\partial x}+\frac{1}{2}\frac{\partial w}{\partial x}[\frac{\partial w}{\partial y}+2\frac{\partial \hat{w}}{\partial y}]+\frac{1}{2}\frac{\partial w}{\partial y}[\frac{\partial w}{\partial x}+2\frac{\partial \hat{w}}{\partial x}]$$

The transverse normal and shear strains, namely ε_{zz}, γ_{yz} and γ_{xz}, keep the same form as in equation (2.3).

4.2.3 Virtual Work Statement

The principle of virtual work for an imperfect cylindrical shell has the same form as equations (2.5) and (2.6). Substituting the strain-displacement relationships for an imperfect shell given by equation (4.2) into the energy equations (2.5) and (2.6) gives:

$$\begin{aligned}0=\int_{\Omega}\Big\{ & N_x^i\frac{\partial \delta u_i}{\partial x}+N_y^i(\frac{\partial \delta v_i}{\partial y}+\frac{\delta w_i}{R})+N_{xy}^i(\frac{\partial \delta u_i}{\partial y}+\frac{\delta \delta v_i}{R})+M_x^{ij}\frac{\partial \delta w_i}{\partial x}(\frac{\partial w_j}{\partial x}+\frac{\partial \hat{w}_j}{\partial x})\\ & +M_y^{ij}\frac{\partial \delta w_i}{\partial y}(\frac{\partial w_j}{\partial y}+\frac{\partial \hat{w}_j}{\partial y})+M_{xy}^{ij}[\frac{\partial \delta w_i}{\partial x}(\frac{\partial w_j}{\partial y}+\frac{\partial \hat{w}_j}{\partial y})+\frac{\partial \delta w_i}{\partial y}(\frac{\partial w_j}{\partial x}+\frac{\partial \hat{w}_j}{\partial x})]\\ & +Q_{xz}^i\delta u_i+Q_{yz}^i\delta v_i+Q_{zz}^i\delta w_i+K_{xz}^i\frac{\partial \delta w_i}{\partial x}+K_{yz}^i(\frac{\partial \delta w_i}{\partial y}+\frac{\delta v_i}{R})\\ & +\overline{M}_x^{ij}\frac{\partial \delta w_i}{\partial x}(\frac{\partial w_j}{\partial x}+\frac{\partial \hat{w}_j}{\partial x})+\overline{M}_y^{ij}\frac{\partial \delta w_i}{\partial y}(\frac{\partial w_j}{\partial y}+\frac{\partial \hat{w}_j}{\partial y})\\ & +M_{xy}^{ij}[\frac{\partial \delta w_i}{\partial x}(\frac{\partial w_j}{\partial y}+\frac{\partial \hat{w}_j}{\partial y})+\frac{\partial \delta w_i}{\partial y}(\frac{\partial w_j}{\partial x}+\frac{\partial \hat{w}_j}{\partial x})+p_i\delta w_i\Big\}\,dA\end{aligned} \qquad (4.3)$$

The laminate resultant forces used in equation (4.3), in the presence of initial imperfections, are given in terms of the displacement as:

$$N_x^i = A_{11}^{ij}\frac{\partial u_j}{\partial x} + A_{12}^{ij}\left(\frac{\partial v_j}{\partial y} + \frac{w_j}{R}\right) + \overline{A}_{13}^{ij}\, w_j + A_{16}^{ij}\left(\frac{\partial u_j}{\partial y} + \frac{\partial v_j}{\partial x}\right) +$$
$$\frac{1}{2} D_{11}^{ijk}\frac{\partial w_j}{\partial x}\left(\frac{\partial w_k}{\partial x} + 2\frac{\partial \hat{w}_k}{\partial x}\right) + \frac{1}{2} D_{12}^{ijk}\frac{\partial w_j}{\partial y}\left(\frac{\partial w_k}{\partial y} + 2\frac{\partial \hat{w}_k}{\partial y}\right) +$$
$$D_{16}^{ijk}\frac{\partial w_j}{\partial x}\left(\frac{\partial w_k}{\partial y} + 2\frac{\partial \hat{w}_k}{\partial y}\right)$$

$$N_y^i = A_{12}^{ij}\frac{\partial u_j}{\partial x} + A_{22}^{ij}\left(\frac{\partial v_j}{\partial y} + \frac{w_j}{R}\right) + \overline{A}_{23}^{ij}\, w_j + A_{26}^{ij}\left(\frac{\partial u_j}{\partial y} + \frac{\partial v_j}{\partial x}\right) +$$
$$\frac{1}{2} D_{12}^{ijk}\frac{\partial w_j}{\partial x}\left(\frac{\partial w_k}{\partial x} + 2\frac{\partial \hat{w}_k}{\partial x}\right) + \frac{1}{2} D_{22}^{ijk}\frac{\partial w_j}{\partial y}\left(\frac{\partial w_k}{\partial y} + 2\frac{\partial \hat{w}_k}{\partial y}\right) + \qquad (4.4)$$
$$D_{26}^{ijk}\frac{\partial w_j}{\partial x}\left(\frac{\partial w_k}{\partial y} + 2\frac{\partial \hat{w}_k}{\partial y}\right)$$

$$N_{xy}^i = A_{16}^{ij}\frac{\partial u_j}{\partial x} + A_{26}^{ij}\left(\frac{\partial v_j}{\partial y} + \frac{w_j}{R}\right) + \overline{A}_{36}^{ij}\, w_j + A_{66}^{ij}\left(\frac{\partial u_j}{\partial y} + \frac{\partial v_j}{\partial x}\right) +$$
$$\frac{1}{2} D_{16}^{ijk}\frac{\partial w_j}{\partial x}\left(\frac{\partial w_k}{\partial x} + 2\frac{\partial \hat{w}_k}{\partial x}\right) + \frac{1}{2} D_{26}^{ijk}\frac{\partial w_j}{\partial y}\left(\frac{\partial w_k}{\partial y} + 2\frac{\partial \hat{w}_k}{\partial y}\right) +$$
$$D_{66}^{ijk}\frac{\partial w_j}{\partial x}\left(\frac{\partial w_k}{\partial y} + 2\frac{\partial \hat{w}_k}{\partial y}\right)$$

$$Q_{zz}^i = \overline{A}_{13}^{ji}\frac{\partial u_j}{\partial x} + \overline{A}_{23}^{ji}\left(\frac{\partial v_j}{\partial y} + \frac{w_j}{R}\right) + \overline{\overline{A}}_{33}^{ji}\, w_j + \overline{A}_{36}^{ji}\left(\frac{\partial u_j}{\partial y} + \frac{\partial v_j}{\partial x}\right) +$$
$$\frac{1}{2}\overline{D}_{13}^{jki}\frac{\partial w_j}{\partial x}\left(\frac{\partial w_k}{\partial x} + 2\frac{\partial \hat{w}_k}{\partial x}\right) + \frac{1}{2}\overline{D}_{23}^{jki}\frac{\partial w_j}{\partial y}\left(\frac{\partial w_k}{\partial y} + 2\frac{\partial \hat{w}_k}{\partial y}\right) +$$
$$\overline{D}_{36}^{jki}\frac{\partial w_j}{\partial x}\left(\frac{\partial w_k}{\partial y} + 2\frac{\partial \hat{w}_k}{\partial y}\right)$$

$$M_x^{ij} = D_{11}^{ijk}\frac{\partial u_k}{\partial x} + D_{12}^{ijk}\left(\frac{\partial v_k}{\partial y} + \frac{w_k}{R}\right) + \overline{D}_{13}^{ijk}\, w_k + D_{16}^{ijk}\left(\frac{\partial u_k}{\partial y} + \frac{\partial v_k}{\partial x}\right) +$$
$$\frac{1}{2} F_{11}^{ijkl}\frac{\partial w_k}{\partial x}\left(\frac{\partial w_l}{\partial x} + 2\frac{\partial \hat{w}_l}{\partial x}\right) + \frac{1}{2} F_{12}^{ijkl}\frac{\partial w_k}{\partial y}\left(\frac{\partial w_l}{\partial y} + 2\frac{\partial \hat{w}_l}{\partial y}\right) +$$
$$F_{16}^{ijkl}\left[\frac{\partial w_k}{\partial x}\left(\frac{1}{2}\frac{\partial w_l}{\partial y} + \frac{\partial \hat{w}_l}{\partial y}\right) + \frac{\partial w_k}{\partial y}\left(\frac{1}{2}\frac{\partial w_l}{\partial x} + \frac{\partial \hat{w}_l}{\partial x}\right)\right]$$

$$M_y^{ij} = D_{12}^{ijk}\frac{\partial u_k}{\partial x} + D_{22}^{ijk}\left(\frac{\partial v_k}{\partial y} + \frac{w_k}{R}\right) + \overline{D}_{23}^{ijk}\, w_k + D_{26}^{ijk}\left(\frac{\partial u_k}{\partial y} + \frac{\partial v_k}{\partial x}\right) +$$
$$\frac{1}{2} F_{12}^{ijkl}\frac{\partial w_k}{\partial x}\left(\frac{\partial w_l}{\partial x} + 2\frac{\partial \hat{w}_l}{\partial x}\right) + \frac{1}{2} F_{22}^{ijkl}\frac{\partial w_k}{\partial y}\left(\frac{\partial w_l}{\partial y} + 2\frac{\partial \hat{w}_l}{\partial y}\right) +$$
$$F_{26}^{ijkl}\left[\frac{\partial w_k}{\partial x}\left(\frac{1}{2}\frac{\partial w_l}{\partial y} + \frac{\partial \hat{w}_l}{\partial y}\right) + \frac{\partial w_k}{\partial y}\left(\frac{1}{2}\frac{\partial w_l}{\partial x} + \frac{\partial \hat{w}_l}{\partial x}\right)\right]$$

$$M_{xy}^{ij} = D_{16}^{ijk}\frac{\partial u_k}{\partial x} + D_{26}^{ijk}\left(\frac{\partial v_k}{\partial y} + \frac{w_k}{R}\right) + \overline{D}_{36}^{ijk}\, w_k + D_{66}^{ijk}\left(\frac{\partial u_k}{\partial y} + \frac{\partial v_k}{\partial x}\right) +$$
$$\frac{1}{2} F_{16}^{ijkl}\frac{\partial w_k}{\partial x}\left(\frac{\partial w_l}{\partial x} + 2\frac{\partial \hat{w}_l}{\partial x}\right) + \frac{1}{2} F_{26}^{ijkl}\frac{\partial w_k}{\partial y}\left(\frac{\partial w_l}{\partial y} + 2\frac{\partial \hat{w}_l}{\partial y}\right) +$$
$$F_{66}^{ijkl}\left[\frac{\partial w_k}{\partial x}\left(\frac{1}{2}\frac{\partial w_l}{\partial y} + \frac{\partial \hat{w}_l}{\partial y}\right) + \frac{\partial w_k}{\partial y}\left(\frac{1}{2}\frac{\partial w_l}{\partial x} + \frac{\partial \hat{w}_l}{\partial x}\right)\right]$$

The terms with a hat on them represent the additional terms due to initial imperfections. The imperfections have no influence on the remaining terms defined in section 2.1.7. The ply stiffnesses $A_{\alpha\beta}^{ij}$, $D_{\alpha\beta}^{ijk}$ etc., are as defined in equation (2.13) of Chapter 2.

4.2.4 Finite Element Model

As in the case of perfect cylindrical shells, the finite element model is developed by expanding the interface displacements (u_i, v_i, w_i, $\hat{w}_i$) over each element as a linear combination of the two dimensional Lagrange interpolation function φ^j and the nodal values u_i^j, v_i^j, w_i^j and $\hat{w}_i^j$ as follows:

$$(u_i, v_i, w_i, \hat{w}_i) = \sum_{j=1}^{p} (u_i^j, v_i^j, w_i^j, \hat{w}_i^j)\, \varphi^j \tag{4.5}$$

where p is the number of nodes in each element. Substitution of equation (4.5) into the weak form of the virtual work statement defined by equation (4.3) gives the finite element model of a typical element as:

$$\begin{bmatrix} {}_{11}K_{ij}^{\alpha\beta} & {}_{12}K_{ij}^{\alpha\beta} & {}_{13}K_{ij}^{\alpha\beta} & {}_{14}K_{ij}^{\alpha\beta} \\ {}_{21}K_{ij}^{\alpha\beta} & {}_{22}K_{ij}^{\alpha\beta} & {}_{23}K_{ij}^{\alpha\beta} & {}_{24}K_{ij}^{\alpha\beta} \\ {}_{31}K_{ij}^{\alpha\beta} & {}_{32}K_{ij}^{\alpha\beta} & {}_{33}K_{ij}^{\alpha\beta} & {}_{34}K_{ij}^{\alpha\beta} \\ {}_{41}K_{ij}^{\alpha\beta} & {}_{42}K_{ij}^{\alpha\beta} & {}_{43}K_{ij}^{\alpha\beta} & {}_{44}K_{ij}^{\alpha\beta} \end{bmatrix} \begin{Bmatrix} \{u\} \\ \{v\} \\ \{w\} \\ \{\hat{w}\} \end{Bmatrix} = \begin{Bmatrix} \{q_u\} \\ \{q_v\} \\ \{q_w\} \\ \{q_{\hat{w}}\} \end{Bmatrix} \tag{4.6}$$

Here i, j = 1, 2, ..., p and α, β = 1, 2, ..., N+1.

The additional components of the stiffness matrix for shells containing initial imperfections are given in Appendix E. Note that the presence of imperfections introduces the additional terms corresponding to the 4-th row and column. All the other components are the same as the ones given in Appendix B.

4.2.5 Solution of Finite Element Equations

Since the initial imperfection at each node and interface is known or prescribed, it is entered as a boundary condition. Hence, the displacement components to be evaluated are only u_i^j, v_i^j, and w_i^j. Having prescribed the initial imperfections, the element stiffness matrix as given in equation (4.6) can be re-written as:

$$\begin{aligned}
&\left[{}^{11}K^{\alpha\beta}\right]\{u\}+\left[{}^{12}K^{\alpha\beta}\right]\{v\}+\left[{}^{13}K^{\alpha\beta}\right]\{w\}=\{q_u\}-\left[{}^{14}K^{\alpha\beta}\right]\{\hat{w}\}\\
&\left[{}^{21}K^{\alpha\beta}\right]\{u\}+\left[{}^{22}K^{\alpha\beta}\right]\{v\}+\left[{}^{23}K^{\alpha\beta}\right]\{w\}=\{q_v\}-\left[{}^{24}K^{\alpha\beta}\right]\{\hat{w}\}\\
&\left[{}^{31}K^{\alpha\beta}\right]\{u\}+\left[{}^{32}K^{\alpha\beta}\right]\{v\}+\left[{}^{33}K^{\alpha\beta}\right]\{w\}=\{q_w\}-\left[{}^{34}K^{\alpha\beta}\right]\{\hat{w}\}
\end{aligned} \tag{4.7}$$

Since the tangent stiffness matrices are nonlinear, any of the standard iterative numerical algorithms for the solution of nonlinear systems of equations may be used. In this study, the Newton-Raphson method is used for nonlinear analysis and the Riks-Wempner method for post-buckling analysis. These are discussed in the next chapter.

CHAPTER 5

SOLUTION PROCEDURES

5.1 INTRODUCTION

The solution of the equations of motion for the layerwise theory for both cylindrical shell and stiffener elements poses a computational challenge. For stiffened cylindrical shells with simply supported and clamped boundary conditions, the traditional energy methods like the Rayleigh-Ritz method offer an economical computational tool. For cross-ply laminates, the coupling terms like A_{i6}, B_{i6}, F_{i6}, A_{45}, and A_{54} terms are zero, which naturally reduces the computational effort.

However, for more general lay-ups and boundary conditions, the finite element method is a natural choice. The finite element model has the clear advantage of generality in terms of ply material properties, lay-up scheme, boundary conditions and loading. The finite element equations developed here are nonlinear and any of the standard iterative schemes may be used for solving them. In the finite element analysis of nonlinear problems, two iterative schemes are often used. They are the Picard method, sometimes known as the Direct Iteration method, and the Newton-Raphson method. For nonlinear problems which have a limit point, both methods fail at the limit point and resort should be made to a specialized numerical technique. The modified Riks-Wempner method, one such efficient technique, is used in this study. In the following sections, the solution techniques used in this study are discussed. A discussion of the solution techniques for eigenvalue problems is also included.

5.2 Newton-Raphson Method

The nonlinear set of finite element equations to be solved has the form:

$$[K(u)]\{u\} = \{f\} \tag{5.1.a}$$

or

$$R(u) = 0 \tag{5.1.b}$$

where [K] is the tangent stiffness matrix, {u} is the displacement vector, {F} is the force vector and{R} is the out-of-balance load vector, also called the residual vector. The scheme is used for the solution at the r-th iteration, when the solution at the (r-1)-st iteration is known.

The Taylor series expansion of the residual vector R(u) about the known solution u^{r-1} takes the form:

$$R(u) = R(u^{r-1}) + \left(\frac{\partial R}{\partial u}\right)_{u^{r-1}} . \delta u + \frac{1}{2}\left(\frac{\partial^2 R}{\partial u^2}\right)_{u^{r-1}} . (\delta u)^2 + \ldots\ldots = 0 \tag{5.2}$$

where the increment δu is given as:

$$\delta u = u^r - u^{r-1} \tag{5.3}$$

The higher order derivatives in δu are neglected due to their small magnitude. As a result, equation (5.2) simplifies into:

$$\delta u = - [K_T (u^{r-1})]^{-1} . R (u^{r-1}) \quad (5.4.a)$$

$$\delta u = - [K_T (u^{r-1})]^{-1} [F - K(u^{r-1}) . u^{r-1}] \quad (5.4.b)$$

where the tangent stiffness matrix $[K_T]$ is given as:

$$K_T = \left(\frac{\partial R}{\partial u}\right)_{u^{r-1}} \quad (5.5)$$

The total solution at the end of the r-th iteration is updated as

$$u^r = u^{r-1} + \delta u \quad (5.6)$$

The iteration is repeated until a specified convergence criterion is satisfied. In this study the modified Newton-Raphson scheme is used, where the tangent stiffness matrix is updated only at the beginning of the current load step. This saves some of the computational time, even though it may result in additional iterations for convergence. The convergence criterion used here is that of the normalized incremental displacement approaching or being less than a specified limit ε:

$$\sqrt{\frac{\sum_{i=1}^{N} (u_i^r - u_i^{r-1})^2}{\sum_{i=1}^{N} (u_i^r)^2}} < \varepsilon \quad (5.7)$$

Figure 7 shows a schematic representation of the modified Newton-Raphson Method.

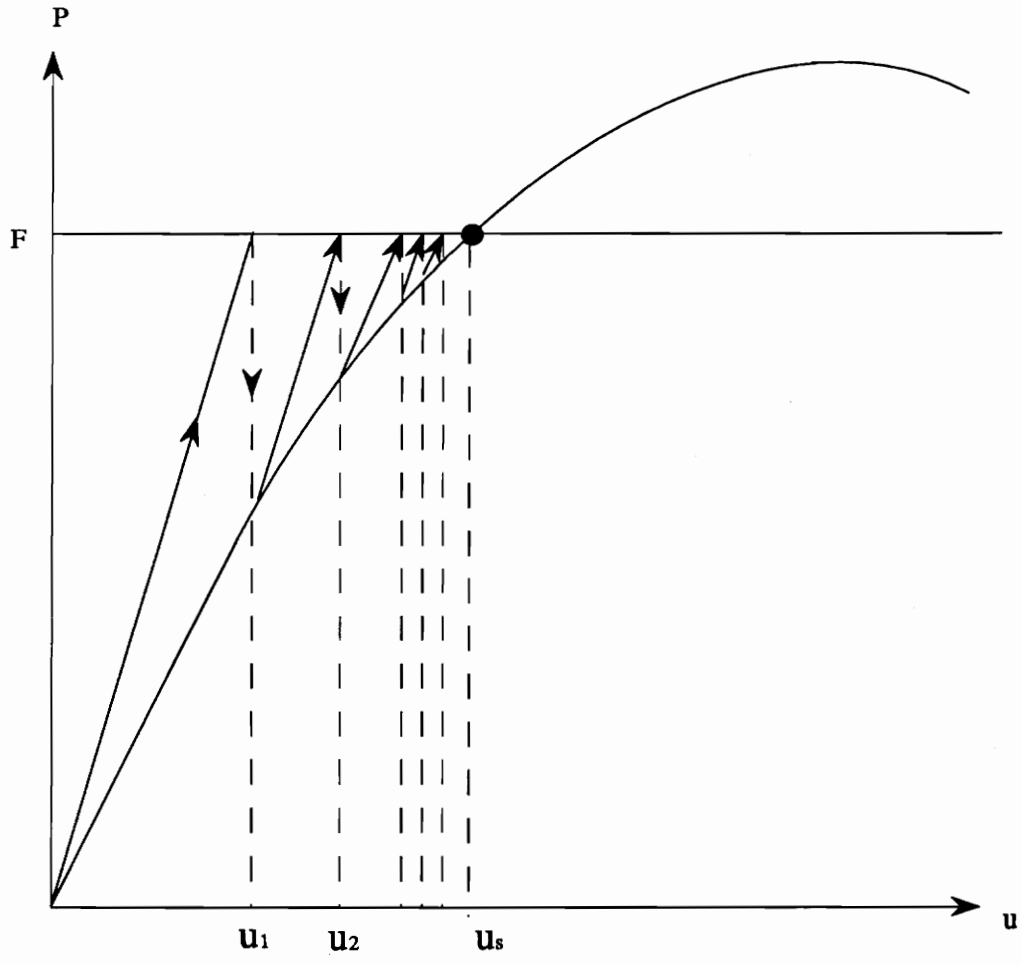

Figure 7. Modified Newton-Raphson Iteration Scheme.

5.3 Modified Riks-Wempner Method

In shell structures under transverse or inplane loading, a phenomenon of snapping may occur depending on the lamination scheme, boundary condition and geometry. Snapping is characterized by what are called limit points where the tangent stiffness matrix becomes singular. The Newton-Raphson method fails in navigating through the limit points and the procedure diverges.

The modified Riks-Wempner method introduces an additional unknown, i.e., the load increment, which is solved as part of the solution. The equilibrium equation to be solved is of the form:

$$[K]\{u\} - \lambda\{F\} = R(\{u\}, \lambda) = 0 \qquad (5.8)$$

where λ is the load factor.

The N number of equilibrium equations in equation (5.8) involve N+1 unknowns $\{u\}$ and λ. The Modified Riks technique adds a "constant arc length" as a constraint equation to the usual N equilibrium equations. The "arc length" ΔL is fixed to a prescribed value. Then the iteration path follows a circular plane with center O and radius ΔL, as shown in Figure 8. Here S1 denotes the locus of the initial solution; then the solution moves to S2 in the next iteration. Convergence is achieved at point S.

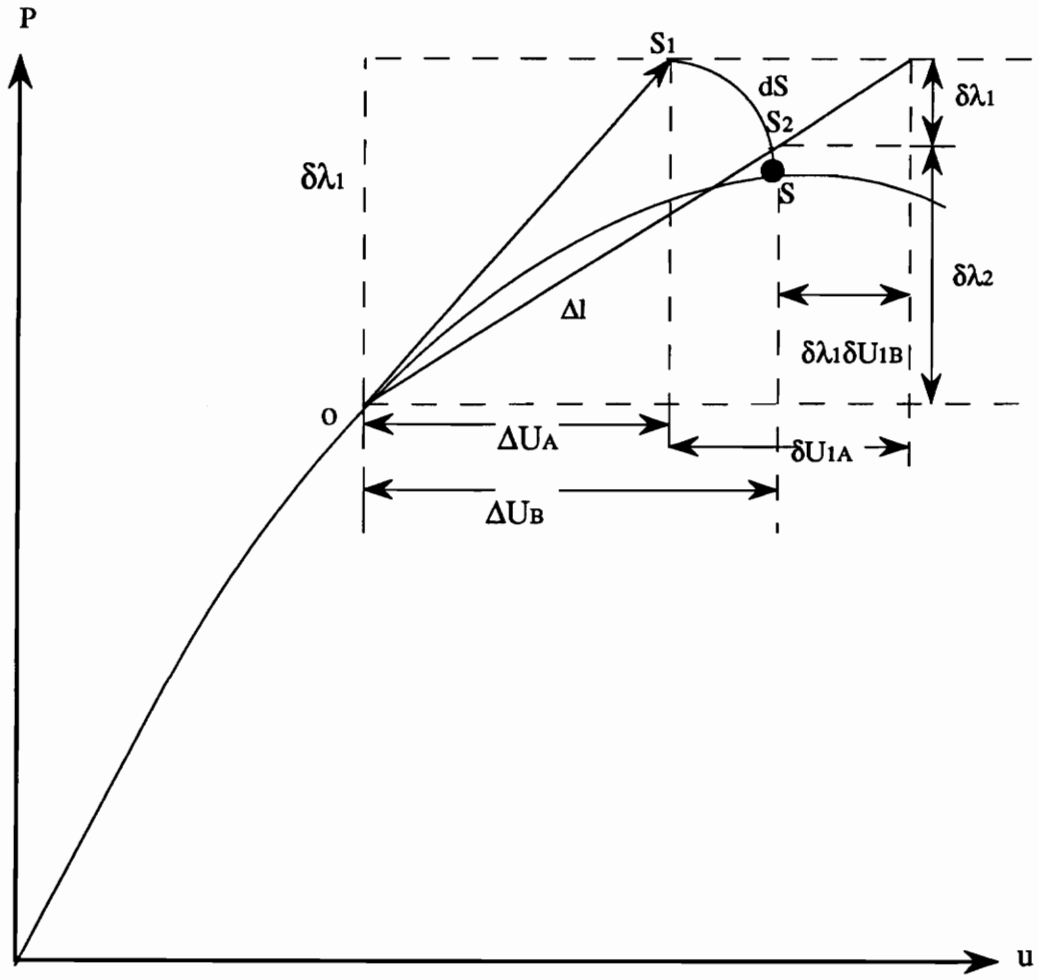

Figure 8. Modified Riks-Wempner Scheme.

A detailed discussion of the method may be found in References [73, 75]. Here only the salient features of the method will be discussed. The equilibrium equation to be solved as given by equation (5.8) may be re-written as:

$$\delta u_i = \delta u_{iA} + \delta\lambda i \, \delta u_{iB} \tag{5.9}$$

where

$$\delta u_{iA} = -[K_T]^{-1} R(u_i, \lambda i) \tag{5.10}$$

$$\delta u_{iB} = [K_T]^{-1} F \tag{5.11}$$

The increments in displacement ΔU_{i+1} and load parameter $\Delta\lambda_{i+1}$ are updated during each iteration as:

$$\Delta U_{i+1} = \Delta U_i + \delta u_i \tag{5.12}$$

$$\Delta\lambda_{i+1} = \Delta\lambda_i + \delta\lambda_i \tag{5.13}$$

Various investigations [73] have shown that fixing the "incremental length" ΔL as shown below by the following constraint equation ensures a better convergence rate:

$$\Delta L^2 = \Delta U_i^T \Delta U_i \tag{5.14}$$

A quadratic equation in $\delta\lambda_i$ given below is obtained by substituting equation (5.12) into equation (5.14):

$$a\delta\lambda_i^2 + 2b\delta\lambda_i + c = 0 \tag{5.15}$$

where

$$a = \delta u_{iB}^T \delta u_{iB} \tag{5.16a}$$

$$b = (\Delta U_i + \delta U_{iA})^T \delta u_{iB} \tag{5.16b}$$

$$c = (\Delta Ui + \delta u_{iA})^T (\Delta Ui + \delta u_{iA}) - \Delta L^2 \tag{5.16c}$$

At the end of the iterative procedure for a given load step r, the total load parameter λr and the total displacement vector U_r are given as:

$$U_r = U_{r-1} + \Delta U_r \tag{5.17a}$$

$$\lambda_r = \lambda_{r-1} + \Delta\lambda_r \tag{5.17b}$$

5.4 Eigenvalue Analysis

Linearized buckling and natural vibration problems require the solution of an eigenvalue problem. Though a number of direct and iterative schemes are available for extracting the eigenvalues and eigenvectors, the IMSL subroutine DVGLRG has been used in this study. This subroutine is suitable for large real and positive definite matrices.

5.5 Observations on the Solution Techniques

The modified Newton-Raphson and Modified Riks-Wempner methods have been incorporated into the finite element computer program developed in this study. The program named COSHELL has the option for both the full Newton-Raphson scheme, where the tangent stiffness matrix is updated at each iteration, and the modified Newton-Raphson scheme, where the tangent stiffness matrix is updated only at the beginning of each load step. For all the problems reported here, unless otherwise stated, the modified Newton-Raphson scheme has been used, resulting in a reduced computational expense. The use of the full Newton-Raphson scheme becomes necessary when the response of the shell under consideration exhibits multiple or steep snap-back phenomena.

CHAPTER 6

SAMPLE ANALYSES and NUMERICAL RESULTS

6.1 Introduction

The layerwise cylindrical shell and stiffener finite elements developed in this study are investigated for accuracy and efficiency using a wide variety of sample problems. Most of the problems solved here are taken from the literature. The layerwise cylindrical shell element, along with the plate/shell stiffener element, is used to analyze stiffened shells, plates and cylindrical panels. In the limiting case, the shell element is reduced to a plate element by setting the radius to infinity (i.e., a large value in the program). A number of stiffened and unstiffened laminated and single-layer plates and shells are analyzed and documented in this study. Stress, vibration, linearized buckling, post-buckling and imperfection sensitivity analyses are carried out for a variety of shell structures. The results reported here are grouped in four parts. In section 6.2, results for unstiffened plate and shell structures are presented. The main focus of this section is testing the accuracy and efficiency of the layerwise shell element through bench-mark test problems taken from the literature. The superiority of the layerwise theory in accurately determining the displacement field and state of stress through the thickness is emphasized. Global responses like buckling and nonlinear load-deflection are also reported. The analysis of stiffened plates and shells is presented in section 6.3. In this section, emphasis is placed on the effect of stiffeners on the local responses, i.e., stress and strain distributions. In section 6.4, global responses like post-buckling and imperfection sensitivity are reported, whereas section 6.5 deals with stand-alone laminated beams modeled by the stiffener element developed in Chapter 3.

6.2 Plate and Shell Structures

6.2.1 Natural Vibration of (0/90/0) Simply Supported Plate

The geometrical details of this problem are given in Figure 9. The material properties are:

$E_{22} = E_{33} = 1.0 \times 10^6$ psi

$E_{11}/E_{22} = 3, 10, 20, 30$

$G_{12} = G_{13} = 0.6 \times 10^6$ psi, $G_{23} = 0.5 \times 10^6$ psi

$\nu_{12} = \nu_{13} = 0.25$, $\nu_{23} = 0.24$

$a/h = 10$

The non-dimensionalized fundamental frequency is given as:

$$\bar{\omega} = \omega h \sqrt{\frac{\rho}{E_{22}}}$$

The results are summarized in Table 1. Convergence was achieved for a 2x2 mesh of nine-noded quadratic elements. Through the thickness, two linear elements are used for each layer. The results obtained demonstrate the influence of the degree of orthotropy and number of layers on the accuracy of the element. A comparison of the results with the Classical Plate Theory (CPT) and the Generalized Lamination Plate Theory (GLPT) is also included. GLPT, though identical in formulation with the Layerwise Shell Theory (LWST), does not consider the variation of the transverse displacement, w, through the thickness; hence a slight difference exists between the results obtained from the two models. The results reported by Noor [78] were obtained from a 3-D orthotropic elasticity theory.

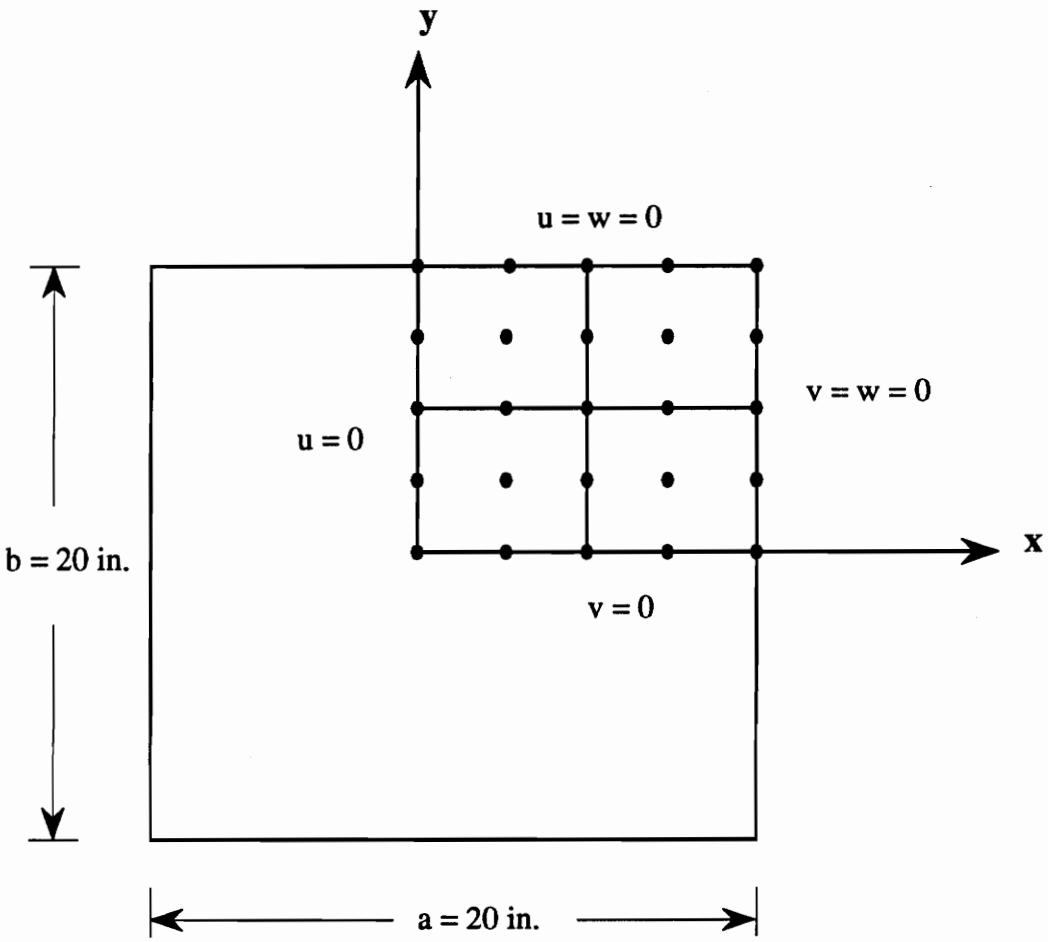

Figure 9. Geometry and finite element mesh of a simply supported plate.

Table 1. Natural vibration of (0/90/0) cross-ply simply supported plates.

No. of Layers	Method	E_{11}/E_{22}			
		3	10	20	30
3	LWST	0.2671	0.3380	0.3897	0.4197
	GLPT [77]	0.2645	0.3368	0.3897	0.4205
	Noor [78]	0.2647	0.3284	0.3824	0.4109
	CPT	0.2919	0.4126	0.5404	0.6433
5	LWST	0.2671	0.3429	0.4012	0.4354
	GLPT [77]	0.2645	0.3415	0.4012	0.4367
	Noor [78]	0.2659	0.3409	0.3997	0.4314
	CPT	0.2919	0.4126	0.5404	0.6433

6.2.2 Cylindrical Bending of (0/90/0) Plate Under Sinusoidal Load

A cross-ply plate (0/90/0) with a/h = 4 is subjected to a sinusoidal load of intensity q_o. The plate is simply supported along the long edges and undergoes a cylindrical bending where every line along the length deforms into the same shape. The distribution of longitudinal normal stress and the u-displacement through the thickness are given in Figures 10 and 11. A mesh of 4x1 nine-node quadrilateral elements is used with a uniform reduced integration. Two linear elements are used through the thickness. The exact solution to this problem is given by Pagano [76], who used a three-dimensional elasticity theory. The u-displacement and the longitudinal stress σ_{xx} are normalized as:

$$\bar{u} = \frac{100\, E_2\, h^2}{q_o\, a^3}\, u$$

$$\bar{\sigma}_{xx} = \frac{\sigma_{xx}}{q_o}$$

Figures 10 and 11 show good agreement between the present model and the three-dimensional elasticity solution. The classical plate theory fails to accurately determine the stress and displacement variation through the thickness, both qualitatively and quantitatively. Note that both the three-dimensional elasticity theory and LWST assume that the load is applied at the top surface of the top ply. This gives rise to an unsymmetrical stress distribution through the thickness, as expected. In the conventional plate theories, however, the load can be applied at the mid-plane only, thereby resulting in equal but opposite stresses at the top and bottom of the plate.

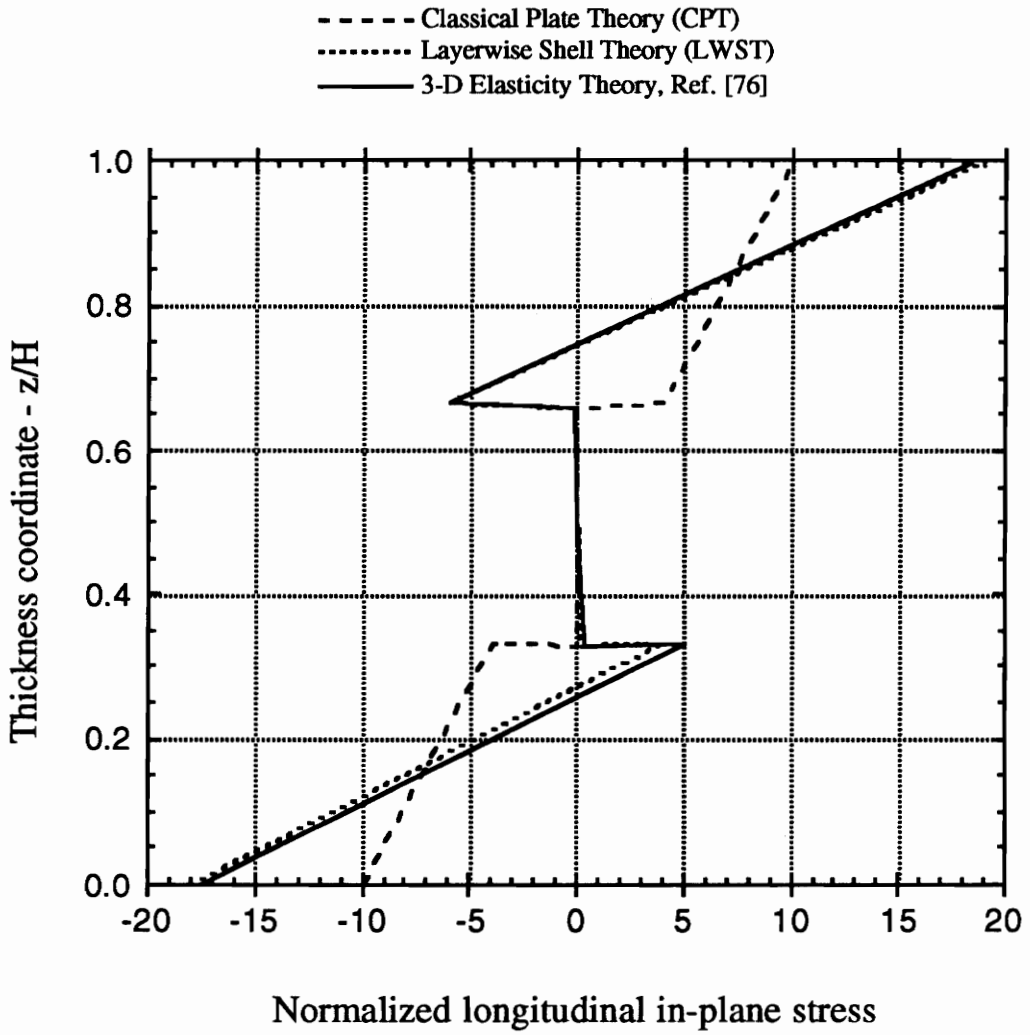

Figure 10. Longitudinal normal stress distribution through the thickness of (0/90/0) plate.

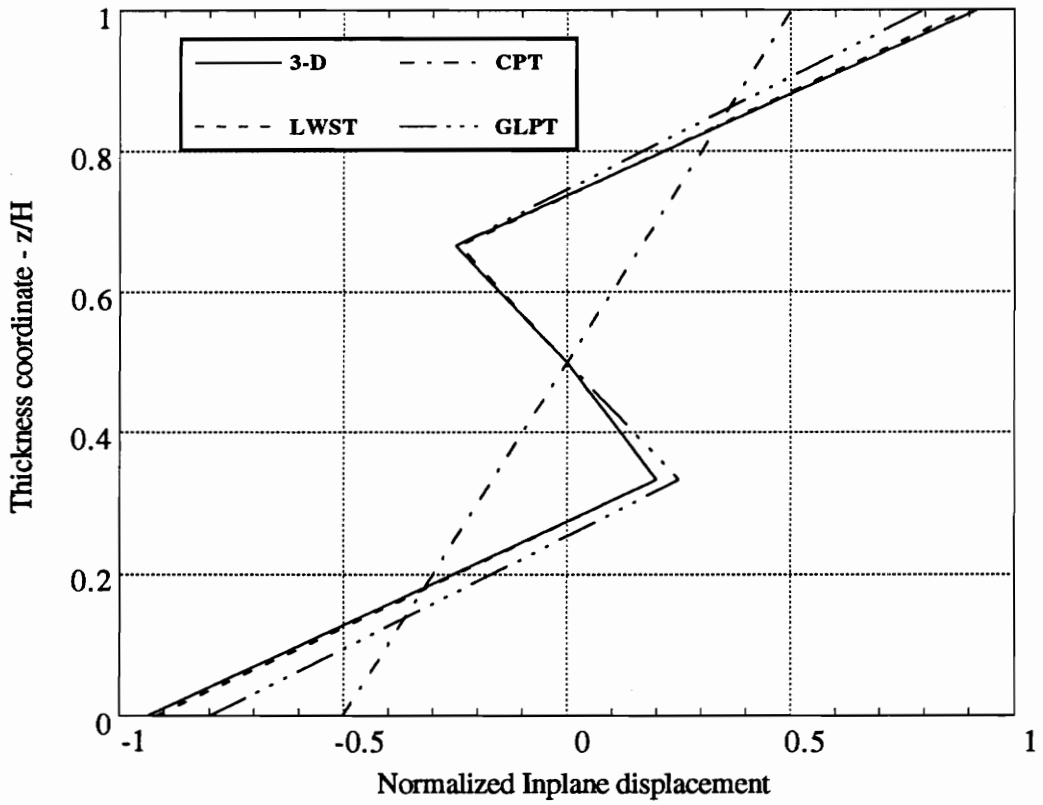

Figure 11. Through the thickness distribution of the normalized u displacement of (0/90/0) plate.

6.2.3 Buckling of Orthotropic Plates

A number of simply supported orthotropic plates subjected to axial loads in x, y or a combination of them are analyzed for critical buckling loads.

Material Properties:

$E_{xx} = 3.29 \times 10^7$ psi $E_{yy} = E_{zz} = 0.18 \times 10^7$ psi

$G_{yz} = 0.50 \times 10^6$ psi $G_{xy} = G_{xz} = 0.88 \times 10^6$ psi

$\nu_{xy} = \nu_{xz} = 0.25$ $\nu_{yz} = 0.24$

t = 0.096 inch.

The results obtained are compared with the ones from References [79] and [80]. Table 2 summarizes the results obtained. A convergence study was carried out first. Surface-wise, a mesh of 4x4 nine-noded quadrilateral elements gave convergent results, whereas through the thickness, two linear elements were required. Note that a full model is used. As shown in Table 2, the layerwise theory gives very good results as compared to the results reported in the literature. The inclusion of transverse normal strains by the layerwise model does not seem to have a significant effect on the buckling load for this particular geometry and material property of the plate. For thin plates and shells, such as the orthotropic plates analyzed in this section, the transverse strains are very small.

6.2.4 A Clamped Cylinder Under Hydrostatic Pressure

The element developed is used here to analyze a thin cylindrical shell subjected to a hydrostatic pressure. Due to the symmetry in loading and geometry, only an octant of the shell is taken as shown in Figure 12. Convergent results were obtained for a mesh of 2x2 nine-noded quadrilateral elements on the surface and two linear elements through the thickness. The comparison is given in Table 3.

Material and Geometry Properties:

$E_{xx} = 7.5 \times 10^7$ psi, $E_{yy} = E_{zz} = 2.0 \times 10^7$ psi

$G_{xy} = G_{xz} = 1.25 \times 10^6$ psi, $G_{yz} = 1.25 \times 10^6$ psi

$\nu_{xy} = \nu_{xz} = 0.25$, $\nu_{yz} = 0.24$

$t = 1.0$ inch

$R = 20$ inch.

As indicated in the table, the layerwise shell theory accurately determines the displacements. The inclusion of transverse normal strains and a refined displacement field by the present model, as compared to Reference [81], does not have any tangible effects for this particular case, mainly due to the fact that the shell is very thin.

Table 2. Buckling loads for simply supported orthotropic plates (lb/in).

Size (in)	Nx	Ny	PANDA2[79]	Ref [80]	Present
10x10	-1	0	285.0	292.0	293.0
	-1	-1	116.0	124.0	127.0
20x20	-1	0	144.0	145.0	147.0
	-1	-1	29.0	30.0	30.5

Table 3. Maximum deflection in inches of a clamped cylinder under hydrostatic pressure.

Pressure	Ref [81]	Present Study
4 Psi	0.00072	0.000718
6 Psi	0.00083	0.000812

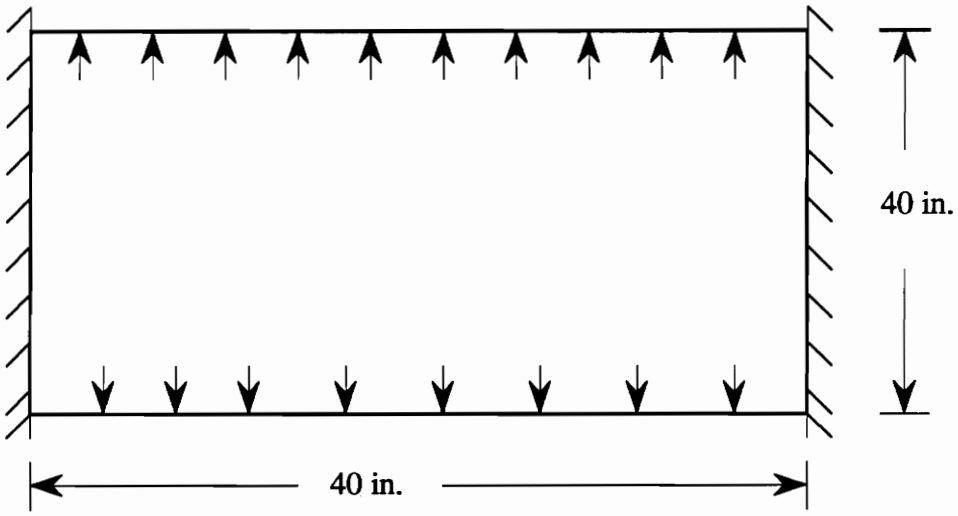

a) Geometry of a cylindrical shell

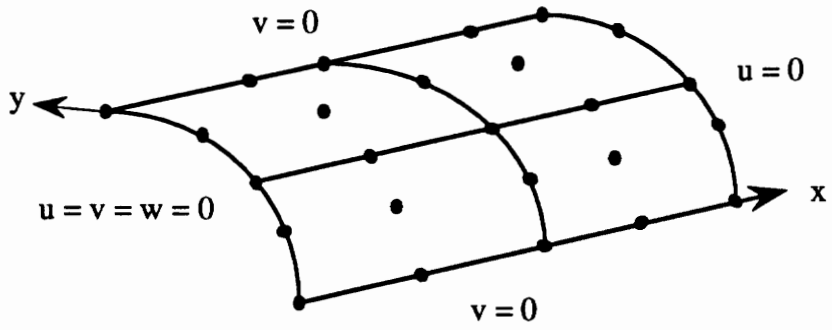

b) Representative octant

Figure 12. Clamped orthotropic cylinder under hydrostatic pressure.

6.2.5 Buckling of Simply Supported Cylindrical Panel

An isotropic cylindrical panel of the following geometry and material properties is analyzed for a critical buckling load:

Panel size: a = 12.70 cm, b = 13.36 cm, R = 50.8 cm, t = 0.2 cm.
Material properties: E =179.27 GPa, $\nu = 0.3$

A convergent result is obtained for a 2x2 mesh of nine-noded quadratic elements surface-wise and two linear elements through the thickness. The critical buckling load found using the present model is 8800.0 N/cm compared to that of 8616.0 N/cm of Reference [80].

6.2.6 Nonlinear Analysis of (0/90) Cylindrical Panel Under a Central Point Load

A laminated composite cylindrical panel is investigated for a nonlinear response under different boundary conditions. Due to the symmetry in loading and geometry, a quarter model is analyzed with a 2x2 nine-node quadratic element mesh. Through the thickness, two linear elements are used for each layer.

Panel size: a = 20.00 in., b = 20.00 in., R =100.00 in., t =1 in.

Material properties:

$E_{xx} = 4.0x10^7$ psi $E_{yy} = E_{zz} = 1.0x10^6$ psi

$G_{yz} = 0.6x10^6$ psi $G_{xy} = G_{xz} = 0.5x10^6$ psi

$\nu_{xy} = \nu_{xz} = 0.25$ $\nu_{yz} = 0.25$

The geometry and boundary conditions are shown in Figure 13, whereas Figure 14 shows the nonlinear response of the panel. The results obtained using the layerwise theory are compared with those reported in reference [82], where an equivalent single-layer shell theory based on assumptions of moderate rotations is used. At higher loads, the layerwise theory tends to give more deflections compared to those from reference [82]. This discrepancy is due to the fact that the Donnell type strain-displacement relationships, which are employed in the present study, assume small rotations and deflections.

6.2.7 Buckling of a Cylindrical Shell under Axial Load.

A cylinder subjected to axial load is investigated for critical buckling load using the layerwise theory. Due to the axisymmetry in the fundamental buckling mode, only a strip of the shell is analyzed using 1x4 mesh of nine node quadratic elements and two linear elements through the thickness as shown in Fig 15. The present model gives a critical load of 6060 lb/in as compared to 6135.1 lb/in reported in Ref [83]. The result is in good agreement with the classical solution of 6050 lb/in obtained from the following formula.

$N_{cr} = 0.605\ Et^2/R$

Note that the critical load does not depend on the length of the cylindrical shell.

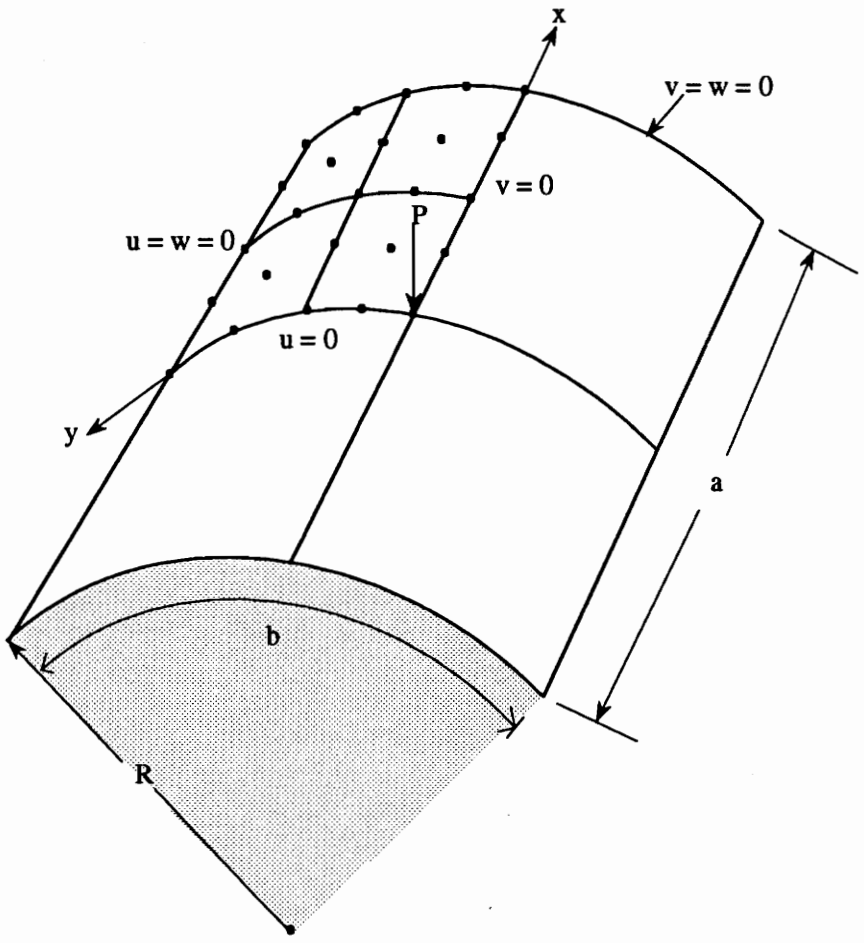

Figure 13. Simply supported (0/90) cylindrical panel.

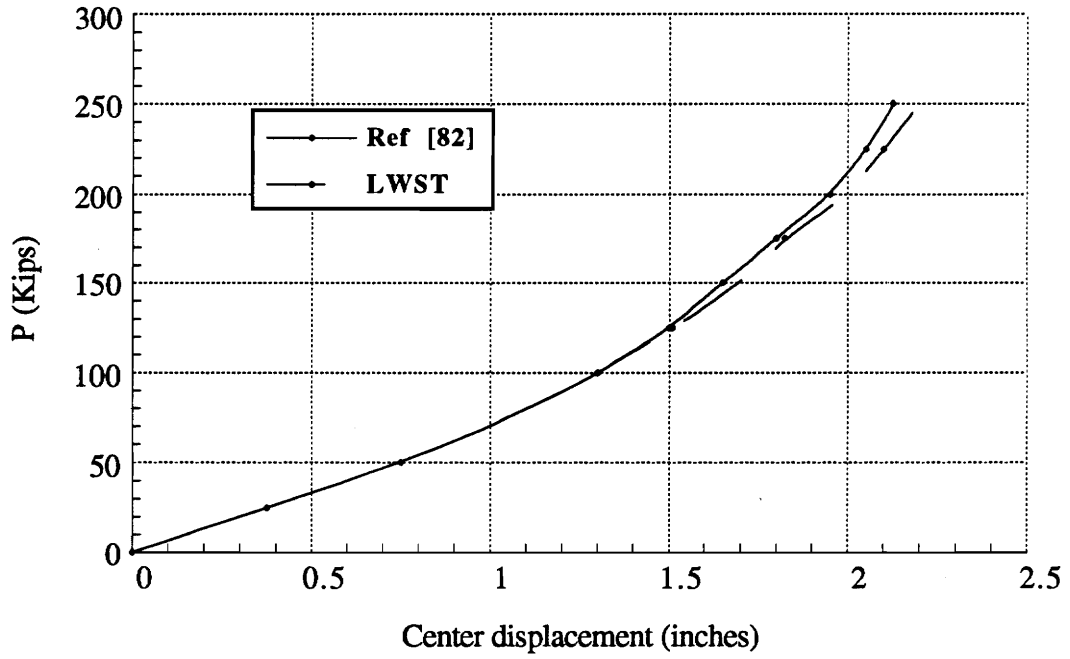

Figure 14. Nonlinear response of a simply supported (0/90) cylindrical panel.

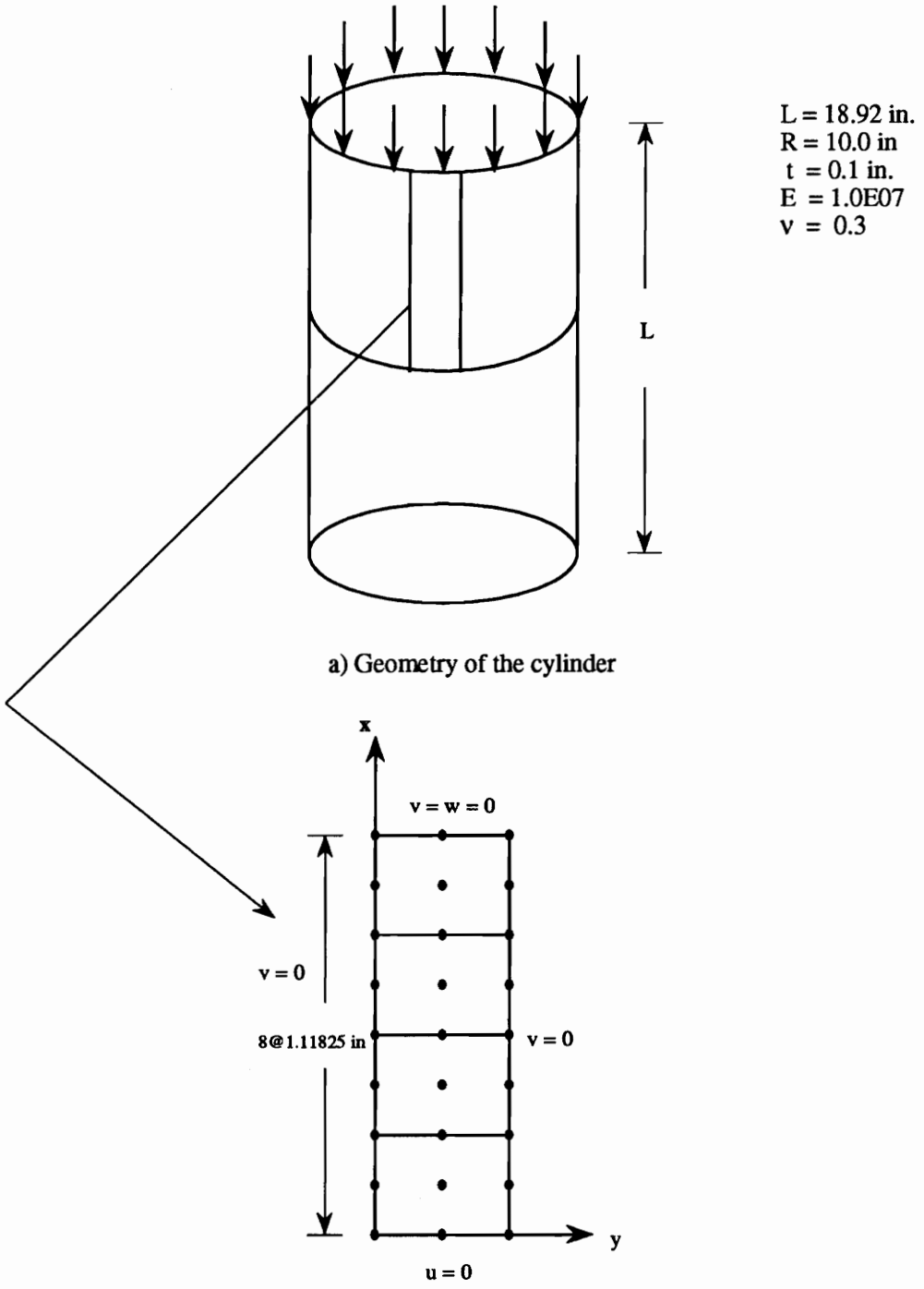

Fig 15. Cylindrical shell under axial load.

6.3 Stiffened Plate and Shell Structures

In this section, a number of plates and laminated cylindrical shells stiffened by stringers or rings or a combination of them are analyzed for buckling and stresses. The stiffeners may be located on the inside or outside of the shell skin. The solved examples illustrate that there is a marked difference between the behavior of internally and externally stiffened shells. The comparison is given wherever appropriate. The stiffeners are modeled as discrete unless otherwise specified. For shells with a large number of stiffeners, the smeared approach as outlined in chapter 3 is employed.

6.3.1 Buckling of Stiffened Orthotropic Plate

An orthotropic plate subjected to inplane axial load is shown in Figure 16. The stiffener is placed along the loading direction at the middle of the plate. Though in practice a single stiffener is not common, this example taken from the literature [84,85] demonstrates the capacity of the discrete model to capture the response quite accurately. To study the effect of the number of stiffeners on the buckling load, the same plate is investigated for the case of 3 and 7 equally spaced stiffeners placed along the loading direction.

Geometric properties:

Plate: b = 2000 mm, h = 10 mm, 'a' is varied to get different aspect ratios.
Stiffener: w_s = 10 mm, t_s = 50 mm,

Material properties:

E_{xx} = 100 GPa, $E_{yy} = E_{zz}$ =10 GPa

$G_{yz} = G_{xy} = G_{xz}$ = 15.0 GPa

ν_{xy} = 0.3

Both "smeared" stiffness and discrete approaches are used to model the stiffener. For the unstiffened plate, convergence is achieved for a mesh of 2x2 nine-noded quadratic elements surface-wise and one linear element through the thickness. The same mesh gives convergence for the stiffened plate modeled by the "smeared" stiffness approach. However, for the discrete model, a non-uniform mesh of 4x2 nine-noded quadratic elements is required for convergence. Through the thickness, three linear elements are required at locations where the stiffeners are attached to the plate. All other points in the plate are modeled by only one linear element, as shown in Figure 17. The buckling loads obtained for different aspect ratios and combinations of loads are given in Table 4. Except for low aspect ratios, there is a good agreement between the results. The references mentioned here, i.e. References [84] and [85], use the discrete approach. For an aspect ratio of 1, the "smeared" approach gives results as good as those from the discrete approach. However, at low aspect ratios, the "smeared" approach gives significantly lower values. The "smeared" approach averages out the stiffness of the stiffeners over the whole surface in both the length and width directions. Therefore for plates or shells loaded and stiffened in one direction only, the "smeared" approach gives lower critical loads because the stiffness of the stiffeners is weakened by distributing it one more direction other than the loading direction. Note that the single stiffener, with a total volume of only 2% of that of the plate, has increased the critical load by 20-30%. Multiple stiffeners increase the critical load very significantly. For example, seven stiffeners placed along the length of the plate increase the critical load almost ten fold.

Table 4. Stiffened axially loaded panel.

	Critical Load (kN/m)			
	a/b	Tripathy and Rao [84]	Ref [85]	Present
Unstiffened	0.6	-	-	108.0
	1.0	-	-	64.0
Stiffened (1 stiffener)	0.6	133.61	163.9	149.0 (discrete) 128.0 (smeared)
	1.0	75.79	78.92	76.7 (discrete) 75.8 (smeared)
(3 stiffeners)	1.0	-	-	471.0 (discrete)
(7 stiffeners)	1.0	-	-	646.0 (discrete)

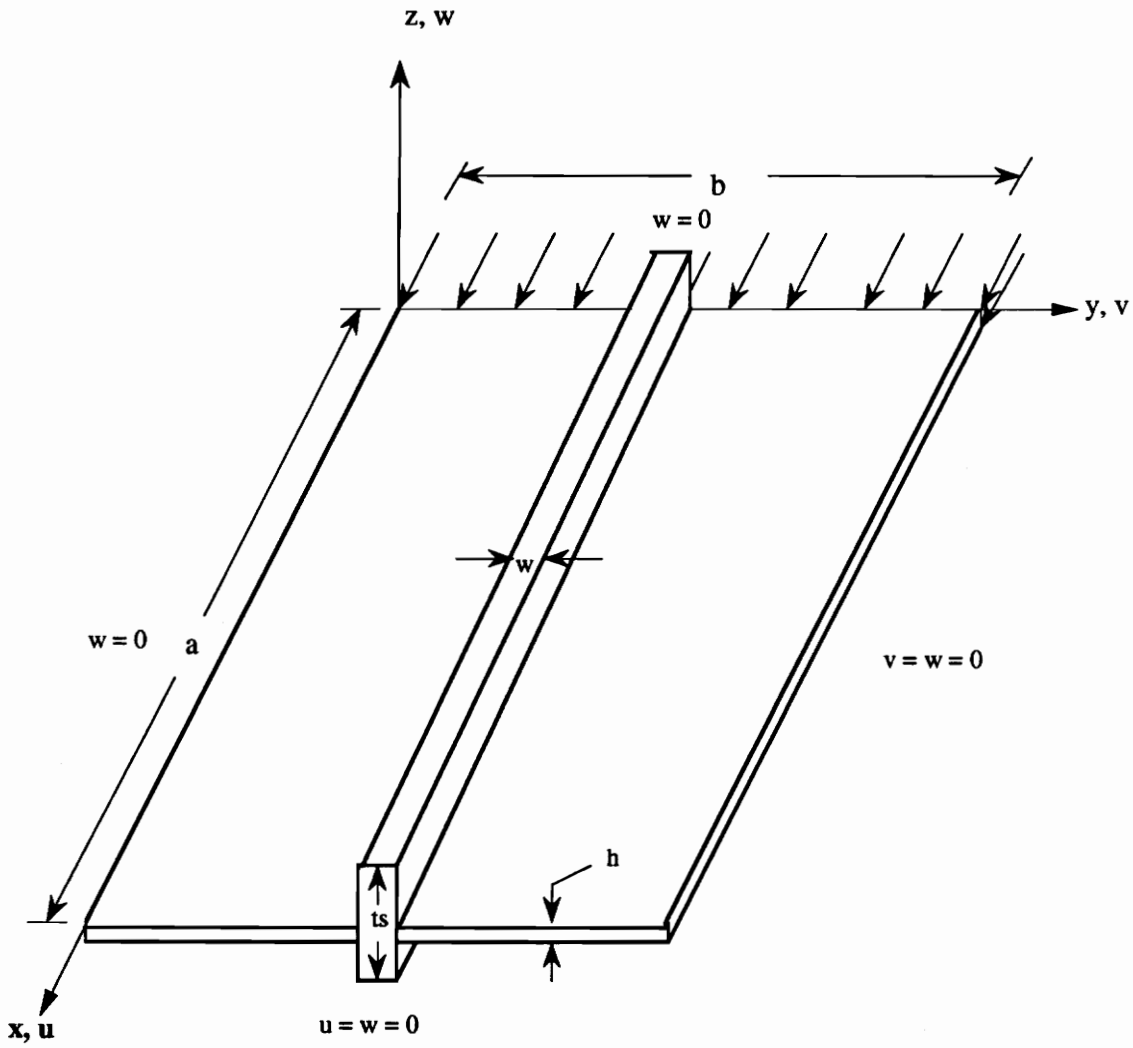

Figure 16. Geometry and loading of a stiffened orthotropic plate.

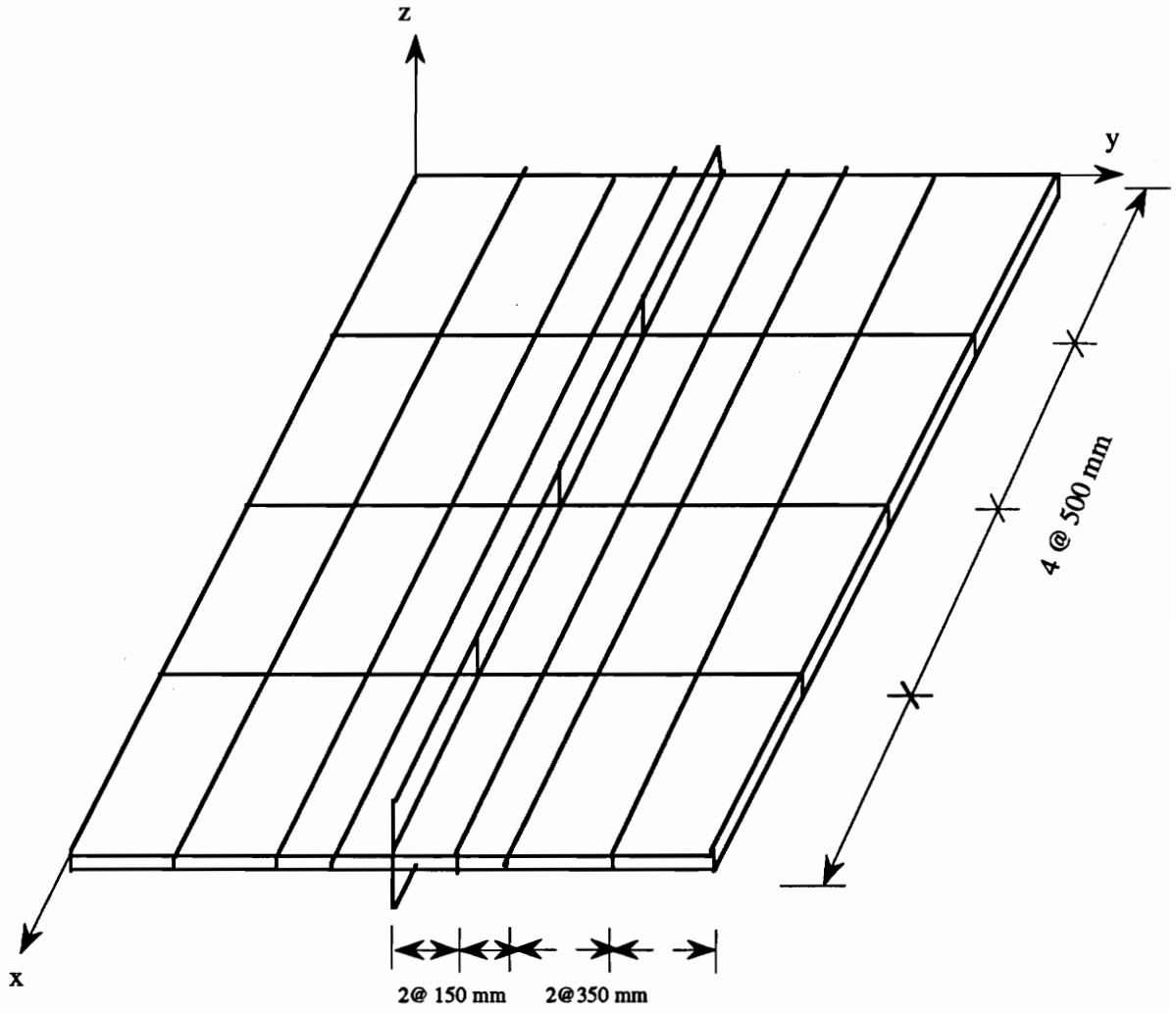

Figure 17. Finite element mesh for a stiffened orthotropic plate.

6.3.2 Stiffened Cylindrical Panel Under a Point Load

A simply supported cylindrical roof panel is stiffened with stringers and rings and subjected to a central point load of magnitude P = 150 Kips. A comparative study is made for different locations of the stringer and the rings as summarized in Table 5. Figure 18 shows the geometry and the boundary conditions of the cylindrical panel. The geometry and material properties are the same as the cylindrical panel analyzed in section 6.2.6. The stiffeners have the same material property as that of the shell skin material.

A convergence study was performed by increasing the number of two-dimensional elements surface-wise and one-dimensional elements through the thickness. Due to the steep gradient in strains and stresses at and near the interface between the shell and the stiffeners, a non-uniform mesh was used. The displacements converged for a non-uniform mesh consisting of 16 nine-noded quadratic elements and 81 nodes as shown in Figure 19. Through the thickness of the shell, only one linear element was used. Again one linear element was used through the thickness of each stiffener, primarily due to the high computational cost.

The distribution of the longitudinal normal stress σ_{xx} at the mid-point of the panel for different stiffening schemes is given in Figure 20. The stiffeners have a significant effect on the distribution of the stresses both qualitatively and quantitatively. All stiffening schemes reduce the longitudinal normal stress quite significantly. With regard to reducing stresses, rings placed externally and stringers placed internally provide the most efficient stiffening scheme. Externally placed stringers are relatively the least efficient.

The whole section at the mid-point of the cylindrical panel is under tensile stresses when only external stringers are used. Note that, even though there is continuity in displacements and strains at the point of attachment of stiffeners and the shell skin, there is a marked jump in stresses at these points. This is due to the change in cross-sectional area at these points.

With regard to the transverse displacement w, it can be observed that rings and stringers used together internally and externally consecutively or vise versa result in the minimum displacements and are therefore more efficient here. The least efficient stiffening scheme for this particular case is where rings or stringers are used alone. With regard to the u and v displacements, there is a clear indication that the neutral axis shifts significantly due to the presence of the stiffeners. In most cases, the neutral axis even moves out of the shell skin plane, resulting in the skin being totally in compression or tension.

In Figure 21, the distribution of the circumferential strain ε_{yy} along $x = a/2$ is plotted for different stiffening schemes. The strain under consideration is evaluated at interface number 3, i.e., at the top of the shell skin (Figure 18). As expected, the strain peaks at the point of load application, which is the mid-point of the cylindrical panel. The stiffeners tend to smooth out the peak. Rings, however, play the major part in reducing the circumferential strain from a peak strain of 0.146 for the unstiffened case down to 0.0081 for the case of a ring stiffened panel. In overall considerations, a combination of stringers and rings placed alternately internally or externally provides the most effective stiffening scheme.

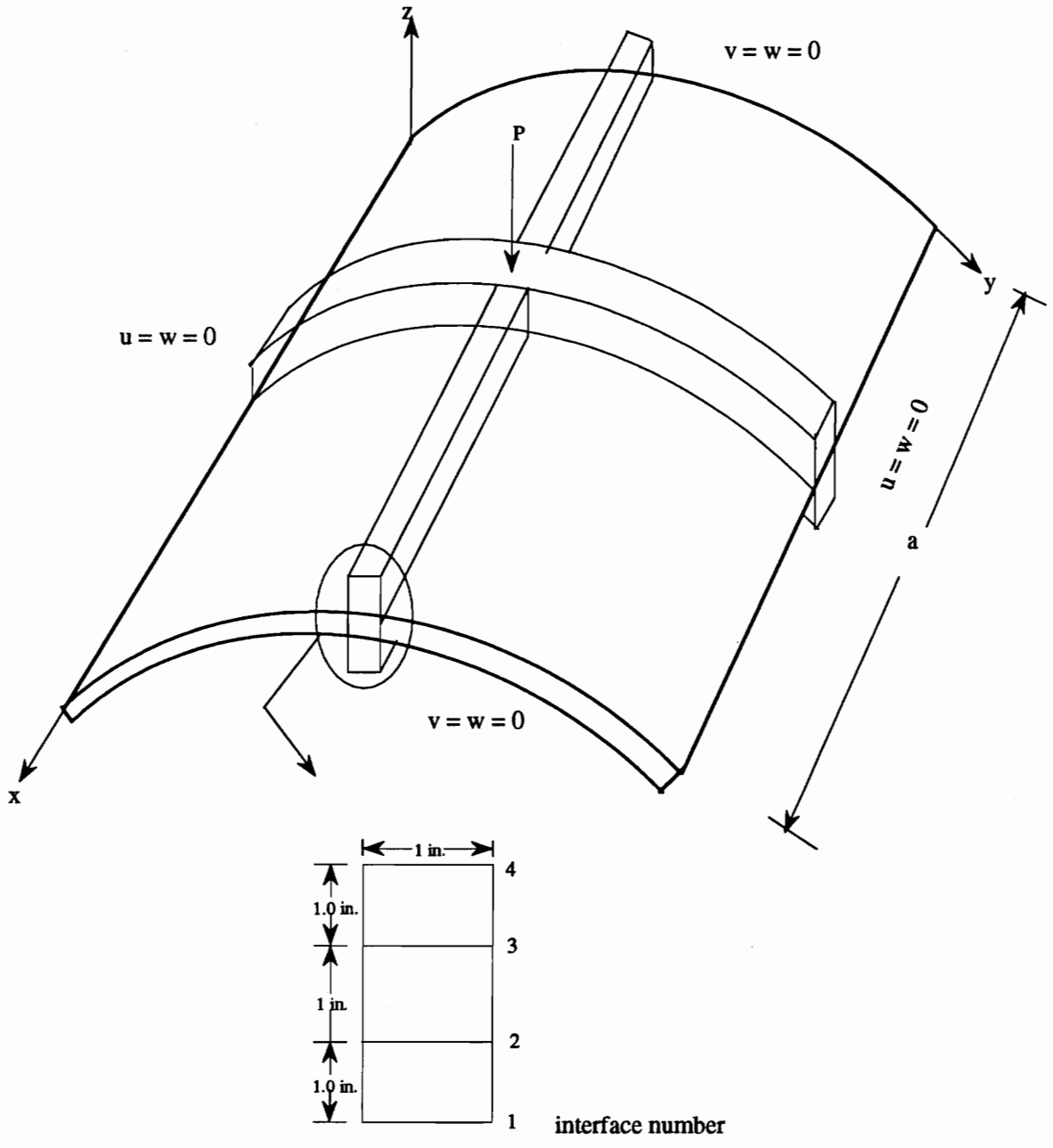

Figure 18. Stiffened orthotropic cylindrical panel.

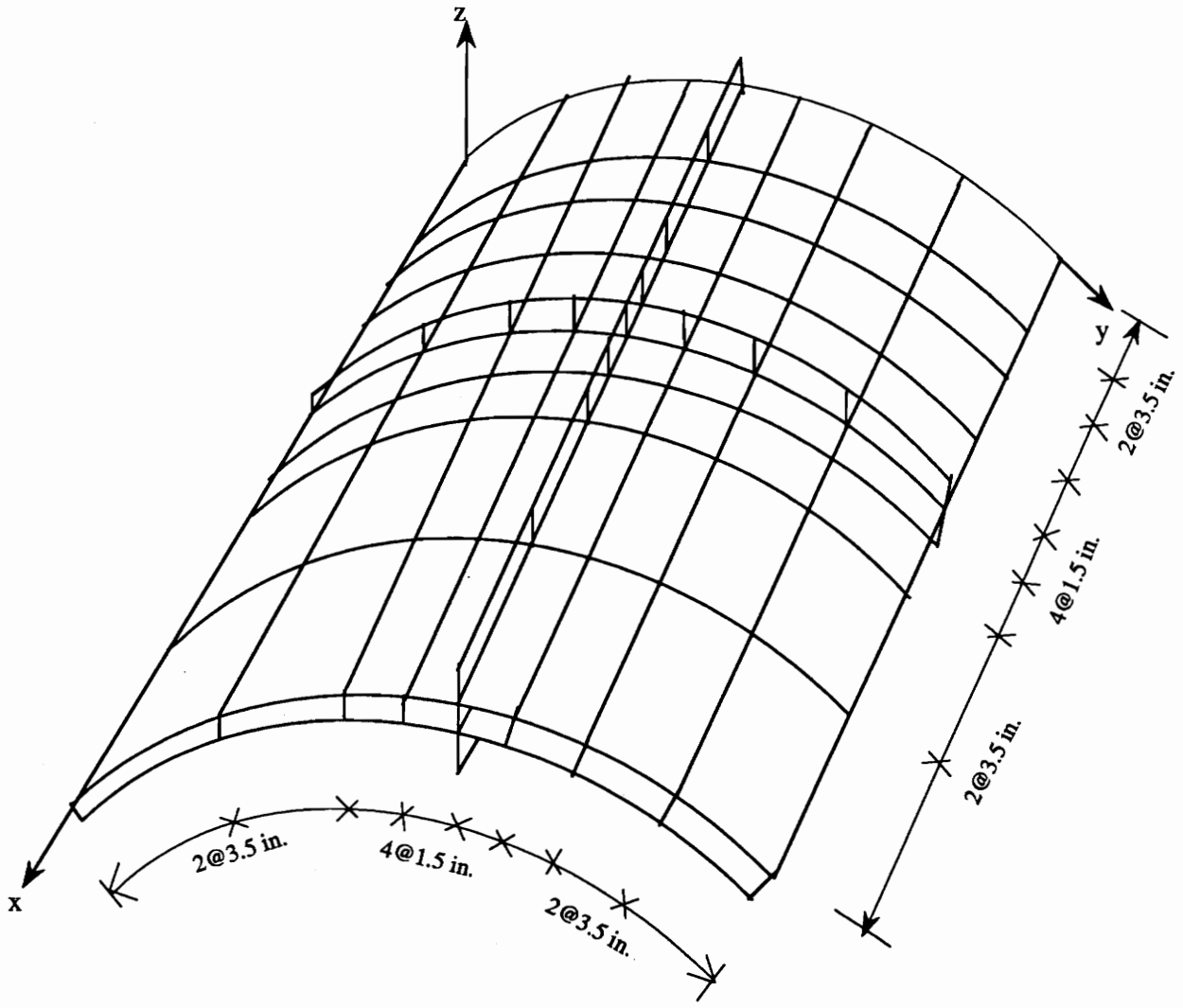

Figure 19. Finite element mesh for a stiffened cylindrical panel.

Table 5. Effect of location of stiffeners on the displacement pattern of a cylindrical panel.

___	Unstiffened	Stiffened					
Interface Disp. (inches)	___	external stringer only	internal ring only	internal ring, external stringer	external ring, internal stringer	external ring, external stringer	internal ring, internal stringer
u^1	-	-	-	-	-0.0496	-	-0.0484
u^2	-0.0619	-0.0419	-0.0468	-0.0349	-0.0030	-0.0354	-0.0031
u^3	0.0630	0.0038	0.0462	0.0028	0.0354	0.0029	0.0343
u^4	-	0.0595	-	0.04843	-	0.0497	-
v^1	-	-	-0.0669	-0.0476	-	-	-0.0469
v^2	0.0163	0.0085	0.0101	0.0069	0.0084	0.0083	0.0074
v^3	0.0355	0.0278	-0.0356	-0.0244	-0.0418	-0.0425	-0.0262
v^4	-	-		-	0.0002	0.0001	-
w^1	-	-	-0.7969	-0.5711	-0.5895	-	-0.5942
w^2	-1.4200	-0.8451	-0.8380	-0.6131	-0.6309	-0.7074	-0.5851
w^3	-1.4100	-0.7584	-0.9211	-0.6162	-0.6234	-0.6040	-0.6427
w^4	-	-0.7165	-	-0.5752	-0.5783	-0.5775	-

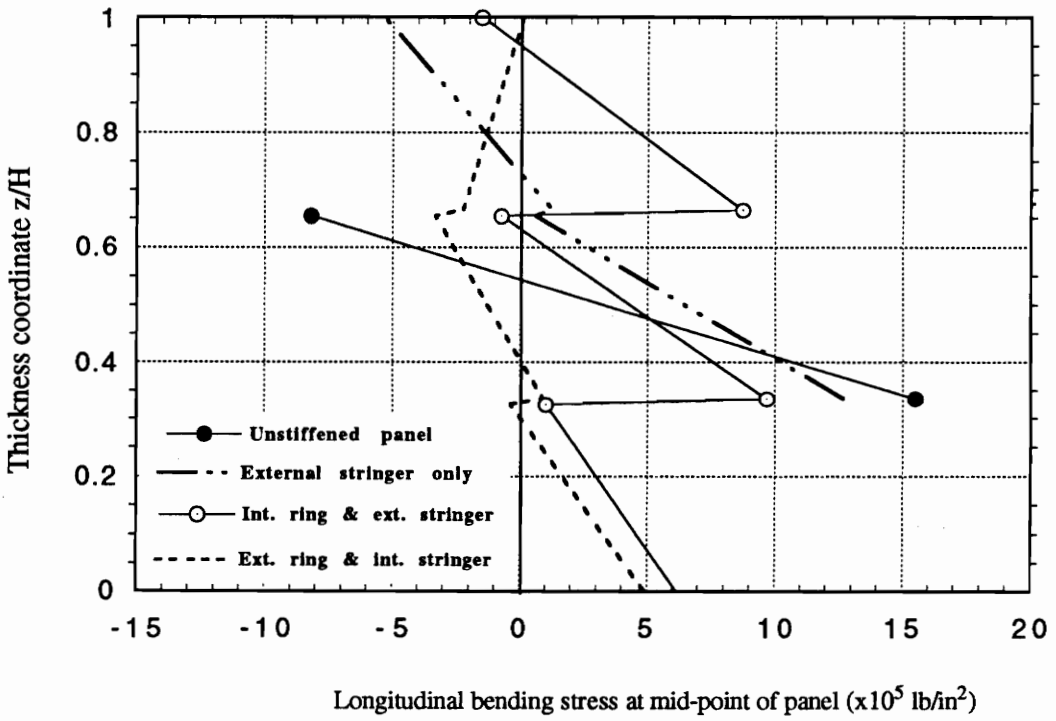

Figure 20. Through-the-thickness distribution of longitudinal bending stress under different stiffening schemes.

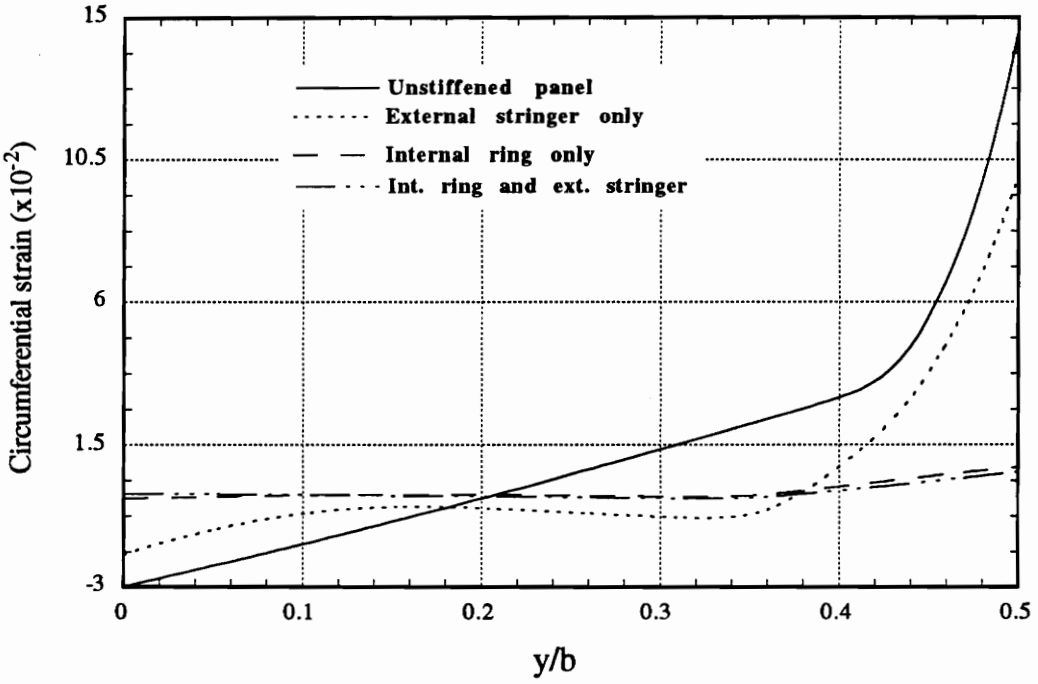

Figure 21. Distribution of circumferential strain for a stiffened cylindrical panel.

6.3.3 Stiffened cylindrical panel under internal pressure

The same cylindrical panel of section 6.3.2 is subjected to an internal pressure of intensity p_o = 375 lb/in^2 and its response under different stiffening schemes is investigated here. The mesh shown in Figure 19 consisting of 16 nine-noded quadratic elements surface-wise and 3 linear elements depth-wise, at points where the stiffeners are attached to the shell, and one linear element elsewhere is used here.

The distribution of the circumferential strain ε_{yy} at interface number 3 along x = a/2 is plotted for different stiffening schemes in Figure 22. The response of this cylindrical panel under internal pressure is quite different from its response under a transverse point load. At mid-span, the stiffeners tend to give a steep increase in strains unlike the case of a transverse point load where the stiffeners smoothen out the peak strains. For the case of external stringers and internal rings, the increase in strains is almost 8 times from a minimum strain value of 2.8 x 10^{-4} at the extreme left to a peak strain of 2.1 x 10^{-3} at the mid span. This peak strain is about 5 times more than the peak strain of the unstiffened cylindrical panel. This phenomenon of pillowing or bulging of the shell skin under pressure load resulting in localized regions of high strains near the stiffeners has been reported in References [90], [92] and [93]. However, note that far from the mid-point where there is a marked inflection point for the unstiffened case, the stiffeners tend to smoothen out the peak in circumferential strains. A similar behavior is observed in the case of longitudinal strains also.

In Figure 23, the through-the-thickness distribution of the longitudinal normal stress σ_{xx} at the mid-point of the panel for different stiffening schemes is given. Internal rings have a minor effect on the distribution of stress through the thickness of the shell skin. However, in the rings themselves, the stresses increase quite significantly. Note that due to the eccentricity of the rings, the stress distribution is not symmetric. External stringers used either alone or coupled with internal rings reduce the stresses through the thickness of the shell skin almost by one-third from a peak tensile stress of about 120,000 lb/in^2 at the top interface of the unstiffened panel to a mere stress of about 4000 lb/in^2 at the same location.

Again from the consideration of through-the thickness stress distribution and length-wise or circumference-wise strain distribution, stringers and rings placed alternately outside or inside of the cylindrical panel provide the most efficient stiffening scheme. Rings and stringers used alone provide a favorable response in the distribution and magnitude of only those stress and strain quantities that coincide with the orientation of the stiffeners. In other words, stringers, for instance, might be effective in reducing the displacements of the nodes and the stresses along their direction but have a very limited influence on the stresses and strains in the circumferential direction.

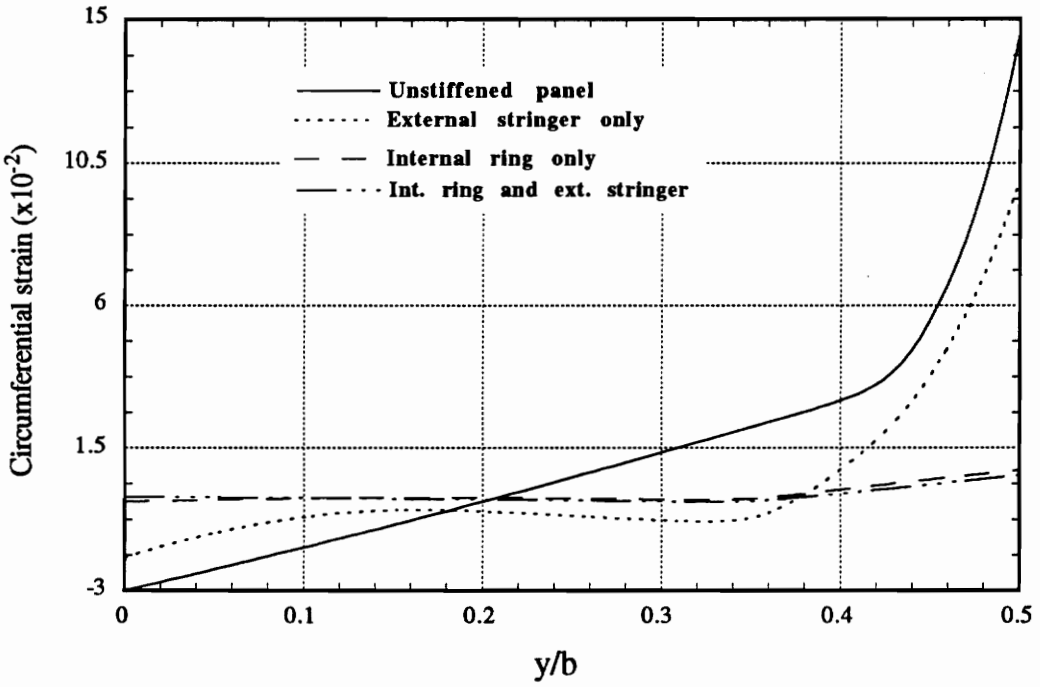

Figure 21. Distribution of circumferential strain for a stiffened cylindrical panel.

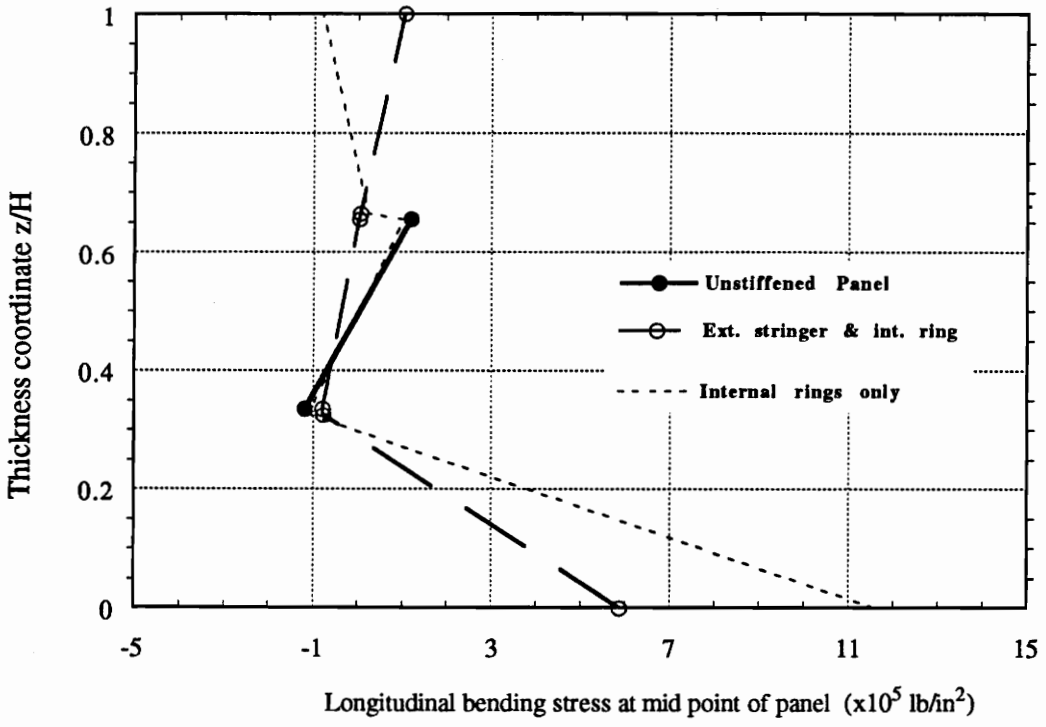

Figure 23. Through-the-thickness distribution of longitudinal bending stress of a panel under internal pressure.

6.3.4 Stiffened Cantilever Shell

A cantilever shell stiffened by symmetrically located rings and stringers is analyzed by the layerwise approach. The shell is loaded by a point load applied at one of the corners. This produces an unsymmetrical complex displacement field which is a combination of membrane stretching, bending and out-of-plane distortion. The capability of the model developed in this study is tested well by this particular example. Figure 24 gives the geometric details of the shell and the stiffeners. Note that for this case where the rings and the stringers are placed symmetrically with respect to the mid-plane of the shell skin, the sections A-A and B-B are the same. For comparison purposes, the mesh used by Liao [86] has been adopted here. The mesh consists of four nine-noded quadratic layerwise shell elements. The results are summarized in Table 6 for the following data:

Material Properties: $E = 1.0 \times 10^6$ Kg/cm^2, $\nu = 0.3$

$t = 6.0$ cm.

6.3.5 Eccentrically Stiffened Cantilever Shell

The same cantilever shell discussed in section 6.3.4 is stiffened by eccentric rings and symmetric stringers. This introduces additional unsymmetrical deformations which are captured by the layerwise model developed here quite accurately as shown in Table 7. The geometry of the ring is shown in Figure 24. Note that sections A-A and B-B are different for this particular type of stiffening scheme. The total thickness of the stringers, t , is 13 cm. for this case.

Figure 25 shows the through-thickness distribution of the normal stress σ_{xx} for the symmetrical stiffening scheme and the unstiffened shell. The stresses are calculated at the loaded corner. The stresses in the unstiffened plate and shell are scaled by a factor of 10 to fit in the plot. It can be seen that the stiffeners reduce the stresses drastically. The presence of the symmetric stiffeners also alters the position of the neutral axis significantly. The whole section of the shell skin at the loaded corner is under tension. Figure 26 shows the distribution of σ_{xx} when eccentric rings and symmetrical stringers are used. Note that, apart from reducing the magnitude of the stresses drastically, this particular stiffening scheme alters the distribution of the stresses qualitatively. The position of the neutral axis is also shifted. The whole section of the shell skin at the loaded corner, which was under tension while stiffened by symmetrical stiffeners, is now completely under compression. The peak stress for this stiffening scheme is only about half of that corresponding to the symmetrically stiffened shell.

With regard to the radial and tangential displacements, the layerwise model gives good results compared to those reported in the literature. Liao's [86] results, reported here for comparison, are based on discrete formulations. However, the inclusion of transverse normal stresses by the layerwise model accounts for the small discrepancies between the two results.

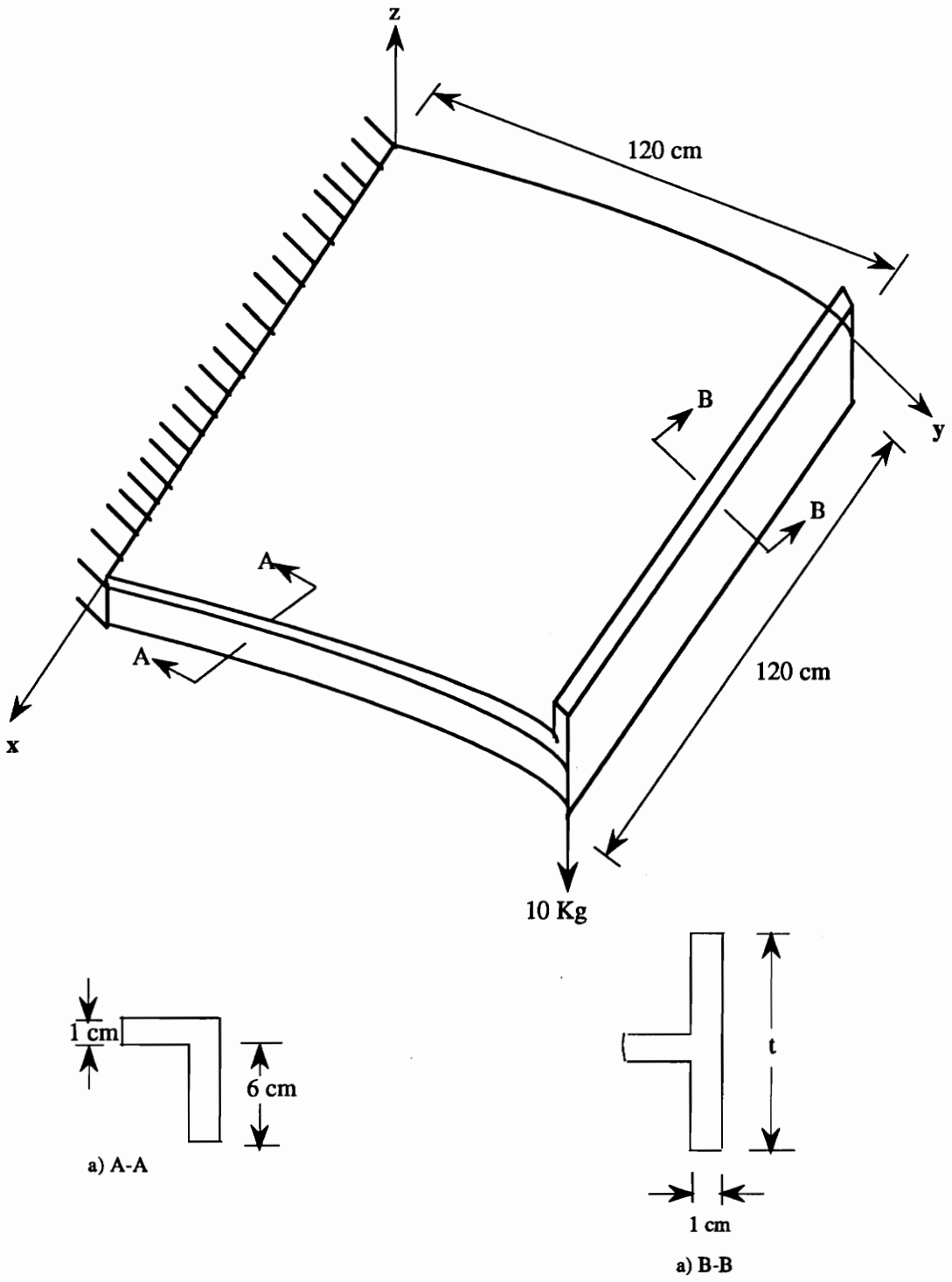

Figure 24. A stiffened cantilever cylindrical shell.

Table 6. Deflections at loaded corner of symmetrically stiffened cantilever shell.

Displacement components	R = Infinity		R = 240 cm.	
	Ref [86]	Present	Ref [86]	Present
w (radial)	-0.1810	-0.1933	-0.1658	-0.1638
v (tangential)	-	0.0011	0.0324	0.0318

Table 7. Deflections at loaded corner of unsymmetrically stiffened cantilever shell.

Displacement components	R = Infinity		R = 240 cm.	
	Ref [86]	Present	Ref [86]	Present
w (radial) cm.	-0.05164	-0.05191	-0.05440	-0.05963
v (tang.) cm.	-	0.00014	0.01142	0.01179

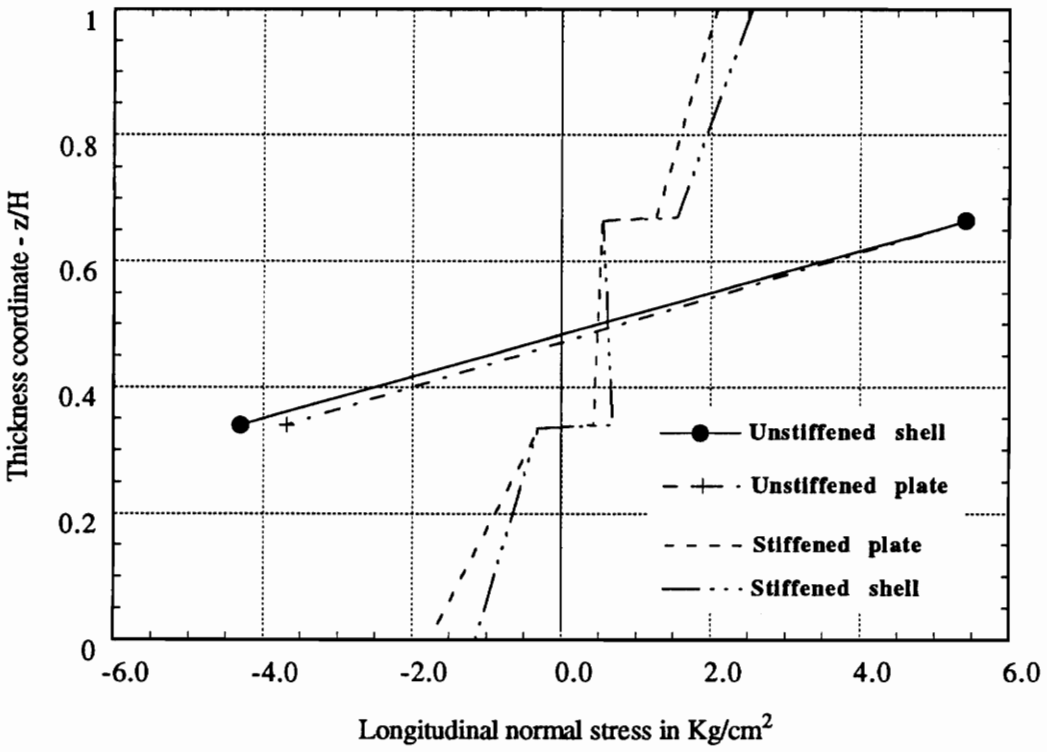

Figure 25. Through-the-thickness distribution of longitudinal normal stress in a symmetrically stiffened shell.

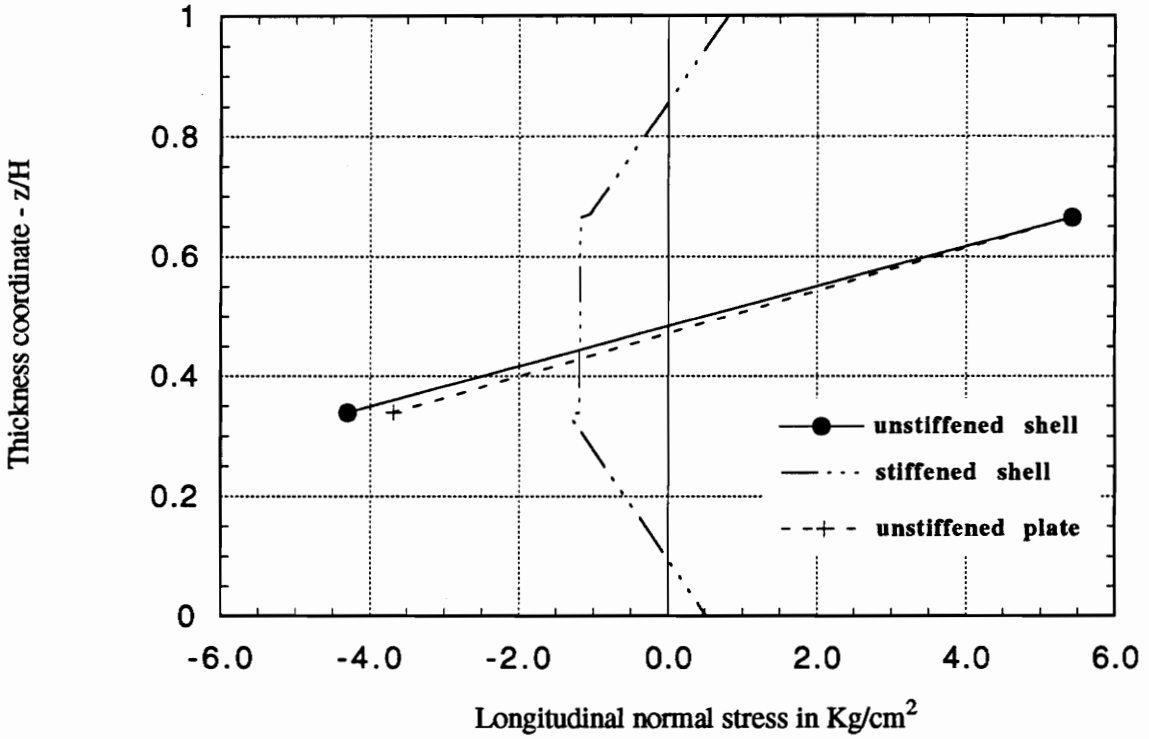

Figure 26. Through-the-thickness distribution of longitudinal normal stress in eccentrically stiffened shell.

6.3.6 Stiffened Cylindrical Shell Under Internal Pressure

A cylindrical shell stiffened by both rings and stringers all around its circumference and length and subjected to an internal pressure of intensity p is analyzed for local responses using the layerwise theory. Figure 26 shows a representative region with its boundary along the midlines between adjacent rings and stringers. It is this representative region which is modeled for analysis. The same shell has been analysed in reference [90], where a discrete analytical approach based on the classical lamination theory was used.

Material Properties:

(i) Shell skin

$E_{xx} = 1.0x10^7$ psi, $E_{yy} = E_{zz} = 1.0x10^6$ psi

$G_{yz} = 0.60x10^6$psi, $G_{xy} = G_{xz} = 0.50x10^6$ psi

$\nu_{yz} = 0.25$, $\nu_{xy} = \nu_{xz} = 0.25$

(ii) stiffener

same as shell material.

Geometric Properties:

a = 20 in.

R = 117.5 in.

b = 5.8 in.

t = 0.075 in.

t1 = 0.05 in., t2 = 0.075 in., w = 1.0 in.

Convergence of displacements is achieved for a non-uniform mesh of 4x4 nine-noded quadrilateral elements as shown in Figure 28. Three linear elements are used through the thickness at nodes where the stiffeners are joined to the shell. All other nodes have only one linear element through the thickness.

For an internal pressure of intensity p = 10 psi, different results obtained from the layerwise theory are compared with those reported in reference [90]. Figure 29 shows the variation of the longitudinal strain ε_{xx} across the circumference and length. Figure 30, on the other hand, shows the variation of the circumferential strain ε_{yy} along x = 0, and y=0. The longitudinal and circumferential strains are evaluated at the inner surface of the shell skin. Note that the local strains peak near the stiffener-skin interface area due to pillowing or bulging of the shell skin under internal pressure. The strains obtained from the finite element model of the layerwise theory tend to have a higher peak at the interface compared to reference [90]. This is partly expected since the results reported in [90] are based on a closed-form analytical solution given by a continuous function, whereas the current study employs the finite element model. More refinement of the mesh at the interface may smoothen the peak to some extent. However, since the layerwise theory accounts for shear deformations and reference [90] does not, there still will be differences in the maximum strains.

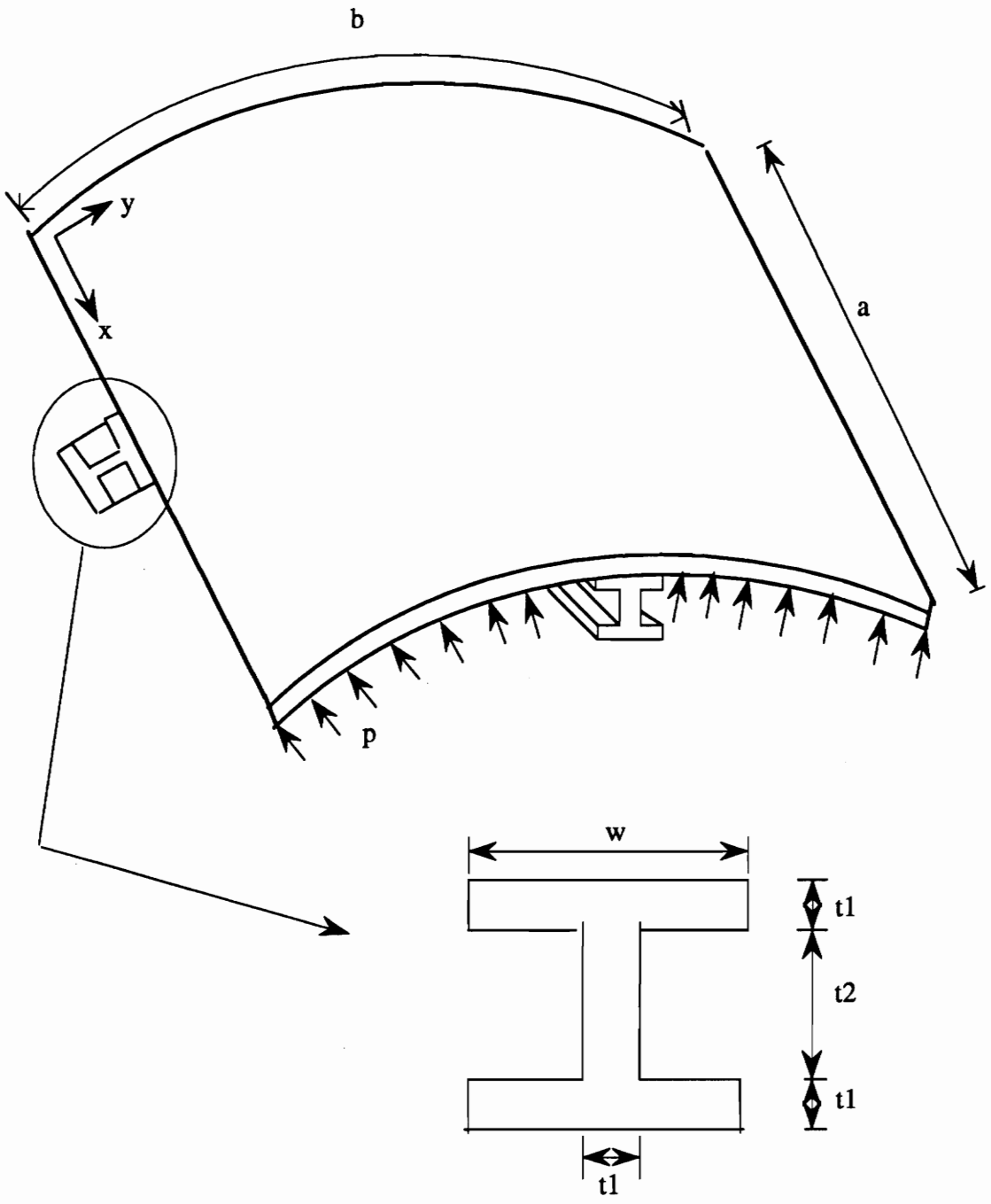

Figure 27. Representative region of a stiffened cylindrical shell.

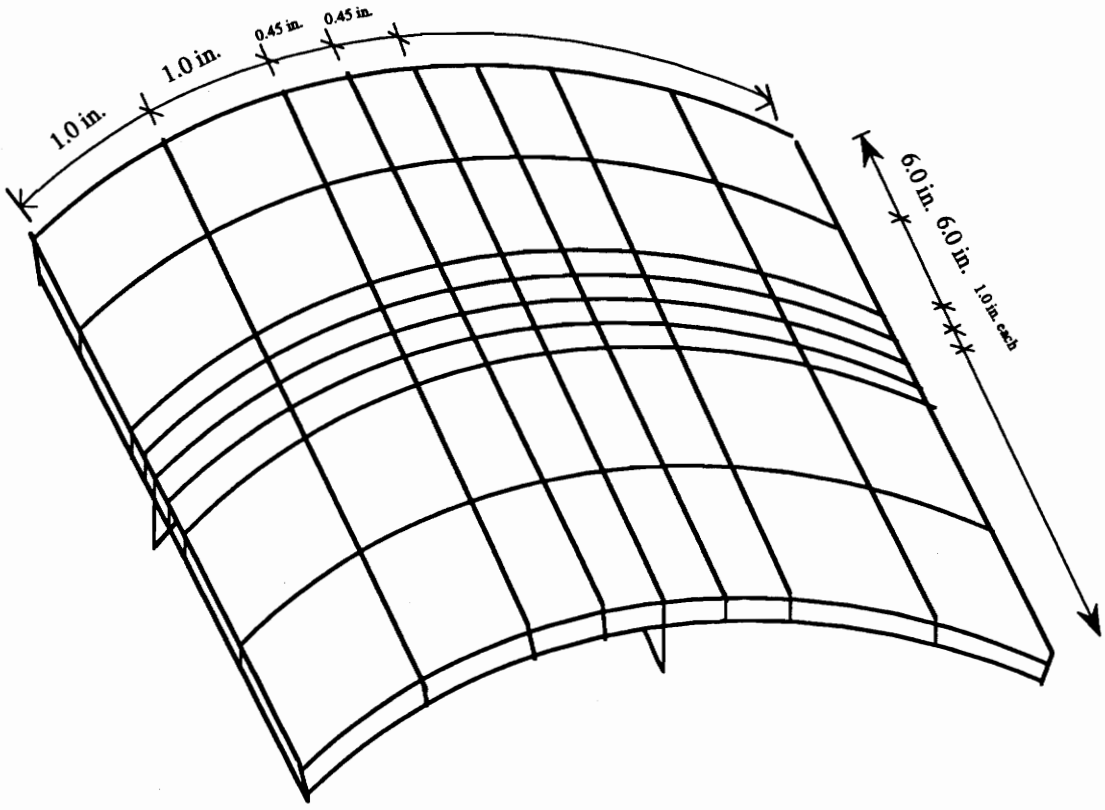

Figure 28. Finite element mesh for a representative region of a stiffened shell.

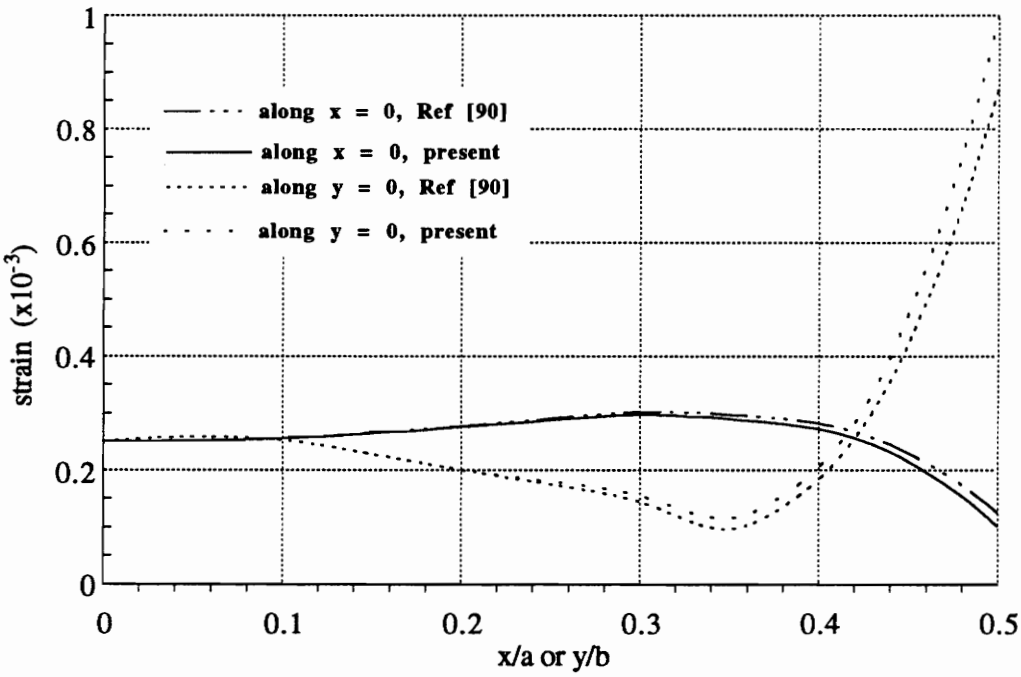

Figure 29. Longitudinal strain of a stiffened shell.

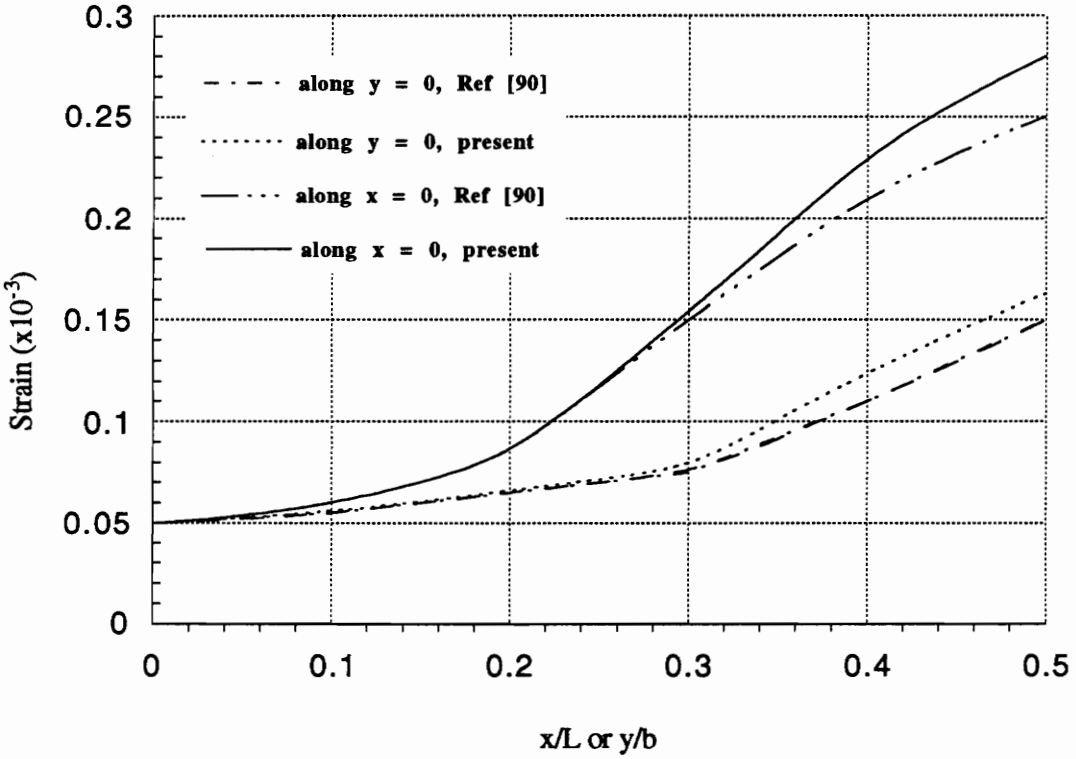

Figure 30. Circumferential strain of a stiffened shell.

6.4 Post-buckling and Imperfection Sensitivity Analysis

6.4.1 Post-buckling of Cylindrical Panels

Isotropic cylindrical panels of different thicknesses are analyzed under a point load to trace the load-displacement curve in the pre-buckling and post-buckling regimes. The geometry and the boundary conditions for the panels are shown in Figure 31. Two linear elements are used through the thickness. Surface-wise, a quarter model of the panels consists of a 2x2 mesh of 9-node quadratic elements. Convergence was achieved for this mesh. The two panels are of the same material and geometry but different thicknesses and exhibit totally different responses as shown in Figures 32 and 33. The thin panel has a snap-through behavior with a defined limit point. The softening of the post-buckling region is also very pronounced. On the other hand, the thick panel shows a plate-like nonlinear response with no definite limit point.

Material Properties:

$E = 450$ ksi

$\nu = 0.3$

Panel Geometry:

$R = 100$ in.

$a = 20$ in.

$b = 20$ in.

$t = 1.0$ in.

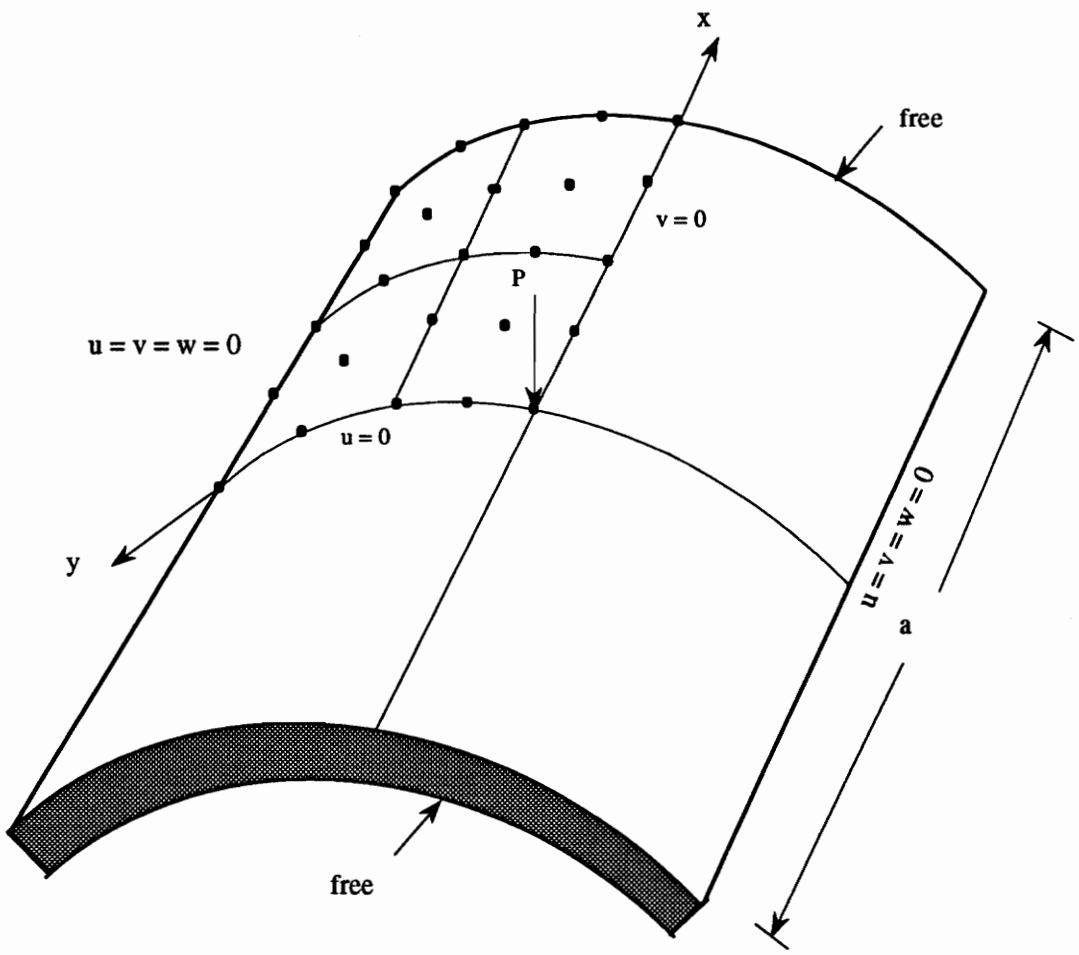

Figure 31. Geometry and boundary conditions for a hinged isotropic cylindrical panel.

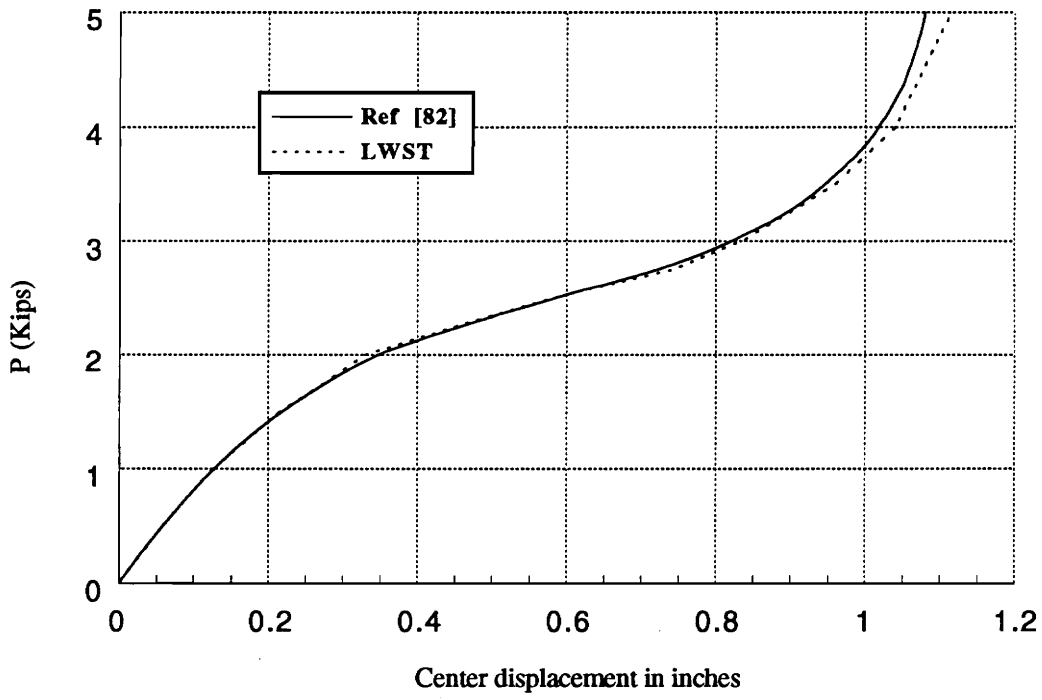

Figure 32. Nonlinear response of a hinged cylindrical panel (t = 1.0 inch).

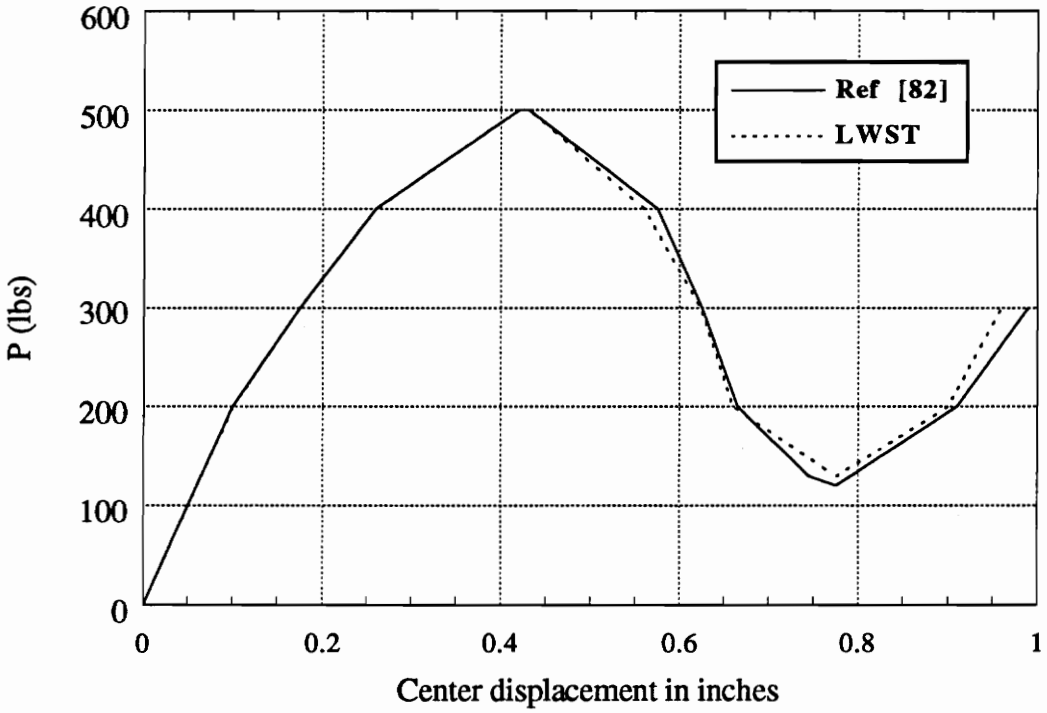

Figure 33. Nonlinear response of a hinged cylindrical panel (t= 0.5 inch).

6.4.2 Postbuckling of a Hinged (0/90) Cylindrical Panel

A two layered composite panel is subjected to a point load at the center. A mesh of 2x2 nine node quadratic elements with two linear elements per layer is used for the analysis. Convergence was achieved for this mesh.

Material Properties:

$E_1 = 4.0 \times 10^7$ lb/in^2; $E_2 = 1.0 \times 10^6$ lb/in^2; $E_3 = 1.0 \times 10^6$ lb/in^2

$G_{12} = G_{23} = 0.6 \times 10^6$ lb/in^2

$G_{23} = 0.5 \times 10^6$ lb/in^2

$\nu_{12} = \nu_{13} = \nu_{23} = 0.25$

Panel Geometry:

R = 100 in.

a = 20 in.

b = 20 in.

t = 1.0 in.

Figure 34 shows the pre-buckling and post-buckling path. The snap-through behavior is well captured by the present model which uses the Modified Riks-Wempner method to navigate the limit point. Near the limit point and in the falling limb region, Reference [82], which is based on the moderate rotation theory, gives larger deflections. This is due to the fact that the theory assumes not small strains and rotations but moderate rotations, as the name implies.

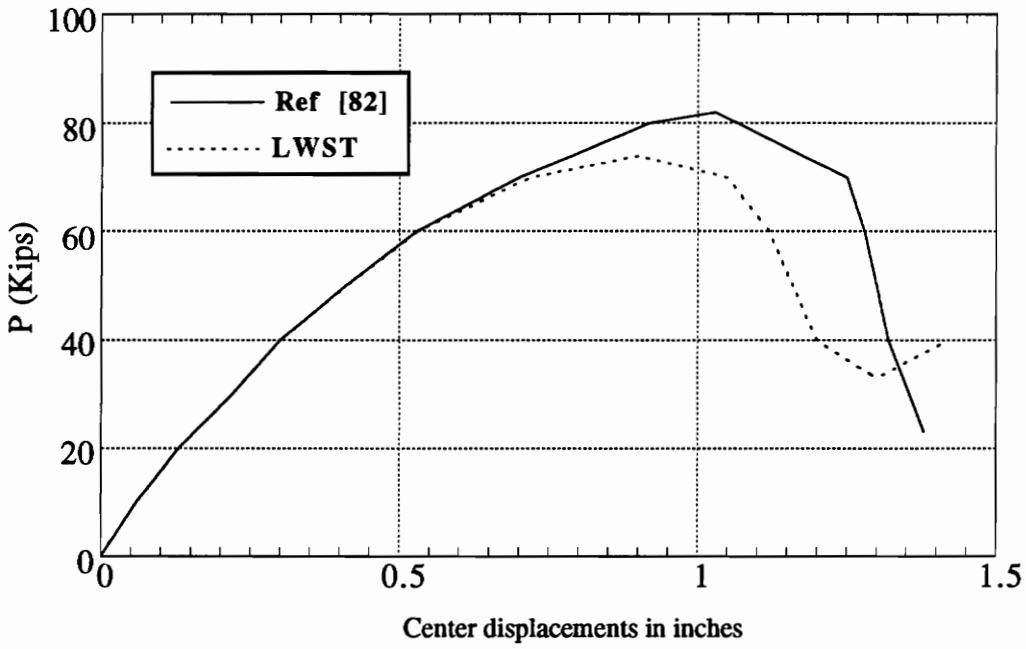

Figure 34. Nonlinear response of a (0/90) hinged cylindrical panel.

6.4.3 Imperfection Sensitivity of a Thin Cylindrical Shell

A thin cross-ply (0-90-0) cylindrical shell is analyzed here to investigate the effect of initial imperfections on its response to an axial loading. The same problem is solved in Reference [89] using the Rayleigh-Ritz method. First, an eigenvalue analysis (linearized buckling) is carried out to determine the critical load and the fundamental mode. The fundamental buckling mode is (1,4). Only one quarter model of a circumferential wave is modeled to save computational expenses.

This quarter model is sufficient because one of the longitudinal edges of this circumferential slice has a symmetric boundary condition with respect to both loading and buckling whereas the other edge has anti-symmetric boundary conditions with respect to buckling [91]. Likewise, due to the symmetry or anti-symmetry about the mid-plane, only half of the span is modeled.

Figure 35 shows the finite element mesh used for this analysis. The load versus axial shortening curves for the cylinder with various magnitudes of initial imperfections are given in Figure 36. Note that the axial load is normalized with respect to the critical buckling load. For very small imperfections, the post-buckling load occurs at around 40% of the buckling load. For higher imperfections, a distinct nonlinear response is obtained. This particular example illustrates the effect of initial imperfections on the response of cylindrical shell structures under external de-stabilizing loads.

The material and geometrical properties are given below.

$E_{LL} = 30x10^6$ psi ; $E_{TT} = 1x10^6$ psi ;

$G_{LT} = 0.5x10^6$ psi; $G_{TT} = 0.2x10^6$ psi

$\nu_{LT} = \nu_{TT} = 0.3$

h = 0.1 inch.

$h_i = h/3$

L = 100 in.

R = 36 inch.

where the subscripts L and T represent the direction along and transverse to that of the fibres.

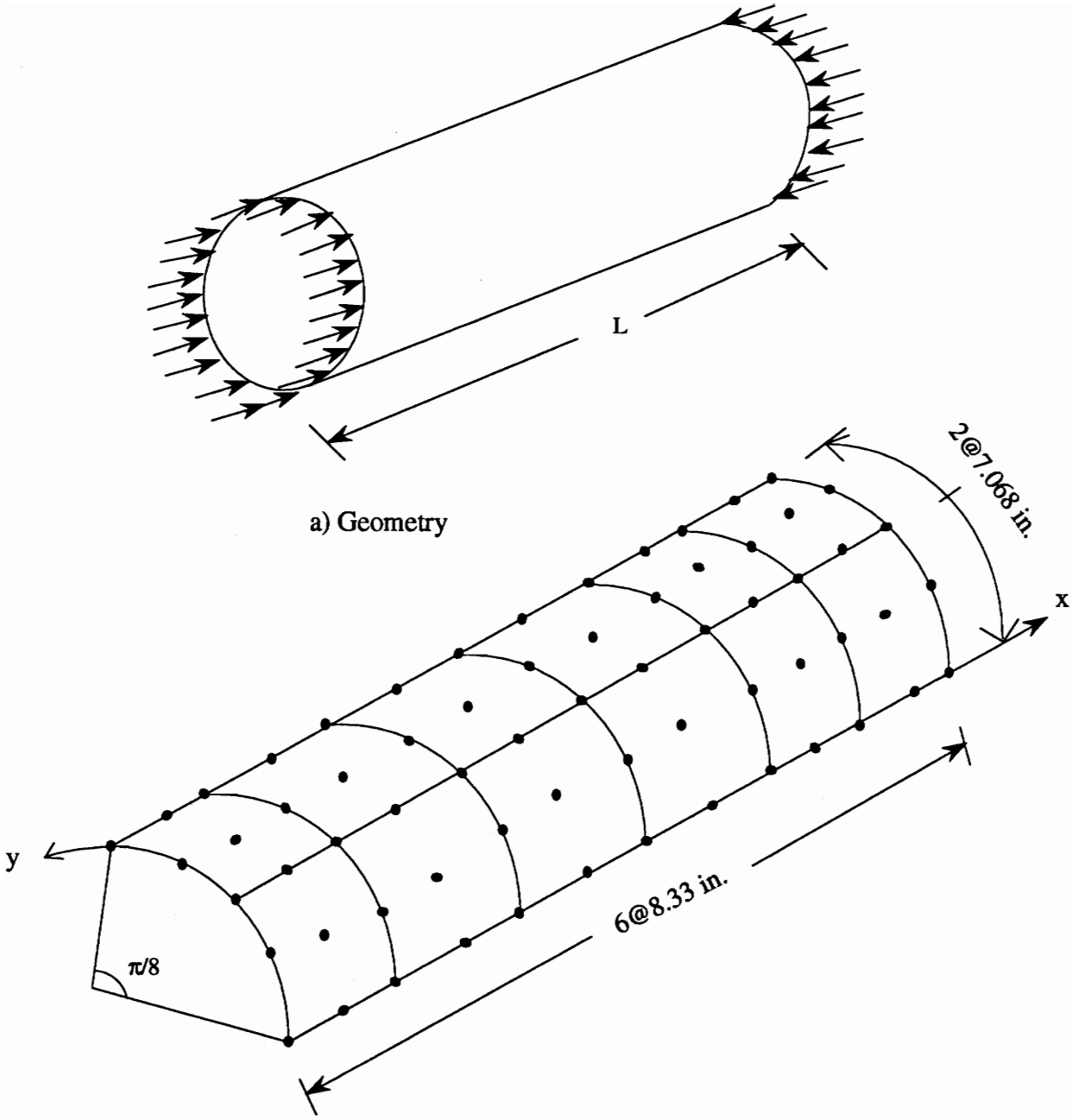

Figure 35. Geometry and finite element mesh of a thin cross-ply cylindrical shell

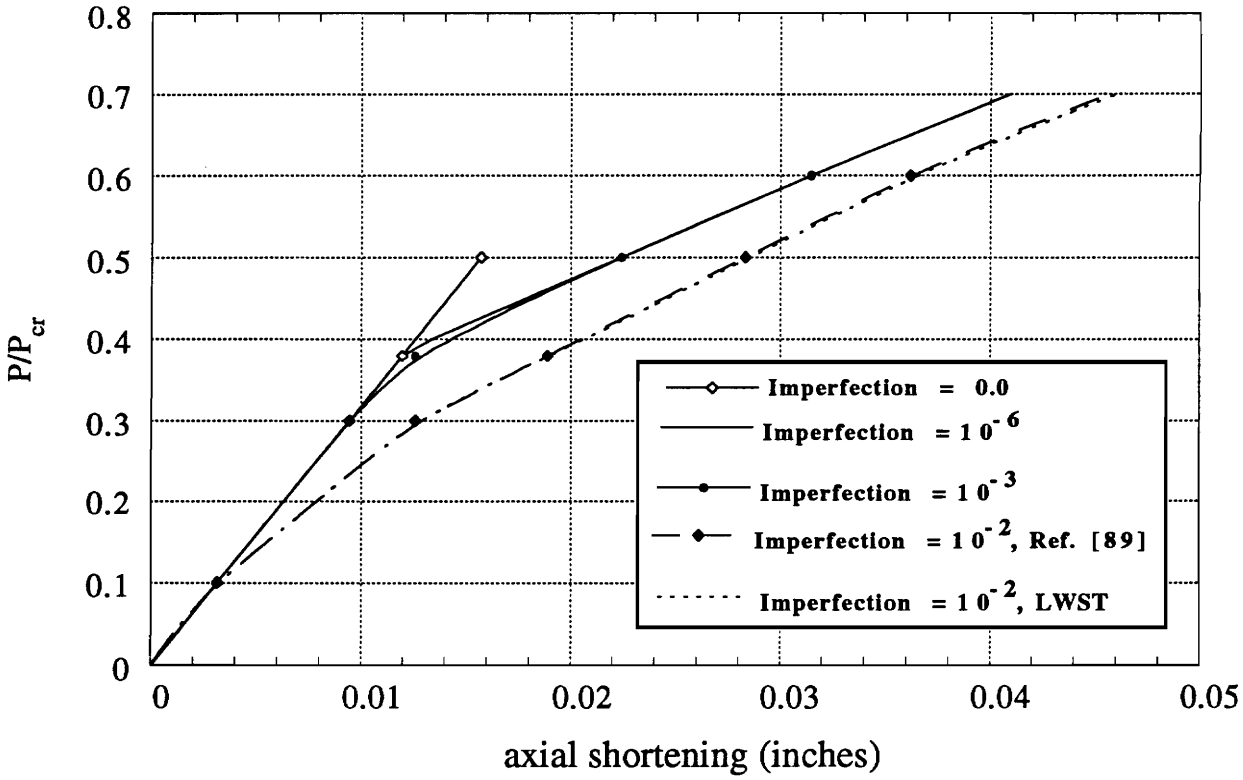

Figure 36. Imperfection sensitivity of a thin cylindrical shell.

6.5 Stand-Alone Beams

The shell stiffener element developed in Chapter 3 can also be used to model stand-alone beams. A separate computer program called COBEAM based on the formulations of Chapter 3 has been developed to analyze stand-alone laminated beams. Such beams are widely used in aircraft and space structures. In this section, a number of single layer and laminated beams are analyzed for natural vibration, critical buckling load and static loads to verify the efficiency and accuracy of the element. Both curved and straight stand-alone beams are investigated.

6.5.1 Straight Isotropic Beam

A cantilever isotropic beam, shown in Figure 37, was analyzed under a tip point load for different L/H ratios. The radius is set to infinity. A convergent solution is obtained for 2 quadratic and 4 linear elements. Through the thickness, four linear elements are used.

The material properties are:

$E = 3.0 \times 10^6$ lb/in^2 ; $\nu = 0$

As shown in Table 8, the layerwise theory gives a very satisfactory result for both deep beams and shallow beams. This particular example illustrates the efficiency of the layerwise model in capturing shear deformations in deep beams.

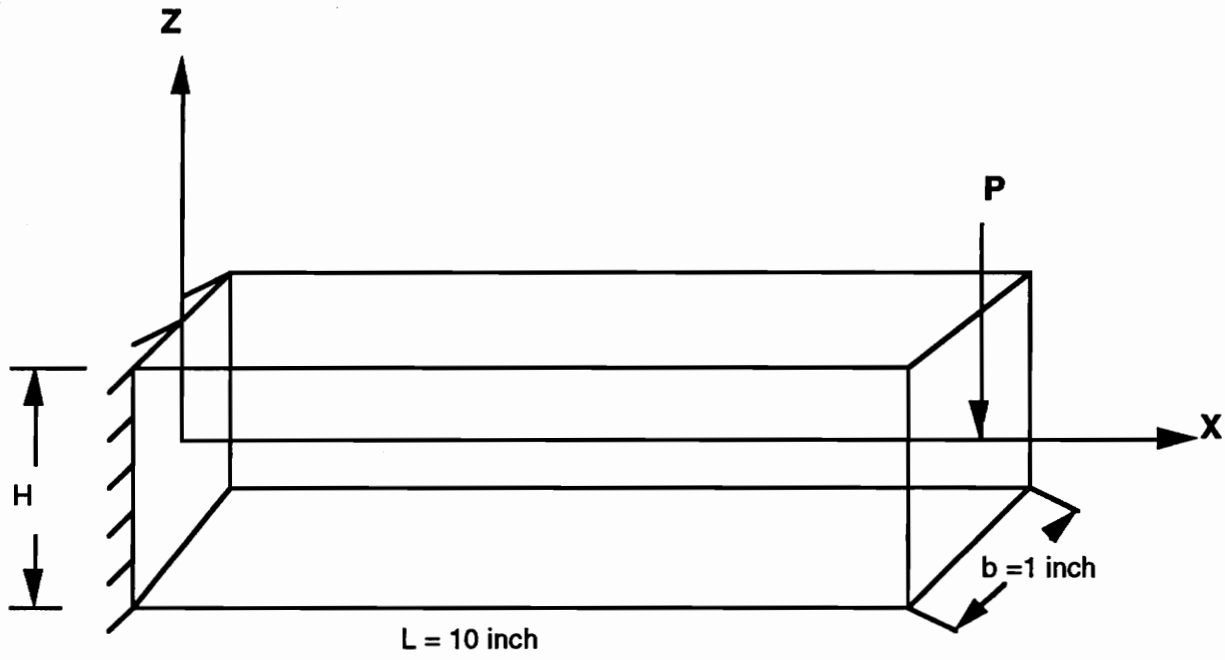

Figure 37. Straight isotropic beam

Table 8. Linear displacement of a straight beam (in inches).

P in lbs	L/H	Displacement in inches		
		Layerwise Theory	Reference [86]	Classical Beam Theory
2.0	1.0	0.400E-05	0.427E-05	0.267E-05
3.0	10.0	0.400E-02	0.402E-02	0.400E-02

6.5.2 Natural Vibration of Orthotropic and Cross-Ply Beams

Simply supported orthotropic and cross-ply beams are investigated to determine their fundamental frequencies using the layerwise theory for beams. The results are given in a non-dimensionalized form as :

$$\Omega^2 = \omega^2 \frac{h^2 E_2}{\rho L^4 (1-\mu_{23}\mu_{23})}$$

The material properties for the Graphite/Epoxy composite laminate are as follows:

$E_{11} = 181$ GPa , $E_{22} = E_{33} = 10.3$ GPa;

$G_{23} = 6.21$GPa , $G_{12} = G_{13} = 7.17$ GPa;

$\mu_{12} = 0.28$, $\mu_{13} = 0.02$, $\mu_{23} = 0.4$, $\rho = 1389.23$ Kg/m^3

The effect of ply orientation on the frequencies is demonstrated in Table 9. Convergent results were obtained for eight linear elements along the length and two linear elements through the thickness. Note that the Euler-Bernoulli theory for beams is inadequate in capturing the effect of the ply orientation. As discussed in section 3.2.4, the layerwise theory, unlike the classical beam theory, does not neglect the out-of-plane normal and transverse shear strains. As a result, these quantities are accounted for in the constitutive equations. This explains the capacity of the present model to capture the effect ply orientation has on the response of the laminate.

Table 9. Comparison of natural frequencies (Ω) of a composite beam.

Lamination Scheme	Present Study	Ref [87]
Isotropic	2.52	2.67
Orthotropic	10.8	10.62
0/90/0	10.0	10.40

Table 10. Effect of ply orientation on the natural frequency Ω.

Angle (θ)	0^o	15^o	75^o
Present Study	10.8	7.42	2.92
Ref [87]	10.62	7.31	2.87
Euler-Bernoulli	11.89	11.11	3.05

6.5.3 Simply Supported (0/90/0) Beam under Sinusoidal Load

This problem has been solved by Pagano [76] using a three-dimensional elasticity theory for the case of a plate in cylindrical bending. The intensity of the sinusoidal load is q_o. The beam consists of three equal thickness graphite-epoxy laminates and has a length to depth ratio of four (L/h = 4).

The material properties for the Graphite/Epoxy composite laminate are as follows:

E_{11} = 172 GPa , $E_{22} = E_{33}$ = 6.9 GPa;
G_{23} = 3.4 GPa , $G_{12} = G_{13}$ = 1.4 GPa;
μ_{12} = 0.25, μ_{13} = 0.25, μ_{23} = 0.25

A convergent solution is obtained for four quadratic elements along the length and two linear elements through the thickness. The through thickness distribution of the longitudinal stress σ_{xx} is given in Figure 38. The stresses are computed at the mid-span and are non-dimensionalized by dividing by q_o. The normal stresses computed by the layerwise theory agree very closely with the exact solutions, whereas CLT fails to predict accurately even the sign of the stress at the interface of the two laminates. The same problem has been solved in section 6.2.2 using a layerwise shell element. Note that the responses predicted by the layerwise shell element and beam element are almost identical.

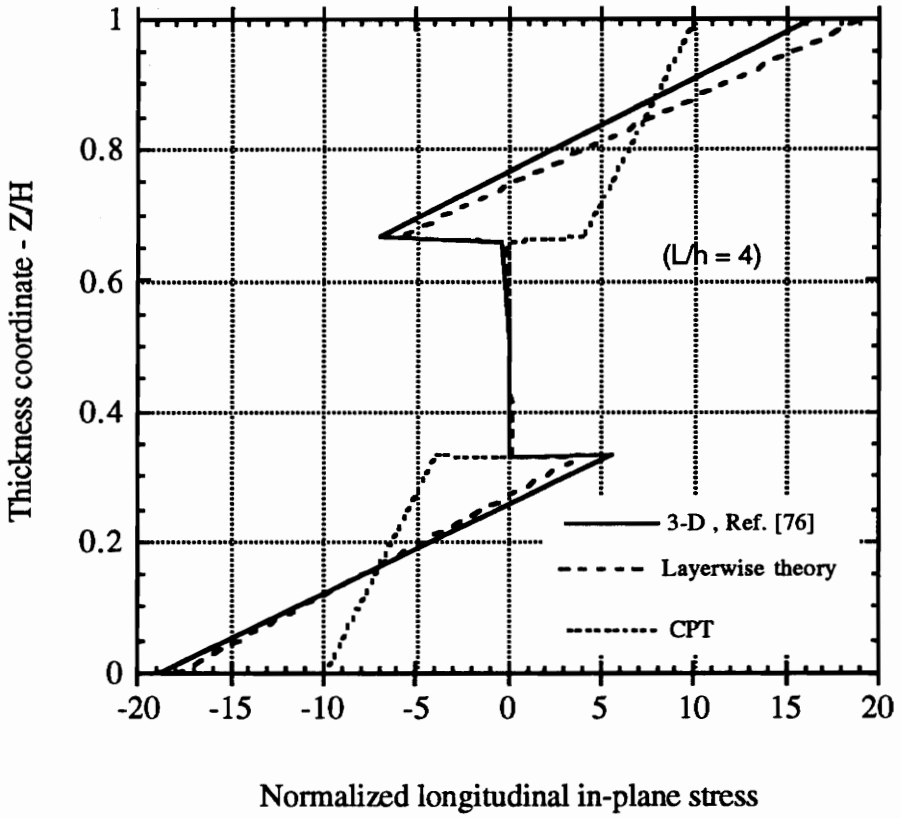

Figure 38. Distribution of longitudinal stress σ_{xx} through the thickness.

6.5.4 Buckling of Curved and Straight Beams

A linearized buckling analysis of straight and curved isotropic beams under different boundary conditions is carried out. The results are compared with those reported by Rao and Tripathy [88]. The beams are modeled with two linear elements through the thickness and eight linear elements along the length.

The material and geometrical properties are:

$E = 2.0 \times 10^6$ lb/in^2; $\nu = 0.3$

H = 25.4 mm; Width = 25.4 mm and L = 508 mm

Table 11. Critical loads of a straight beam under different boundary conditions.

Boundary Condition	Present Study	Ref [88]
Simply Supported	94.43 kN	96.6 kN
Clamped-Free	23.15 kN	24.0 kN

Table 12. Critical loads of a curved beam under uniform radial load (simply supported).

No of Elements	Present Study	Ref [88]
2	78.54 kN/m	78.76 kN/m
6	76.87 kN/m	77.05 kN/m

CHAPTER 7

CONCLUDING REMARKS AND RECOMMENDATIONS

7.1 Summary

The Layerwise Theory of Reddy is used to develop two-dimensional layerwise cylindrical shell and stiffener elements. The elements developed are used alone or together to model such varied structures as unstiffened and stiffened plates and shells, and stand-alone composite beams.

The layerwise format of the elements introduces a three-dimensional kinematics which represents the local and global state of stress and deformation to a high degree of accuracy. Stiffened shells, which have been traditionally modelled by the "stiffness averaging" method are modelled, as discrete stiffeners using a layerwise format. The discrete model gives detailed information about the displacement field and hence the state of stress at the skin-stiffener interface. This information is invaluable for the design of stiffened panels and shells where separation of stiffener and shell skin should be prevented.

Initial imperfections are also incorporated in the formulation of the finite element model of the cylindrical shell element. The accuracy and efficiency of the elements developed is established by solving a wide variety of unstiffened and stiffened plate and shell structures. The elements are tested for natural vibration, linearized buckling and linear static and post-buckling responses. The sample problems demonstrate that the layerwise elements capture the global and local responses to a high degree of accuracy.

7.2 Conclusions

Based on the investigations of different structures carried out in this study, the following conclusions are made:

1. The Layerwise Theory of Reddy is capable of modeling the three-dimensional kinematics and state of stress in cylindrical shells and stiffener elements to a high degree of accuracy. Unlike the conventional equivalent single-layer methods, the layerwise theory, by virtue of its layerwise format, gives detailed information on the state of stress and displacement field at each interface in the shell skin and the stiffeners.

2. The behavior of stiffened panels and shells near the area of attachment of the shell skin and the stiffeners is complex and only a discrete model is capable of capturing the response accurately. In a very localized regions near the stiffeners, there is a steep increase in strains for shells under pressure. This is due to pillowing of the shell skin under the pressure load. Quantification of these strains is very important in the design of stiffened composite shells due to the brittle nature and low transverse strength exhibited by the fibre composite materials of which they are made. Models based on an "average-stiffness" approach cannot accurately determine local variations of stresses and strains, even though they tend to give satisfactory results for global responses.

3. The eccentricity and location of both axial and circumferential stiffeners has a very significant bearing on the response of stiffened shells. For transverse loading, external axial stiffeners and internal rings or internal stringers and external rings used together are more efficient, whereas under hydrostatic loads, internal rings used alone or together with

external stringers respond better. Stringers are very effective in reducing the longitudinal strains but have almost negligible effect on the circumferential strains. On the other hand, rings have little effect on the distribution of the longitudinal strains but reduce circumferential strains significantly. A layerwise format handles the eccentricity and the location of the stiffeners readily.

4. Unlike the equivalent single-layer methods, which can determine the stresses and strains only at the top and bottom of the shell skin, the layerwise theory for discretely stiffened cylindrical shells has the ability to accurately determine the variation of the stresses and strains through the thickness of the stiffeners and the shell skin. Information on the state of stress and strain through the thickness of the stiffeners and the shell skin is very important for the designer who has to decide on the particular lamination scheme to be used for the stiffeners and the shell.

5. For shells with a large number of stiffeners, the discrete model might be expensive computationally, especially at the design stage where cycles of analyses might have to be performed. Therefore, a "smeared" model might be used as an economical alternative for analysis at the preliminary design stage. The use of possible symmetry lines and axes might alleviate this problem to some extent. For the final analysis, the discrete model may be used to obtain an accurate and complete picture of the response of the stiffened plate or shell under the external destabilizing loads.

6. In the example problems visited in this study, a perfect bond between the shell skin and the stiffeners is assumed. For cases where adhesives which result in secondary bonding are used, the adhesive layer should be modeled as a separate layer with its own material properties.

7. The discrete stiffener element developed in Chapter 3 can also be used to model stand-alone composite beams. Keeping the transverse normal and shear strains while eliminating the corresponding stresses in the constitutive equations is found to give a better and more accurate representation of the kinematics and state of stress.

7.3 Recommendations for Further Work

The Layerwise Theory of Reddy has a vast potential for applications in a wide variety of specific problems, where so far the lack of a refined and yet economical computational scheme has discouraged a rigorous treatment. Here, a list of areas which need further investigation is given.

1. The Layerwise Shell Theory can be extended to shells of general geometry such as spherical, conical and toroidal shells. With properly defined kinematics and geometry, the extension will be quite straightforward. The theory might find an important application for the global and local analysis of such shells with structural discontinuities such as cut-outs and free-edges.

2. Stiffened panels and shells do experience separation of the skin material and the stiffener at certain load levels or even at the unstressed configuration due to manufacturing errors. The theory can be extended to such cases by introducing additional unknowns for the separation region and incorporating it in the kinematics.

3. Composite shells are often stiffened by crisscrossing stiffeners called geodesical stiffeners. The layerwise elements developed in this study could be extended to a general case where the stiffeners are oriented at an arbitrary angle to the cylinder coordinate system. Geodesically stiffened shells are gaining more importance because of the ease in manufacturing them and their favorable response characteristics.

4. In the design of stiffened panels and shell structures like aircraft wings and fuselages, a non-detrimental local phenomenon known as panel buckling is often tolerated for a lighter economical design. A global/local analysis based on the Layerwise Shell Theory which can model such a phenomenon accurately should be developed to give the designer a powerful analytical tool.

REFERENCES

1. Love, A. E. H., *"On the Small Free Vibrations and Deformations of the Elastic Shells,"* Philosophical Transaction of the Royal Society (London), Series A, Vol. 17, 1888, pp. 491-549.
2. Reddy, J. N., and Liu, C. F., *"A Higher-order Theory for Geometrically Nonlinear Analysis of Composite Laminates,"* NASA Contractor Report 4056, March 1987.
3. van der Neut, A., *"The General Instability of Stiffened Cylindrical Shells under Axial Compression,"* National Aeronautical Research Institute (Amsterdam), Report Series 314, 1947.
4. Reddy, J.N., *"A Generalization of Two-Dimensional Theories of Laminated Composite Laminates,"* Communications in Applied Numerical Methods, Vol. 3, 1987, pp. 173-180.
5. Robbins, D.H and Reddy, J. N., *"Modelling of Thick Composite Using a Layerwise Laminate Theory, "* International Journal for Numerical Methods in Engineering, in press.
6. Budiansky, B. and Sanders, J. L., *"On the 'Best' First Order Linear Shell Theory,"* Progress in Applied Mechanics (Prager Anniversary Volume), MacMillan, New York, 1963. pp 22-45.
7. Koiter, W.T., *"A Consistent First Approximation in the General Theory of Thin Elastic Shells, "* Theory of Thin Elastic Shells, North Holland, Amsterdam, 1960, pp. 12-33.
8. Donnell, L. H., *"Stability of Thin-walled Tubes Under Torsion,"* NACA, Report 479 1933.
9. Vlasov, V. Z., *"Allgemeine Schalen Theorie und ihre Anwending in der Technik,"* Akademie-Verlag, Berlin, 1958.
10. Novozhilov, V. V., *"Foundations of the Nonlinear Theory of Elasticity, "* Greylock Press, Rochester, New York, 1953.

11. March, S., *"Influence of Predetermined Delaminations on Buckling and Postbuckling Behavior of Composite Sandwich Beams,"* Composite Structures, Vol. 17, 1991, pp. 295-329.

12. Schnaell, W. and Bush, D., *"The Effect of Delamination on the Fundamental and Higher Order Buckling Loads of Laminated Beams,"* Journal of Composite Testing and Research, Vol. 11, 1989, pp. 87-93.

13. Thielmann, W. F., *"New Developments in the Nonlinear Theories of the Buckling of Thin Cylindrical Shells,"* Proceedings of the Durand Centennial Conference, Hoff, N.J., and Vincenti, W.G., (Eds.), Pergamon Press, London, 1960, pp. 76.

14. Hess, H., *"Large Deformation Effects in the Postbuckling Behavior of Composite with Thin Delaminations,"* AIAA Journal, Vol. 27, 1988, pp. 624-631.

15. Cheng, S. and Ho, B.P.C., *"Stability of Heterogeneous Aeolotropic Cylindrical Shells Under Combined Loading,"* AIAA Journal, Vol. 1, 1963, pp. 892-898.

16. Jones, R. M., and Morgan, H. S., *"Buckling and Vibration of Cross-ply Laminated Circular Cylindrical Shells,"* AIAA Journal, Vol. 5, No. 8, 1967, pp. 1463.

17. Jones, R.M., *"Buckling of Circular Cylindrical Shells with Multiple Orthotropic Layers and Eccentric Stiffeners,"* AIAA Journal, Vol. 6, 1968, pp. 2301-2305. Errata, Vol. 7, 1969, p. 2048.

18. Hennemann, and Hirano, *"Allgemeine Schalen Theorie und ihre Anwending in der Technik,"* Akademie-Verlag, Berlin, 1958.

19. Flügge, W., *"Die Stabilität der Kreiszy linderschale,"* Ingenieur Archive, Vol. 3, 1932, pp. 463-506.

20. Tasi, J., Feldman, A., and Starg, D. A., *"The Buckling Strength of Filament-Wound Cylinders Under Axial Compression, "* NASA TR-266, July 1965.

21. Martin, W., and Drew, D., *"The Effect of Delamination on the Fundamental and Higher Order Buckling Loads of Laminated Beams, "* Journal of Composite Testing and Research, Vol. 11, 1989, pp. 87-93.

22. Chao, C., *"New Developments in the Nonlinear Theories of the Buckling of Thin Cylindrical Shells, "* Proceedings of the Durand Centennial Conference, Hoff, N.J., and Vincenti, W.G., (Eds.), Pergamon Press, London, 1960, pp. 83.

23. Reissner, E., *"On The Theory of Bending of Elastic Plates,"* Journal of Mathematics and Physics, Vol. 23, 1944, pp. 184-191.

24. Gol'denveizer, A.C., *"On Reissner's Theory of Bending of Plates,"* Izvestiya An SSSR, OTN., No. 4, 1958.

25. Kromm, A., *"Uber die Randquer Krafte bei gestutzten Platten,"* ZAMM, Vol 35, 1955, pp. 231-242.

26. Basset, A. B., *"On the Extension and Flexure of Cylindrical and Spherical Thin Elastic Shells, "* Philosophical Transaction of the Royal Society, (London), Series A, Vol 6., 1890, pp. 433-480.

27. Hildebrand, F. B., Reissner, E. and Thomas, G.B., *"Notes on the Foundations of the Theory of Small Displacements of Orthotropic Shells,"* NACA TN-1833, Washington, D.C., 1949.

28. Yang, P., Norris, C. H. and Stavsky, Y., *"Elastic Wave Propagation in Heterogeneous Plates, "* International Journal of Solids and Structures, Vol. 2, 1966, pp. 665-684.

29. Librescu, L., Khdeir, A., and Frederick, D., *"A Shear Deformable Theory of Laminated Composite Shallow Shell-Type Panels and Their Response Analysis, I: Free Vibration and Buckling, "* Acta Mechanica, Vol. 76, 1989, pp. 1-33.

30. Reddy, J.N., "A Simple Higher-order Theory for Laminated Composite Plates," Journal of Applied Mechanics, Vol. 51, 1984, pp. 745-752.

31. Schmidt, R., *"A Refined Nonlinear Theory for Plates with Transverse Shear Deformation,"* Journal of the Industrial Mathematics Society, Vol. 27, 1977, pp. 23-38.

32. Levinson, M., *"An Accurate Simple Theory of the Static and Dynamics of Elastic Plates,"* Mechanics Research Communications, Vol. 7, 1980, pp. 343-350.

33. Murthy, M. V. V., *"An Improved Transverse Shear Deformation Theory for Laminated Anisotropic Shells and Plates, "* NASA Technical Paper 1903, November 1981, pp. 1-37.

34. Librescu, L., *"Substantiation of a Theory of Elastic and Anisotropic Shells and Plates, "* St. Cerc. Mech. Appl., Vol. 1, 1968, pp. 105-128.

35. Vlasov, B.F., *"Ob Uravnieniakh izgiba Plastinok (On Equations of Bending of Plates), "* Dokla Ak. Nauh Azerbeijanskoi SSR, Vol. 3, 1957, pp. 955-959.

36. Krishna Murthy, A. V., *"Flexure of Composite Plates, "* AIAA Journal, Vol. 7, 1987, pp. 161-177.

37. Reddy, J. N., *"A Layerwise Shell Theory with Applications to Buckling and Vibration of Cross-Ply Laminated Stiffened Circular Cylindrical Shells,"* Virginia Polytechnic Institute and State University, CCMS-92-01, January, 1992.

38. Wilson, L. B., *"Deformation Under Uniform Pressure of a Circular Cylindrical Shell Supported by Equally Spaced Circular Ring Frames, "* Naval Construction Research Establishment, St. Leonard's Hill, Dunfermline, Fife, Report No. R-337C, December 1956.

39. Baruch, M., and Singer, J., *"Effect of Eccentricity of Stiffeners on the General Instability of Stiffened Cylindrical Shells Under Hydrostatic Pressure, "* Journal of Mechanical Engineering Sciences, Vol. 5, 1963, pp. 23-27.

40. Hedgepth, J. M., and Hall, D. B., *"Stability of Stiffened Cylinders, "* AIAA Journal, Vol. 3, 1965, pp. 2275-2286.

41. Block, D.L., *"Influence of Ring Stiffeners on Instability of Orthotropic Cylinders in Axial Compression, "* NASA TND-2482, 1964.

42. Kohnke, P. C., and Schnobrich, W. C., *"Analysis of Eccentrically Stiffened Cylindrical Shells, "* Journal of the Structural Division, ASCE, Vol. 98, 1972, pp. 1493-1510.

43. Rao, K. P., *"A Rectangular Laminated Anisotropic Shallow Thin Shell Finite Element, "* Computer Methods in Applied Mechanics and Engineering, Vol. 15, 1978, pp. 13-33.

44. Venkatesh, A., and Rao, K. P., *"A Laminated Anisotropic Curved Beam and Shell Stiffening Finite Element, "* Computers and Structures, Vol. 15, 1982, pp. 197-201.

45. Venkatesh, A., and Rao, K. P., *"Analysis of Laminated Shells with Laminated Stiffeners Using Rectangular Finite Elements,"* Computers Methods in Applied Mechanics and Engineering, Vol. 38, 1983 pp. 255-272.

46. Venkatesh, A., and Rao, K. P., *"A Doubly Curved Quadrilateral Finite Element for the Analysis of Laminated Anisotropic Thin Shells of Revolution,"* Computers and Structures, Vol. 12, 1980, pp. 825-832.

47. Carr, A. J., and Clough, R. W., *"Dynamic Earthquake Behavior of Shell Roofs,"* Fourth World Conference on Earthquake Engineering, Santiago, Chile, 1969.

48. Schmit, L. A., *"Developments in Discrete Element Finite Deflection Structural Analysis by Functional Minimization, "* Technical Report AFFDL-TR-68-126, Wright-Patterson Air Force Base, Ohio, 1968.

49. Ferguson, G. H., and Clark, R. H., *"A Variable Thickness Curved Beam and Shell Stiffening Element with Shear Deformations, "* International Journal for Numerical Methods in Engineering, Vol. 14, 1979, pp. 581-592.

50. Ahmad, S., Irons, B. M., and Zienkiewicz, O.C., *"Analysis of Thick and Thin Shell Structures by Curved Finite Elements, "* International Journal for Numerical Methods in Engineering, Vol. 2, 1970, pp. 419-451.

51. Liao, C. L., *"An Incremental Total Lagrangian Formulation for General Anisotropic Shell-Type Structures, "* AIAA Journal, Vol. 2, 1989 , pp. 453-435.

52. Kiciman, O. K., Popov, E. P., *"Post-Buckling Analysis of Cylindrical Shells,"* Journal of the Engineering Mechanics Division, ASCE, Vol 104, 1978, pp. 751-762.

53. Bodner, S. R., *"The Analysis of the General Instability of Ring Reinforced Circular Cylindrical Shells by Orthotropic Shell Theory, "* Polytechnic Institute of Brooklyn, Report No. 291, May 1955.

54. Batdorf, S. B., *"A Simplified Method of Elastic Stability Analysis for Thin Cylindrical Shells, I - Donnell Equations, "* NACA, TN 1341, 1947.

55. Ho, B. P. C. and Cheng, S., *"Some Problems in Stability of Heterogeneous Aeolotropic Cylindrical shells Under Combined Loading, "* AIAA Journal, Vol 1, 1963, pp. 1603-1607.

56. von Kárman, T. and Tsien, H. S., *"The Buckling of Thin Cylinders Under Axial Compression, "* Journal of the Aeronautical. Sciences, Vol. 8, 1941, pp. 302-312.

57. Naghdi, P. M., *"On the Theory of Thin Elastic Shells, "* Quarterly of Applied Mathematics, Vol. 14, 1957, pp. 369-380.

58. Rao, K. P., *"A Review of General Instability,"* Computer Methods in Applied Mechanics and Engineering, Vol. 15, 1978, pp. 13-33.

59. Koiter, W. T., *"The Stability of Elastic Equilibrium, "* Ph.D. Thesis, Delft, Netherlands, 1945, also AFFDL-TR-70-25, 1970.

60. Hutchinson, J. W., *"Axial Buckling of Pressurized Imperfect Cylindrical Shells,"* AIAA Journal, Vol. 3, 1965, pp.1461-1466.

61. Budiansky, B., and Hutchinson, J. W., *"Buckling of Circular Cylindrical Shells Under Axial Compression, "* Contributions to the Theory of Aircraft Structures, Delft University Press, Holland, 1972.

62. Arbocz, J., and Babcock, C. D., *"The Effect of General Imperfections on the Buckling of Cylindrical Shells,"* Journal of Applied Mechanics, Vol. 36, 1969, pp. 23-38.

63. Gallagher, R. H., *"The Finite Element Method in Shell Stability Analysis,"* Computers and Structures, Vol. 3, 1973, pp. 543-557.

64. Sharifi, P. and Popov, E., *"Nonlinear Buckling Analysis of Sandwich Arches,"* Journal of the Engineering Mechanics Division, ASCE, Vol. 97, 1971, pp. 1397-1412.

65. Walker, A. C., *"A Nonlinear Finite Element Analysis of Shallow Circular Arches,"* International Journal of Solids and Structures, Vol. 5, 1969, pp. 97-107.

66. Noor, A. K., Peters, J. M., *"Mixed Models and Reduced/Selective Integration Displacement Models for Nonlinear Analysis of Curved Beams,"* International Journal for Numerical Methods in Engineering, Vol. 17, 1981, pp. 615-631.

67. Bergan, P. G., Horregmoe, Krakeland, B., and Soreide, T. H., *"Solution Techniques for Nonlinear Finite Element Problems, "* International Journal for Numerical Methods in Engineering, Vol. 12, 1978, pp. 1677-1696.

68. Bergan, P. G., and Soreide, T. H., *"Solution of Large Displacement and Instability Problems Using the Current Stiffness Parameters,"* Finite Elements in Nonlinear Mechanics, Tapiv Press, 1978, pp. 647-649.

69. Argyris, J. H., *"Continua and Discontinuum, Proceedings of the First Conference on Matrix Methods in Structural Mechanics, "* Wright-Patterson Air Force Base, Ohio, 1965, pp. 11-189.

70. Batoz, J. C. and Dhatt, G., *"Incremental Displacement Algorithm for Nonlinear Problems,"* International Journal for Numerical Methods in Engineering, Vol. 14, 1979, pp. 1262-1268.

71. Riks, E., *"An Incremental Approach to the Solution of Snapping and Buckling Problems,"* International Journal of Solids and Structures, Vol. 15, 1979, pp. 529-551.

72. Ramm, E., *"Strategies for Tracing the Nonlinear Response Near Limit Points,"* Nonlinear Finite Element Analysis in Structural Mechanics, edited by Stein, M., and Bathe, K. J., Berlin, 1981, pp. 63-89.

73. Crisfield, M. A., *"A Fast Incremental Iterative Solution Procedure that Handles Snap-through,"* Computers and Structures, Vol. 13, 1981, pp. 55-62.

74. Brush, D. and Almroth, B., *"Buckling of Bar, Plates and Shells,"* McGraw Hill, 1977.

75. Reddy, J.N., *"Solution Procedures for Nonlinear Algebraic Equations,"* ESM Class Notes (Finite Element Analysis - A Second Course), Virginia Polytechnic Institute and State University, Blacksburg, VA, 1990.

76. Pagano, N.J., *"Exact Solutions for Composite Laminates in Cylindrical Bending,"* Journal of Composite Materials, Vol 3, pp. 398-411, 1969.

77. Barbero, E., *"On a Generalized Laminate Theory with Application to Bending, Vibration and Delamination Buckling in Composite Laminates, "* Ph. D. Thesis, Virginia Polytechnic Institute and State University, Blacksburg, VA, 1989.

78. Noor, A.K., *"Forced Vibration of Multilayered Composite Plates,"* AIAA Journal, Vol. 11, 1975 pp. 1038-1039.

79. Bushnell, D.,*"PANDA2-Program for Minimum Weight Design of Stiffened, Composite, Locally Buckled Panels,"* LMSC-D067175, Lockheed Missiles and Space Company.

80. Rao, K.P., and Tripathy, B., *"Composite Cylindrical Panels-Optimum Lay-up for Buckling by Ranking, "* Computers and Structures, Vol 38, pp. 217-225, 1991.

81. Kapania, R., and Yang, C., *"Formulation of an Impefect Quadrilateral Doubly-Curved Shell Element for Post-buckling Analysis,"* AIAA Journal, Vol. 24, 1986, p. 310.

82. Palmerio, A.F., *"On a Moderate Rotation Theory for Anisotropic Shells, "* Ph.D. Thesis, Virginia Polytechnic Institute and State University, Blacksburg, VA, 1988.

83. Shen-yu, L., *"Finite Element Elastic Thin Shell Pre-buckling and Post-buckling Analysis,'* Ph.D. Thesis, Cornell University, Ithaca, NY, 1971.

84. Tripathy, B., and Rao, K.P., *"Stiffened Composite Cylindrical Panels-Optimum Lay-up for Buckling by Ranking,"* Computers and Structures, Vol. 42, No 4, pp. 481-488.

85. Lekhnitskii, S.G., Tsai, S.W., and Cheron, T., *"Anisotropic Plates,"* Second Edition, Chapter 16, pp. 492-502, 1968.

86. Liao, C-L., *"Incremental Total Lagrangian Formulation for General Anisotropic Shell-Type Structures, "* Ph. D. Thesis, Virginia Polytechnic Institute and State University, Blacksburg, VA, 1987.

87. Bhimaraddi, A., and Chandrashekara, K., *"Some Observations on the Modeling of Laminated Composite Beams With General Lay-ups, "* Composite Structures, Vol. 13, 1991, pp. 371-380.

88. Tripathy, B., and Rao, K.P., *"Curved Composite Beams - Optimum Lay-up for Buckling by Ranking, "* Computers and Structures, Vol. 41, pp. 75-82, 1991.

89. Reddy, J. N., and Savoia, M., *"Post-buckling of Laminated Circular Cylindrical Shells According to the Layerwise Shell Theory,"* Virginia Polytechnic Institute and State University, CCMS-92-02, January, 1992.

90. Wang, J. T-S., and Hsu, T.M., *"Discrete Analysis of Stiffened Composite Cylindrical Shells,"* AIAA Journal, Vol 23, 1985, pp. 1753-1761.

91. Hibbitt, Karlsson and Sorensen, Inc., *"ABAQUS"*, version 4.6, pp. 3.2.12.1-3.2.12.22, 1988.

92. Ley, R.P., *"Analysis and Optimal Design of Pressurized, Imperfect, Anisotropic Ring-Stiffened Cylinders,"* Ph. D. Thesis, Virginia Polytechnic Institute and State University, Blacksburg, VA, 1987.

93. Hyer, M.W., Loup, D.C., and Starnes, J.H., Jr., *"Stiffener/Skin Interactions in Pressure Loaded Composite Panels,"* AIAA Journal, Vol. 28, 1990, pp. 532-537.

APPENDIX A

The algorithm for evaluating the tangent stiffness matrix of a layerwise cylindrical shell element is discussed here.

As indicated in Chapter 5, the Newton-Raphson and Modified Riks methods require the evaluation of of the tangent stiffness matrix. Equation (5.5) could be re-written, in more general terms, as:

$$\left[{}^{mn}K^{\alpha\beta} \right]^{tan} = \frac{\partial R_{\alpha}^{m}}{\partial \Delta_{\beta}^{n}} \tag{D.1}$$

where $\alpha, \beta = 1, 2, ..., N+1$ and $m,n = 1, 2, 3$. N is the number of mathematical layers in the shell.

$$\Delta_{\beta}^{1} = u_{\beta},\ \Delta_{\beta}^{2} = v_{\beta},\ \Delta_{\beta}^{3} = w_{\beta},\ \text{and}\ \widehat{\Delta}_{\beta}^{3} = \widehat{w}_{\beta} \tag{D.2}$$

Equation (D.1) can be expanded as:

$$\left[{}^{mn}K^{\alpha\beta} \right]^{tan} = \frac{\partial}{\partial \Delta_{\beta}^{n}} \left[\sum_{r} \sum_{p} \left[{}^{mn}K^{\alpha\beta} \right] \Delta_{p}^{r} - {}^{m}F^{\alpha} \right] \tag{D.3}$$

which reduces to:

$$\left[{}^{mn}K^{\alpha\beta} \right]^{tan} = \left[{}^{mn}K^{\alpha\beta} \right]^{direct} + \sum_{r} \sum_{p} \frac{\partial\, {}^{mn}K^{\alpha\beta}}{\partial\, \Delta_{\beta}^{n}} \Delta_{p}^{r} \tag{D.4}$$

For m and n varying from 1 to 2, the tangent stiffness matrix assumes the same value as the direct stiffness matrix as given in Equation (D.5):

$$\left[{}^{mn}K^{\alpha\beta}\right]^{tan} = \left[{}^{mn}K^{\alpha\beta}\right]^{direct} \qquad (m,n = 1, 2) \qquad (D.5)$$

$$\left[{}^{3n}K^{\alpha\beta}\right]^{tan} = \left[{}^{3n}K^{\alpha\beta}\right]^{direct} \qquad (n = 1, 2) \qquad (D.6)$$

The direct stiffness matrices $\left[{}^{13}K^{\alpha\beta}\right]$, $\left[{}^{23}K^{\alpha\beta}\right]$ and $\left[{}^{33}K^{\alpha\beta}\right]$ may be re-written in a convenient form to systematically keep track of the different indices as follows:

$$\left[{}^{m3}K^{\alpha\beta}\right] = \left[{}^{m3}K^{\alpha\beta}\right]^{L} + \left[{}^{m3}K^{\alpha\beta\gamma}\right]\left(\frac{\Delta^3_\gamma}{2} + \hat{\Delta}^3_\gamma\right) \qquad (m = 1, 2) \qquad (D.7)$$

$$\left[{}^{3m}K^{\alpha\beta}\right] = \left[{}^{3m}K^{\alpha\beta}\right]^{L} + \left[{}^{3m}K^{\alpha\beta\gamma}\right]\left(\Delta^3_\gamma + \hat{\Delta}^3_\gamma\right) \qquad (m = 1, 2) \qquad (D.8)$$

$$\begin{aligned}\left[{}^{33}K^{\alpha\beta}\right] = \left[{}^{33}K^{\alpha\beta}\right]^{L} &+ \left[{}^{33}K^{\alpha\beta\gamma}\right]^{NL1}\left(\frac{\Delta^3_\gamma}{2} + \hat{\Delta}^3_\gamma\right) + \left[{}^{33}K^{\alpha\beta\gamma}\right]^{NL2}\left(\Delta^3_\gamma + \hat{\Delta}^3_\gamma\right) \\ &+ \left[{}^{33}K^{\alpha\beta\gamma\rho}\right]^{NL3}\left(\frac{\Delta^3_\gamma}{2} + \hat{\Delta}^3_\gamma\right)\left(\Delta^3_\gamma + \hat{\Delta}^3_\gamma\right)\end{aligned} \qquad (D.9)$$

Using equations (D.3), (D.7), (D.8) and (D.9), the remaining tangent stiffness matrices are derived as follows:

$$\left[{}^{m3}K^{\alpha\beta} \right]^{tan} = \frac{\partial\, {}^{m3}K_{ij}^{\alpha\beta}}{\partial\, \Delta_\beta^3}\, \Delta_\gamma^3 + \left[{}^{m3}K^{\alpha\gamma} \right]^{direct} \frac{\partial \Delta_\gamma^3}{\partial\, \Delta_\beta^3} \qquad (m = 1, 2) \qquad \text{(D.10.a)}$$

$$= \frac{1}{2}\left[{}^{m3}K^{\alpha\gamma\beta} \right] (\Delta_\gamma^3) + \left[{}^{m3}K^{\alpha\beta} \right] \qquad \text{(D.10.b)}$$

$$= \frac{1}{2}\left[{}^{m3}K^{\alpha\gamma\beta} \right] (\Delta_\gamma^3) + \left[{}^{m3}K^{\alpha\beta\gamma} \right] \left(\frac{\Delta_\gamma^3}{2} + \hat{\Delta}_\gamma^3 \right) + \left[{}^{m3}K^{\alpha\beta} \right]^{L} \qquad \text{(D.10.c)}$$

Similarly,

$$\left[{}^{33}K^{\alpha\beta} \right]^{tan} = \frac{\partial\, {}^{3m}K_{ij}^{\alpha\gamma}}{\partial\, \Delta_\beta^3}\, \Delta_\gamma^m + \frac{\partial\, {}^{33}K_{ij}^{\alpha\gamma}}{\partial\, \Delta_\beta^3}\, \Delta_\gamma^3 + \left[{}^{33}K^{\alpha\gamma} \right]^{direct} \frac{\partial \Delta_\gamma^3}{\partial\, \Delta_\beta^3} \qquad \text{(D.11.a)}$$

$$\left[{}^{33}K^{\alpha\beta} \right]^{tan} = \left[{}^{3m}K^{\alpha\gamma\beta} \right] (\Delta_\gamma^m) + \frac{1}{2}\left[{}^{33}K^{\alpha\gamma\beta} \right]^{NL1} (\Delta_\gamma^3) + \left[{}^{33}K^{\alpha\gamma\beta} \right]^{NL2} (\Delta_\gamma^3)$$
$$+ \frac{1}{2}\left[{}^{33}K^{\alpha\gamma\rho\beta} \right]^{NL3} \left(\frac{\Delta_\rho^3}{2} + \hat{\Delta}_\rho^3 \right) (\Delta_\gamma^3) \qquad \text{(D.11.b)}$$
$$+ \left[{}^{33}K^{\alpha\gamma\rho\beta} \right]^{NL3} \left(\frac{\Delta_\rho^3}{2} + \hat{\Delta}_\rho^3 \right) (\Delta_\gamma^3) + \left[{}^{33}K^{\alpha\beta} \right]^{direct}$$

APPENDIX B

The components of the tangent stiffness matrix for a layerwise cylindrical shell element are given below. Note that initial imperfections are included.

$$\left[{}^{11}K_{ij}^{\alpha\beta}\right] = \int_{\Omega_e} \left[\left(\frac{\partial\varphi_i}{\partial x} A_{11}^{\alpha\beta} \frac{\partial\varphi_j}{\partial x}\right) + \left(\frac{\partial\varphi_i}{\partial x} A_{16}^{\alpha\beta} \frac{\partial\varphi_j}{\partial y}\right) + \left(\frac{\partial\varphi_i}{\partial y} A_{16}^{\alpha\beta} \frac{\partial\varphi_j}{\partial x}\right) + \left(\frac{\partial\varphi_i}{\partial y} A_{66}^{\alpha\beta} \frac{\partial\varphi_j}{\partial y}\right) + \left(\varphi_i \bar{\bar{A}}_{55}^{\alpha\beta} \varphi_j\right) \right] dx\, dy$$

$$\left[{}^{12}K_{ij}^{\alpha\beta}\right] = \int_{\Omega_e} \left[\left(\frac{\partial\varphi_i}{\partial x} A_{12}^{\alpha\beta} \frac{\partial\varphi_j}{\partial y}\right) + \left(\frac{\partial\varphi_i}{\partial x} A_{16}^{\alpha\beta} \frac{\partial\varphi_j}{\partial x}\right) + \left(\frac{\partial\varphi_i}{\partial y} A_{26}^{\alpha\beta} \frac{\partial\varphi_j}{\partial y}\right) + \left(\frac{\partial\varphi_i}{\partial y} A_{66}^{\alpha\beta} \frac{\partial\varphi_j}{\partial x}\right) + \left(\varphi_i \bar{\bar{A}}_{45}^{\alpha\beta} \varphi_j\right) - \left(\varphi_i \bar{A}_{45}^{\beta\alpha} \frac{\varphi_j}{R}\right) \right] dx\, dy$$

$$\left[{}^{21}K_{ij}^{\alpha\beta}\right] = \int_{\Omega_e} \left[\left(\frac{\partial\varphi_i}{\partial y} A_{12}^{\alpha\beta} \frac{\partial\varphi_j}{\partial x}\right) + \left(\frac{\partial\varphi_i}{\partial x} A_{16}^{\alpha\beta} \frac{\partial\varphi_j}{\partial x}\right) + \left(\frac{\partial\varphi_i}{\partial y} A_{26}^{\alpha\beta} \frac{\partial\varphi_j}{\partial y}\right) + \left(\frac{\partial\varphi_i}{\partial x} A_{66}^{\alpha\beta} \frac{\partial\varphi_j}{\partial y}\right) + \left(\varphi_i \bar{\bar{A}}_{45}^{\alpha\beta} \varphi_j\right) - \left(\frac{\varphi_i}{R} \bar{A}_{45}^{\alpha\beta} \varphi_j\right) \right] dx\, dy$$

$$\left[{}^{22}K_{ij}^{\alpha\beta}\right] = \int_{\Omega_e} \left[\left(\frac{\partial\varphi_i}{\partial y} A_{22}^{\alpha\beta} \frac{\partial\varphi_j}{\partial y}\right) + \left(\frac{\partial\varphi_i}{\partial y} A_{26}^{\alpha\beta} \frac{\partial\varphi_j}{\partial x}\right) + \left(\frac{\partial\varphi_i}{\partial x} A_{26}^{\alpha\beta} \frac{\partial\varphi_j}{\partial y}\right) + \left(\frac{\partial\varphi_i}{\partial x} A_{66}^{\alpha\beta} \frac{\partial\varphi_j}{\partial x}\right) + \left(\varphi_i \bar{\bar{A}}_{44}^{\alpha\beta} \varphi_j\right) - \left(\varphi_i \bar{A}_{44}^{\beta\alpha} \frac{\varphi_j}{R}\right) - \left(\frac{\varphi_i}{R} \bar{A}_{44}^{\alpha\beta} \varphi_j\right) + \left(\frac{\varphi_i}{R^2} A_{44}^{\alpha\beta} \varphi_j\right) \right] dx\, dy$$

$$\left[{}^{13}K_{ij}^{\alpha\beta}\right] = \int_{\Omega_e} \Big[\left(\frac{\partial \varphi_i}{\partial x} A_{12}^{\alpha\beta} \frac{\varphi_j}{R}\right) + \left(\frac{\partial \varphi_i}{\partial x} \overline{A}_{13}^{\alpha\beta} \varphi_j\right) + \left(\frac{\partial \varphi_i}{\partial y} A_{26}^{\alpha\beta} \frac{\varphi_j}{R}\right) + \left(\frac{\partial \varphi_i}{\partial y} \overline{A}_{36}^{\alpha\beta} \varphi_j\right)$$

$$+ \left(\varphi_i \overline{A}_{55}^{\beta\alpha} \frac{\partial \varphi_j}{\partial x}\right) + \left(\varphi_i \overline{A}_{45}^{\beta\alpha} \frac{\partial \varphi_j}{\partial y}\right)$$

$$+ \frac{\partial \varphi_i}{\partial x} D_{11}^{\alpha\beta\gamma} \frac{\partial \varphi_j}{\partial x} \left(\frac{\partial w_\gamma}{\partial x} + \frac{\partial \hat{w}_\gamma}{\partial x}\right) + \frac{\partial \varphi_i}{\partial x} D_{12}^{\alpha\beta\gamma} \frac{\partial \varphi_j}{\partial y} \left(\frac{\partial w_\gamma}{\partial y} + \frac{\partial \hat{w}_\gamma}{\partial y}\right)$$

$$+ 2 \frac{\partial \varphi_i}{\partial x} D_{16}^{\alpha\beta\gamma} \frac{\partial \varphi_j}{\partial x} \left(\frac{\partial w_\gamma}{\partial y} + \frac{\partial \hat{w}_\gamma}{\partial y}\right) + \frac{\partial \varphi_i}{\partial y} D_{16}^{\alpha\beta\gamma} \frac{\partial \varphi_j}{\partial x} \left(\frac{\partial w_\gamma}{\partial x} + \frac{\partial \hat{w}_\gamma}{\partial x}\right)$$

$$+ \frac{\partial \varphi_i}{\partial y} D_{26}^{\alpha\beta\gamma} \frac{\partial \varphi_j}{\partial y} \left(\frac{\partial w_\gamma}{\partial y} + \frac{\partial \hat{w}_\gamma}{\partial y}\right) + 2 \frac{\partial \varphi_i}{\partial y} D_{66}^{\alpha\beta\gamma} \frac{\partial \varphi_j}{\partial x} \left(\frac{\partial w_\gamma}{\partial y} + \frac{\partial \hat{w}_\gamma}{\partial y}\right) \Big] dx\, dy$$

$$\left[{}^{31}K_{ij}^{\alpha\beta}\right] = \int_{\Omega_e} \Big[\left(\frac{\varphi_i}{R} A_{12}^{\alpha\beta} \frac{\partial \varphi_j}{\partial x}\right) + \left(\varphi_i \overline{A}_{13}^{\beta\alpha} \frac{\partial \varphi_j}{\partial x}\right) + \left(\frac{\varphi_i}{R} A_{26}^{\alpha\beta} \frac{\partial \varphi_j}{\partial y}\right) + \left(\varphi_i \overline{A}_{36}^{\beta\alpha} \frac{\partial \varphi_j}{\partial y}\right)$$

$$+ \left(\frac{\partial \varphi_i}{\partial x} \overline{A}_{55}^{\alpha\beta} \varphi_j\right) + \left(\frac{\partial \varphi_i}{\partial y} \overline{A}_{45}^{\alpha\beta} \varphi_j\right)$$

$$+ \frac{\partial \varphi_i}{\partial x} D_{11}^{\alpha\beta\gamma} \frac{\partial \varphi_j}{\partial x} \left(\frac{\partial w_\gamma}{\partial x} + \frac{\partial \hat{w}_\gamma}{\partial x}\right) + \frac{\partial \varphi_i}{\partial y} D_{12}^{\alpha\beta\gamma} \frac{\partial \varphi_j}{\partial x} \left(\frac{\partial w_\gamma}{\partial y} + \frac{\partial \hat{w}_\gamma}{\partial y}\right)$$

$$+ \frac{\partial \varphi_i}{\partial x} D_{16}^{\alpha\beta\gamma} \frac{\partial \varphi_j}{\partial y} \left(\frac{\partial w_\gamma}{\partial x} + \frac{\partial \hat{w}_\gamma}{\partial x}\right) + \frac{\partial \varphi_i}{\partial y} D_{26}^{\alpha\beta\gamma} \frac{\partial \varphi_j}{\partial y} \left(\frac{\partial w_\gamma}{\partial y} + \frac{\partial \hat{w}_\gamma}{\partial y}\right)$$

$$+ \frac{\partial \varphi_j}{\partial x} D_{16}^{\alpha\beta\gamma} \left(\frac{\partial \varphi_i}{\partial x} \left(\frac{\partial w_\gamma}{\partial y} + \frac{\partial \hat{w}_\gamma}{\partial y}\right) + \frac{\partial \varphi_i}{\partial y} \left(\frac{\partial w_\gamma}{\partial x} + \frac{\partial \hat{w}_\gamma}{\partial x}\right)\right)$$

$$+ \frac{\partial \varphi_j}{\partial x} D_{66}^{\alpha\beta\gamma} \left(\frac{\partial \varphi_i}{\partial x} \left(\frac{\partial w_\gamma}{\partial y} + \frac{\partial \hat{w}_\gamma}{\partial y}\right) + \frac{\partial \varphi_i}{\partial y} \left(\frac{\partial w_\gamma}{\partial x} + \frac{\partial \hat{w}_\gamma}{\partial x}\right)\right) \Big] \; dx\, dy$$

$$\left[{}^{23}K_{ij}^{\alpha\beta}\right] = \int_{\Omega_e} \Big[\left(\frac{\partial\varphi_i}{\partial y} A_{22}^{\alpha\beta} \frac{\varphi_j}{R}\right) + \left(\frac{\partial\varphi_i}{\partial y} \overline{A}_{23}^{\alpha\beta} \varphi_j\right) + \left(\frac{\partial\varphi_i}{\partial x} A_{26}^{\alpha\beta} \frac{\varphi_j}{R}\right) + \left(\frac{\partial\varphi_i}{\partial x} \overline{A}_{36}^{\alpha\beta} \varphi_j\right)$$

$$+ \left(\varphi_i \overline{A}_{45}^{\beta\alpha} \frac{\partial\varphi_j}{\partial x}\right) + \left(\varphi_i \overline{A}_{44}^{\beta\alpha} \frac{\partial\varphi_j}{\partial y}\right) - \left(\frac{\varphi_i}{R} A_{45}^{\alpha\beta} \frac{\partial\varphi_j}{\partial x}\right) - \left(\frac{\varphi_i}{R} A_{44}^{\alpha\beta} \frac{\partial\varphi_j}{\partial y}\right)$$

$$+ \frac{\partial\varphi_i}{\partial y} D_{12}^{\alpha\beta\gamma} \frac{\partial\varphi_j}{\partial x} \left(\frac{\partial w_\gamma}{\partial x} + \frac{\partial\hat{w}_\gamma}{\partial x}\right) + \frac{\partial\varphi_i}{\partial y} D_{22}^{\alpha\beta\gamma} \frac{\partial\varphi_j}{\partial y} \left(\frac{\partial w_\gamma}{\partial y} + \frac{\partial\hat{w}_\gamma}{\partial y}\right)$$

$$+ \frac{\partial\varphi_i}{\partial x} D_{16}^{\alpha\beta\gamma} \frac{\partial\varphi_j}{\partial x} \left(\frac{\partial w_\gamma}{\partial x} + \frac{\partial\hat{w}_\gamma}{\partial x}\right) + 2 \frac{\partial\varphi_i}{\partial y} D_{26}^{\alpha\beta\gamma} \frac{\partial\varphi_j}{\partial x} \left(\frac{\partial w_\gamma}{\partial y} + \frac{\partial\hat{w}_\gamma}{\partial y}\right)$$

$$+ \frac{\partial\varphi_i}{\partial x} D_{26}^{\alpha\beta\gamma} \frac{\partial\varphi_j}{\partial y} \left(\frac{\partial w_\gamma}{\partial y} + \frac{\partial\hat{w}_\gamma}{\partial y}\right) + 2 \frac{\partial\varphi_i}{\partial x} D_{66}^{\alpha\beta\gamma} \frac{\partial\varphi_j}{\partial x} \left(\frac{\partial w_\gamma}{\partial y} + \frac{\partial\hat{w}_\gamma}{\partial y}\right) dx\, dy$$

$$\left[{}^{32}K_{ij}^{\alpha\beta}\right] = \int_{\Omega_e} \Big[\left(\frac{\varphi_i}{R} A_{22}^{\alpha\beta} \frac{\partial\varphi_j}{\partial y}\right) + \left(\varphi_i \overline{A}_{23}^{\beta\alpha} \frac{\partial\varphi_j}{\partial y}\right) + \left(\frac{\varphi_i}{R} A_{26}^{\alpha\beta} \frac{\partial\varphi_j}{\partial x}\right) + \left(\varphi_i \overline{A}_{36}^{\beta\alpha} \frac{\partial\varphi_j}{\partial x}\right)$$

$$+ \left(\frac{\partial\varphi_i}{\partial y} \overline{A}_{44}^{\alpha\beta} \varphi_j\right) + \left(\frac{\partial\varphi_i}{\partial x} \overline{A}_{54}^{\alpha\beta} \varphi_j\right) - \left(\frac{\partial\varphi_i}{\partial y} A_{44}^{\alpha\beta} \frac{\varphi_j}{R}\right) - \left(\frac{\partial\varphi_i}{\partial x} A_{45}^{\alpha\beta} \frac{\varphi_j}{R}\right)$$

$$+ \frac{\partial\varphi_i}{\partial x} D_{12}^{\alpha\beta\gamma} \frac{\partial\varphi_j}{\partial y} \left(\frac{\partial w_\gamma}{\partial x} + \frac{\partial\hat{w}_\gamma}{\partial x}\right) + \frac{\partial\varphi_i}{\partial y} D_{22}^{\alpha\beta\gamma} \frac{\partial\varphi_j}{\partial y} \left(\frac{\partial w_\gamma}{\partial y} + \frac{\partial\hat{w}_\gamma}{\partial y}\right)$$

$$+ \frac{\partial\varphi_i}{\partial x} D_{16}^{\alpha\beta\gamma} \frac{\partial\varphi_j}{\partial x} \left(\frac{\partial w_\gamma}{\partial x} + \frac{\partial\hat{w}_\gamma}{\partial x}\right) + \frac{\partial\varphi_i}{\partial y} D_{26}^{\alpha\beta\gamma} \frac{\partial\varphi_j}{\partial x} \left(\frac{\partial w_\gamma}{\partial y} + \frac{\partial\hat{w}_\gamma}{\partial y}\right)$$

$$+ \frac{\partial\varphi_j}{\partial y} D_{26}^{\alpha\beta\gamma} \left(\frac{\partial\varphi_i}{\partial x} \left(\frac{\partial w_\gamma}{\partial y} + \frac{\partial\hat{w}_\gamma}{\partial y}\right) + \frac{\partial\varphi_i}{\partial y} \left(\frac{\partial w_\gamma}{\partial x} + \frac{\partial\hat{w}_\gamma}{\partial x}\right)\right)$$

$$+ \frac{\partial\varphi_j}{\partial x} D_{66}^{\alpha\beta\gamma} \left(\frac{\partial\varphi_i}{\partial x} \left(\frac{\partial w_\gamma}{\partial y} + \frac{\partial\hat{w}_\gamma}{\partial y}\right) + \frac{\partial\varphi_i}{\partial y} \left(\frac{\partial w_\gamma}{\partial x} + \frac{\partial\hat{w}_\gamma}{\partial x}\right)\right)\Big] dx\, dy$$

$$\left[{}^{33}K_{ij}^{\alpha\beta}\right] = \int_{\Omega_e} \Big[\left(\frac{\varphi_i}{R^2} A_{22}^{\alpha\beta} \varphi_j\right) + \left(\frac{\varphi_i}{R} \overline{A}_{23}^{\alpha\beta} \varphi_j\right) + \left(\frac{\varphi_i}{R} \overline{A}_{23}^{\beta\alpha} \varphi_j\right) + \left(\varphi_i \overline{\overline{A}}_{33}^{\alpha\beta} \varphi_j\right)$$

$$+ \left(\frac{\partial\varphi_i}{\partial x} A_{55}^{\beta\alpha} \frac{\partial\varphi_j}{\partial x}\right) + \left(\frac{\partial\varphi_i}{\partial x} A_{45}^{\alpha\beta} \frac{\partial\varphi_j}{\partial y}\right) + \left(\frac{\partial\varphi_i}{\partial y} A_{45}^{\alpha\beta} \frac{\partial\varphi_j}{\partial x}\right)$$

$$+ \left(\frac{\partial\varphi_i}{\partial y} A_{44}^{\alpha\beta} \frac{\partial\varphi_j}{\partial y}\right)$$

$$+ \frac{\partial\varphi_i}{\partial x} D_{11}^{\alpha\beta\gamma} \frac{\partial\varphi_j}{\partial x} \frac{\partial u_\gamma}{\partial x} + \frac{\partial\varphi_i}{\partial y} D_{12}^{\alpha\beta\gamma} \frac{\partial\varphi_j}{\partial x} \frac{\partial u_\gamma}{\partial y}$$

$$+ \frac{\partial\varphi_i}{\partial x} D_{16}^{\alpha\beta\gamma} \frac{\partial\varphi_j}{\partial y} \frac{\partial u_\gamma}{\partial x} + \frac{\partial\varphi_i}{\partial y} D_{26}^{\alpha\beta\gamma} \frac{\partial\varphi_j}{\partial y} \frac{\partial u_\gamma}{\partial y}$$

$$+ \frac{\partial\varphi_j}{\partial x} D_{16}^{\alpha\beta\gamma} \left(\frac{\partial\varphi_i}{\partial x} \frac{\partial u_\gamma}{\partial y} + \frac{\partial\varphi_i}{\partial y} \frac{\partial u_\gamma}{\partial x}\right)$$

$$+ \frac{\partial\varphi_j}{\partial y} D_{66}^{\alpha\beta\gamma} \left(\frac{\partial\varphi_i}{\partial x} \frac{\partial u_\gamma}{\partial y} + \frac{\partial\varphi_i}{\partial y} \frac{\partial u_\gamma}{\partial x}\right)$$

$$+ \frac{\partial\varphi_i}{\partial x} D_{12}^{\alpha\beta\gamma} \frac{\partial\varphi_j}{\partial y} \frac{\partial v_\gamma}{\partial x} + \frac{\partial\varphi_i}{\partial y} D_{22}^{\alpha\beta\gamma} \frac{\partial\varphi_j}{\partial y} \frac{\partial v_\gamma}{\partial y}$$

$$+ \frac{\partial\varphi_i}{\partial x} D_{16}^{\alpha\beta\gamma} \frac{\partial\varphi_j}{\partial x} \frac{\partial v_\gamma}{\partial x} + \frac{\partial\varphi_i}{\partial y} D_{26}^{\alpha\beta\gamma} \frac{\partial\varphi_j}{\partial x} \frac{\partial v_\gamma}{\partial y}$$

$$+ \frac{\partial\varphi_j}{\partial y} D_{26}^{\alpha\beta\gamma} \left(\frac{\partial\varphi_i}{\partial x} \frac{\partial v_\gamma}{\partial y} + \frac{\partial\varphi_i}{\partial y} \frac{\partial v_\gamma}{\partial x}\right)$$

$$+ \frac{\partial\varphi_j}{\partial y} D_{66}^{\alpha\beta\gamma} \left(\frac{\partial\varphi_i}{\partial x} \frac{\partial v_\gamma}{\partial y} + \frac{\partial\varphi_i}{\partial y} \frac{\partial v_\gamma}{\partial x}\right)$$

$$+ \frac{1}{2R} \varphi_i D_{12}^{\alpha\beta\gamma} \frac{\partial\varphi_j}{\partial x} \left(\frac{\partial w_\gamma}{\partial x} + 2\frac{\partial\hat{w}_\gamma}{\partial x}\right) + \frac{1}{2R} \varphi_i D_{22}^{\alpha\beta\gamma} \frac{\partial\varphi_j}{\partial y} \left(\frac{\partial w_\gamma}{\partial y} + 2\frac{\partial\hat{w}_\gamma}{\partial y}\right)$$

$$+ \frac{1}{R} \varphi_i D_{26}^{\alpha\beta\gamma} \frac{\partial\varphi_j}{\partial x} \left(\frac{\partial w_\gamma}{\partial y} + \frac{\partial\hat{w}_\gamma}{\partial y}\right) + \frac{1}{2} \varphi_i \overline{D}_{13}^{\beta\gamma\alpha} \frac{\partial\varphi_j}{\partial x} \left(\frac{\partial w_\gamma}{\partial x} + 2\frac{\partial\hat{w}_\gamma}{\partial x}\right)$$

$$+ \frac{1}{2} \varphi_i \overline{D}_{23}^{\beta\gamma\alpha} \frac{\partial\varphi_j}{\partial y} \left(\frac{\partial w_\gamma}{\partial y} + 2\frac{\partial\hat{w}_\gamma}{\partial y}\right) + \varphi_i \overline{D}_{36}^{\beta\gamma\alpha} \frac{\partial\varphi_j}{\partial x} \left(\frac{\partial w_\gamma}{\partial y} + \frac{\partial\hat{w}_\gamma}{\partial y}\right)$$

$$+\frac{1}{R}\frac{\partial\varphi_i}{\partial x}D_{12}^{\alpha\beta\gamma}\varphi_j\left(\frac{\partial w_\gamma}{\partial x}+\frac{\partial\hat{w}_\gamma}{\partial x}\right)+\frac{\partial\varphi_i}{\partial x}\overline{D}_{13}^{\alpha\beta\gamma}\varphi_j\left(\frac{\partial w_\gamma}{\partial x}+\frac{\partial\hat{w}_\gamma}{\partial x}\right)$$

$$+\frac{1}{R}\frac{\partial\varphi_i}{\partial y}D_{22}^{\alpha\beta\gamma}\varphi_j\left(\frac{\partial w_\gamma}{\partial y}+\frac{\partial\hat{w}_\gamma}{\partial y}\right)+\frac{\partial\varphi_i}{\partial y}\overline{D}_{23}^{\alpha\beta\gamma}\varphi_j\left(\frac{\partial w_\gamma}{\partial y}+\frac{\partial\hat{w}_\gamma}{\partial y}\right)$$

$$+\left(\frac{\partial\varphi_i}{\partial x}\left(\frac{\partial w_\gamma}{\partial y}+\frac{\partial\hat{w}_\gamma}{\partial y}\right)+\frac{\partial\varphi_i}{\partial y}\left(\frac{\partial w_\gamma}{\partial x}+\frac{\partial\hat{w}_\gamma}{\partial x}\right)\right)D_{26}^{\alpha\beta\gamma}\frac{\varphi_j}{R}$$

$$+\left(\frac{\partial\varphi_i}{\partial x}\left(\frac{\partial w_\gamma}{\partial y}+\frac{\partial\hat{w}_\gamma}{\partial y}\right)+\frac{\partial\varphi_i}{\partial y}\left(\frac{\partial w_\gamma}{\partial x}+\frac{\partial\hat{w}_\gamma}{\partial x}\right)\right)\overline{D}_{36}^{\alpha\beta\gamma}\varphi_j$$

$$+\frac{1}{2}\frac{\partial\varphi_i}{\partial x}F_{11}^{\alpha\beta\gamma\rho}\frac{\partial\varphi_j}{\partial x}\left(\frac{\partial w_\gamma}{\partial x}+\frac{\partial\hat{w}_\gamma}{\partial x}\right)\left(\frac{\partial w_\rho}{\partial x}+2\frac{\partial\hat{w}_\rho}{\partial x}\right)$$

$$+\frac{1}{2}\frac{\partial\varphi_i}{\partial x}F_{12}^{\alpha\beta\gamma\rho}\frac{\partial\varphi_j}{\partial y}\left(\frac{\partial w_\gamma}{\partial x}+\frac{\partial\hat{w}_\gamma}{\partial x}\right)\left(\frac{\partial w_\rho}{\partial y}+2\frac{\partial\hat{w}_\rho}{\partial y}\right)$$

$$+\frac{1}{2}\frac{\partial\varphi_i}{\partial x}F_{16}^{\alpha\beta\gamma\rho}\left(\frac{\partial w_\gamma}{\partial x}+\frac{\partial\hat{w}_\gamma}{\partial x}\right)\left(\frac{\partial\varphi_j}{\partial x}\left(\frac{\partial w_\rho}{\partial y}+2\frac{\partial\hat{w}_\rho}{\partial y}\right)+\frac{\partial\varphi_j}{\partial y}\left(\frac{\partial w_\rho}{\partial x}+2\frac{\partial\hat{w}_\rho}{\partial x}\right)\right)$$

$$+\frac{1}{2}\frac{\partial\varphi_i}{\partial y}F_{12}^{\alpha\beta\gamma\rho}\frac{\partial\varphi_j}{\partial x}\left(\frac{\partial w_\gamma}{\partial y}+\frac{\partial\hat{w}_\gamma}{\partial y}\right)\left(\frac{\partial w_\rho}{\partial x}+2\frac{\partial\hat{w}_\rho}{\partial x}\right)$$

$$+\frac{1}{2}\frac{\partial\varphi_i}{\partial y}F_{22}^{\alpha\beta\gamma\rho}\frac{\partial\varphi_j}{\partial y}\left(\frac{\partial w_\gamma}{\partial y}+\frac{\partial\hat{w}_\gamma}{\partial y}\right)\left(\frac{\partial w_\rho}{\partial y}+2\frac{\partial\hat{w}_\rho}{\partial y}\right)$$

$$+\frac{1}{2}\frac{\partial\varphi_i}{\partial y}F_{26}^{\alpha\beta\gamma\rho}\left(\frac{\partial w_\gamma}{\partial y}+\frac{\partial\hat{w}_\gamma}{\partial y}\right)\left(\frac{\partial\varphi_j}{\partial x}\left(\frac{\partial w_\rho}{\partial y}+2\frac{\partial\hat{w}_\rho}{\partial y}\right)+\frac{\partial\varphi_j}{\partial y}\left(\frac{\partial w_\rho}{\partial x}+2\frac{\partial\hat{w}_\rho}{\partial x}\right)\right)$$

$$+\left(\frac{\partial\varphi_i}{\partial x}\left(\frac{\partial w_\gamma}{\partial y}+\frac{\partial\hat{w}_\gamma}{\partial y}\right)+\frac{\partial\varphi_i}{\partial y}\left(\frac{\partial w_\gamma}{\partial x}+\frac{\partial\hat{w}_\gamma}{\partial x}\right)\right)F_{16}^{\alpha\beta\gamma\rho}\frac{\partial\varphi_j}{\partial x}\left(\frac{\partial w_\rho}{\partial x}+2\frac{\partial\hat{w}_\rho}{\partial x}\right)$$

$$+\left(\frac{\partial\varphi_i}{\partial x}\left(\frac{\partial w_\gamma}{\partial y}+\frac{\partial\hat{w}_\gamma}{\partial y}\right)+\frac{\partial\varphi_i}{\partial y}\left(\frac{\partial w_\gamma}{\partial x}+\frac{\partial\hat{w}_\gamma}{\partial x}\right)\right)F_{26}^{\alpha\beta\gamma\rho}\frac{\partial\varphi_j}{\partial y}\left(\frac{\partial w_\rho}{\partial y}+2\frac{\partial\hat{w}_\rho}{\partial y}\right)$$

$$+\left(\frac{\partial\varphi_i}{\partial x}\left(\frac{\partial w_\gamma}{\partial y}+\frac{\partial\hat{w}_\gamma}{\partial y}\right)+\frac{\partial\varphi_i}{\partial y}\left(\frac{\partial w_\gamma}{\partial x}+\frac{\partial\hat{w}_\gamma}{\partial x}\right)\right)$$

$$x\{F_{66}^{\alpha\beta\gamma\rho}\left(\frac{\partial\varphi_j}{\partial x}\left(\frac{\partial w_\rho}{\partial y}+2\frac{\partial\hat{w}_\rho}{\partial y}\right)+\frac{\partial\varphi_j}{\partial y}\left(\frac{\partial w_\rho}{\partial x}+2\frac{\partial\hat{w}_\rho}{\partial x}\right)\right)\}$$

$$+\frac{1}{2R}\varphi_i D_{12}^{\alpha\gamma\beta}\frac{\partial\varphi_j}{\partial x}\frac{\partial w_\gamma}{\partial x}+\frac{1}{2R}\varphi_i D_{22}^{\alpha\gamma\beta}\frac{\partial\varphi_j}{\partial y}\frac{\partial w_\gamma}{\partial y}+\frac{1}{R}\varphi_i D_{26}^{\alpha\gamma\beta}\frac{\partial\varphi_j}{\partial x}\frac{\partial w_\gamma}{\partial y}$$

$$+\frac{1}{2}\varphi_i \overline{D}_{13}^{\beta\alpha\gamma}\frac{\partial\varphi_j}{\partial x}\frac{\partial w_\gamma}{\partial x}+\frac{1}{2}\varphi_i \overline{D}_{23}^{\beta\alpha\gamma}\frac{\partial\varphi_j}{\partial y}\frac{\partial w_\gamma}{\partial y}+\varphi_i \overline{D}_{36}^{\beta\alpha\gamma}\frac{\partial\varphi_j}{\partial x}\frac{\partial w_\gamma}{\partial y}$$

$$+\frac{1}{R}\frac{\partial\varphi_i}{\partial x}D_{12}^{\alpha\beta\gamma}\varphi_j\frac{\partial w_\gamma}{\partial x}+\frac{\partial\varphi_i}{\partial x}\overline{D}_{13}^{\alpha\gamma\beta}\varphi_j\frac{\partial w_\gamma}{\partial x}+\frac{1}{R}\frac{\partial\varphi_i}{\partial y}D_{22}^{\alpha\beta\gamma}\varphi_j\frac{\partial w_\gamma}{\partial y}$$

$$+\frac{\partial\varphi_i}{\partial y}\overline{D}_{23}^{\alpha\gamma\beta}\varphi_j\frac{\partial w_\gamma}{\partial y}+\left(\frac{\partial\varphi_i}{\partial x}\frac{\partial w_\gamma}{\partial y}+\frac{\partial\varphi_i}{\partial y}\frac{\partial w_\gamma}{\partial x}\right)D_{26}^{\alpha\gamma\beta}\frac{\varphi_j}{R}$$

$$+\left(\frac{\partial\varphi_i}{\partial x}\frac{\partial w_\gamma}{\partial y}+\frac{\partial\varphi_i}{\partial y}\frac{\partial w_\gamma}{\partial x}\right)\overline{D}_{36}^{\alpha\gamma\beta}\varphi_j$$

$$+\frac{1}{2}\frac{\partial\varphi_i}{\partial x}F_{11}^{\alpha\gamma\beta\rho}\frac{\partial\varphi_j}{\partial x}\frac{\partial w_\gamma}{\partial x}\left(\frac{\partial w_\rho}{\partial x}+\frac{\partial\hat{w}_\rho}{\partial x}\right)$$

$$+\frac{1}{2}\frac{\partial\varphi_i}{\partial x}F_{12}^{\alpha\gamma\beta\rho}\frac{\partial\varphi_j}{\partial y}\frac{\partial w_\gamma}{\partial y}\left(\frac{\partial w_\rho}{\partial x}+\frac{\partial\hat{w}_\rho}{\partial x}\right)$$

$$+\frac{1}{2}\frac{\partial\varphi_i}{\partial x}F_{16}^{\alpha\gamma\beta\rho}\left(\frac{\partial\varphi_j}{\partial x}\frac{\partial w_\gamma}{\partial y}+\frac{\partial\varphi_j}{\partial y}\frac{\partial w_\gamma}{\partial x}\right)\left(\frac{\partial w_\rho}{\partial x}+\frac{\partial\hat{w}_\rho}{\partial x}\right)$$

$$+\frac{1}{2}\frac{\partial\varphi_i}{\partial y}F_{12}^{\alpha\gamma\beta\rho}\frac{\partial\varphi_j}{\partial x}\frac{\partial w_\gamma}{\partial x}\left(\frac{\partial w_\rho}{\partial y}+\frac{\partial\hat{w}_\rho}{\partial y}\right)$$

$$+\frac{1}{2}\frac{\partial\varphi_i}{\partial y}F_{22}^{\alpha\gamma\beta\rho}\frac{\partial\varphi_j}{\partial y}\frac{\partial w_\gamma}{\partial y}\left(\frac{\partial w_\rho}{\partial y}+\frac{\partial\hat{w}_\rho}{\partial y}\right)$$

$$+\frac{1}{2}\frac{\partial\varphi_i}{\partial y}F_{26}^{\alpha\gamma\beta\rho}\left(\frac{\partial\varphi_j}{\partial x}\frac{\partial w_\gamma}{\partial y}+\frac{\partial\varphi_j}{\partial y}\frac{\partial w_\gamma}{\partial x}\right)\left(\frac{\partial w_\rho}{\partial y}+\frac{\partial\hat{w}_\rho}{\partial y}\right)$$

$$+\frac{1}{2}\left(\frac{\partial\varphi_i}{\partial x}\frac{\partial w_\gamma}{\partial y}+\frac{\partial\varphi_i}{\partial y}\frac{\partial w_\gamma}{\partial x}\right)F_{16}^{\alpha\gamma\beta\rho}\frac{\partial\varphi_j}{\partial x}\left(\frac{\partial w_\rho}{\partial x}+\frac{\partial\hat{w}_\rho}{\partial x}\right)$$

$$+\frac{1}{2}\left(\frac{\partial\varphi_i}{\partial x}\frac{\partial w_\gamma}{\partial y}+\frac{\partial\varphi_i}{\partial y}\frac{\partial w_\gamma}{\partial x}\right)F_{26}^{\alpha\gamma\beta\rho}\frac{\partial\varphi_j}{\partial y}\left(\frac{\partial w_\rho}{\partial y}+\frac{\partial\hat{w}_\rho}{\partial y}\right)$$

$$+\frac{1}{2}\left(\frac{\partial\varphi_i}{\partial x}\frac{\partial w_\gamma}{\partial y}+\frac{\partial\varphi_i}{\partial y}\frac{\partial w_\gamma}{\partial x}\right)F_{66}^{\alpha\gamma\beta\rho}$$

$$x\left(\frac{\partial\varphi_j}{\partial x}\left(\frac{\partial w_\rho}{\partial y}+\frac{\partial\hat{w}_\rho}{\partial y}\right)+\frac{\partial\varphi_j}{\partial y}\left(\frac{\partial w_\rho}{\partial y}+\frac{\partial\hat{w}_\rho}{\partial y}\right)\right)$$

$$+\frac{1}{2}\frac{\partial\varphi_i}{\partial x}F_{11}^{\alpha\gamma\rho\beta}\frac{\partial\varphi_j}{\partial x}\frac{\partial w_\gamma}{\partial x}\left(\frac{\partial w_\rho}{\partial x}+2\frac{\partial\hat{w}_\rho}{\partial x}\right)$$

$$+\frac{1}{2}\frac{\partial\varphi_i}{\partial x}F_{12}^{\alpha\gamma\rho\beta}\frac{\partial\varphi_j}{\partial y}\frac{\partial w_\gamma}{\partial y}\left(\frac{\partial w_\rho}{\partial x}+2\frac{\partial\hat{w}_\rho}{\partial x}\right)$$

$$+\frac{1}{2}\frac{\partial\varphi_i}{\partial x}F_{16}^{\alpha\gamma\rho\beta}\left(\frac{\partial\varphi_j}{\partial x}\frac{\partial w_\gamma}{\partial y}+\frac{\partial\varphi_j}{\partial y}\frac{\partial w_\gamma}{\partial x}\right)\left(\frac{\partial w_\rho}{\partial x}+2\frac{\partial\hat{w}_\rho}{\partial x}\right)$$

$$+\frac{1}{2}\frac{\partial\varphi_i}{\partial y}F_{12}^{\alpha\gamma\rho\beta}\frac{\partial\varphi_j}{\partial x}\frac{\partial w_\gamma}{\partial x}\left(\frac{\partial w_\rho}{\partial y}+2\frac{\partial\hat{w}_\rho}{\partial y}\right)$$

$$+\frac{1}{2}\frac{\partial\varphi_i}{\partial y}F_{22}^{\alpha\gamma\rho\beta}\frac{\partial\varphi_j}{\partial y}\frac{\partial w_\gamma}{\partial y}\left(\frac{\partial w_\rho}{\partial y}+2\frac{\partial\hat{w}_\rho}{\partial y}\right)$$

$$+\frac{1}{2}\frac{\partial\varphi_i}{\partial y}F_{26}^{\alpha\gamma\rho\beta}\left(\frac{\partial\varphi_j}{\partial x}\frac{\partial w_\gamma}{\partial y}+\frac{\partial\varphi_j}{\partial y}\frac{\partial w_\gamma}{\partial x}\right)\left(\frac{\partial w_\rho}{\partial y}+\frac{\partial\hat{w}_\rho}{\partial y}\right)$$

$$+\frac{1}{2}\left(\frac{\partial\varphi_i}{\partial x}\frac{\partial w_\gamma}{\partial y}+\frac{\partial\varphi_i}{\partial y}\frac{\partial w_\gamma}{\partial x}\right)F_{16}^{\alpha\gamma\rho\beta}\frac{\partial\varphi_j}{\partial x}\left(\frac{\partial w_\rho}{\partial x}+2\frac{\partial\hat{w}_\rho}{\partial x}\right)$$

$$+\frac{1}{2}\left(\frac{\partial\varphi_i}{\partial x}\frac{\partial w_\gamma}{\partial y}+\frac{\partial\varphi_i}{\partial y}\frac{\partial w_\gamma}{\partial x}\right)F_{26}^{\alpha\gamma\rho\beta}\frac{\partial\varphi_j}{\partial y}\left(\frac{\partial w_\rho}{\partial y}+2\frac{\partial\hat{w}_\rho}{\partial y}\right)$$

$$+\frac{1}{2}\left(\frac{\partial\varphi_i}{\partial x}\frac{\partial w_\gamma}{\partial y}+\frac{\partial\varphi_i}{\partial y}\frac{\partial w_\gamma}{\partial x}\right)$$

$$x\left\{F_{66}^{\alpha\gamma\rho\beta}\left(\frac{\partial\varphi_j}{\partial x}\left(\frac{\partial w_\rho}{\partial y}+2\frac{\partial\hat{w}_\rho}{\partial y}\right)+\frac{\partial\varphi_j}{\partial y}\left(\frac{\partial w_\rho}{\partial x}+2\frac{\partial\hat{w}_\rho}{\partial x}\right)\right)\right\}\Bigg]\,dx\,dy$$

APPENDIX C

The components of the nonlinear tangent stiffness matrix of a discrete layerwise shell stiffener element are given below. The tangent stiffness matrix given here is for a circumferential stiffener. For longitudinal stiffeners, the same matrix can be used by setting the radius equal to infinity. Note that initial imperfections are included in the formulation.

$$\left[{}^{11}K_{ij}^{\alpha\beta} \right] = \int_{\Omega_e} \left[\left(\frac{\partial \varphi_i}{\partial y} A_{11}^{\alpha\beta} \frac{\partial \varphi_j}{\partial y}\right) + \left(\varphi_i \bar{\bar{A}}_{44}^{\alpha\beta} \varphi_j\right) - \left(\varphi_i \bar{A}_{44}^{\beta\alpha} \frac{\varphi_j}{R}\right) - \left(\frac{\varphi_i}{R} \bar{A}_{44}^{\alpha\beta} \varphi_j\right) + \left(\frac{\varphi_i}{R^2} A_{44}^{\alpha\beta} \varphi_j\right) \right] dy$$

$$\left[{}^{12}K_{ij}^{\alpha\beta} \right] = \int_{\Omega_e} \left[\left(\frac{\partial \varphi_i}{\partial y} A_{11}^{\alpha\beta} \frac{\varphi_j}{R}\right) + \left(\frac{\partial \varphi_i}{\partial y} \bar{A}_{13}^{\alpha\beta} \varphi_j\right) + \left(\varphi_i \bar{A}_{44}^{\beta\alpha} \frac{\partial \varphi_j}{\partial y}\right) - \left(\frac{\varphi_i}{R} A_{44}^{\alpha\beta} \frac{\partial \varphi_j}{\partial y}\right) + \frac{\partial \varphi_i}{\partial y} D_{11}^{\alpha\beta\gamma} \frac{\partial \varphi_j}{\partial y} \left(\frac{\partial w_\gamma}{\partial y} + \frac{\partial \hat{w}_\gamma}{\partial y}\right) \right] dy$$

$$\left[{}^{21}K_{ij}^{\alpha\beta} \right] = \int_{\Omega_e} \left[\left(\frac{\varphi_i}{R} A_{11}^{\alpha\beta} \frac{\partial \varphi_j}{\partial y}\right) + \left(\varphi_i \bar{A}_{13}^{\beta\alpha} \frac{\partial \varphi_j}{\partial y}\right) + \left(\frac{\partial \varphi_i}{\partial y} \bar{A}_{44}^{\alpha\beta} \varphi_j\right) - \left(\frac{\partial \varphi_i}{\partial y} A_{44}^{\alpha\beta} \frac{\varphi_j}{R}\right) + \frac{\partial \varphi_i}{\partial y} D_{11}^{\alpha\beta\gamma} \frac{\partial \varphi_j}{\partial y} \left(\frac{\partial w_\gamma}{\partial y} + \frac{\partial \hat{w}_\gamma}{\partial y}\right) \right] dy$$

$$\left[{}^{22}\mathbf{K}_{ij}^{\alpha\beta}\right] = \int_{\Omega_e} \Big[\left(\frac{\varphi_i}{R^2} A_{11}^{\alpha\beta} \varphi_j\right) + \left(\frac{\varphi_i}{R} \overline{A}_{13}^{\alpha\beta} \varphi_j\right) + \left(\frac{\varphi_i}{R} \overline{A}_{13}^{\beta\alpha} \varphi_j\right) + \left(\varphi_i \overline{\overline{A}}_{33}^{\alpha\beta} \varphi_j\right)$$

$$+ \left(\frac{\partial \varphi_i}{\partial y} A_{44}^{\alpha\beta} \frac{\partial \varphi_j}{\partial y}\right) + \frac{1}{2R} \varphi_i D_{11}^{\alpha\beta\gamma} \frac{\partial \varphi_j}{\partial y} \left(\frac{\partial w_\gamma}{\partial y} + 2 \frac{\partial \hat{w}_\gamma}{\partial y}\right)$$

$$+ \frac{1}{2} \varphi_i \overline{D}_{13}^{\beta\gamma\alpha} \frac{\partial \varphi_j}{\partial y} \left(\frac{\partial w_\gamma}{\partial y} + 2 \frac{\partial \hat{w}_\gamma}{\partial y}\right) + \frac{1}{R} \frac{\partial \varphi_i}{\partial y} D_{11}^{\alpha\beta\gamma} \varphi_j \left(\frac{\partial w_\gamma}{\partial y} + \frac{\partial \hat{w}_\gamma}{\partial y}\right)$$

$$+ \frac{1}{2} \frac{\partial \varphi_i}{\partial y} F_{11}^{\alpha\beta\gamma\rho} \frac{\partial \varphi_j}{\partial y} \left(\frac{\partial w_\gamma}{\partial y} + \frac{\partial w_\gamma}{\partial y}\right) \left(\frac{\partial w_\rho}{\partial y} + \frac{\partial \hat{w}_\rho}{\partial y}\right)$$

$$+ \left(\frac{\partial \varphi_i}{\partial y} D_{11}^{\alpha\beta} \frac{\partial \varphi_j}{\partial y} \frac{\partial v_\gamma}{\partial y}\right) + \frac{1}{2R} \varphi_i D_{11}^{\alpha\beta\gamma} \frac{\partial \varphi_j}{\partial y} \frac{\partial w_\gamma}{\partial y}$$

$$+ \frac{1}{2} \varphi_i \overline{D}_{13}^{\beta\alpha\gamma} \frac{\partial \varphi_j}{\partial y} \frac{\partial w_\gamma}{\partial y} + \frac{1}{R} \frac{\partial \varphi_i}{\partial y} D_{11}^{\alpha\beta\gamma} \varphi_j \frac{\partial w_\gamma}{\partial y}$$

$$+ \frac{1}{2} \frac{\partial \varphi_i}{\partial y} F_{11}^{\alpha\gamma\beta\rho} \frac{\partial \varphi_j}{\partial y} \left(\frac{\partial w_\rho}{\partial y} + \frac{\partial \hat{w}_\rho}{\partial y}\right) \frac{\partial w_\gamma}{\partial y}$$

$$+ \frac{1}{2} \frac{\partial \varphi_i}{\partial y} F_{11}^{\alpha\gamma\rho\beta} \frac{\partial \varphi_j}{\partial y} \left(\frac{\partial w_\rho}{\partial y} + 2 \frac{\partial w_\rho}{\partial y}\right) \frac{\partial w_\gamma}{\partial y} \Big] \, dy$$

APPENDIX D

The components of the tangent stiffness matrix of the stiffeners using the stiffness averaging method is given below. These components are directly added to the corresponding coefficients in the shell stiffness matrix. The superscript n represents the interface number of the skin layer to which the stiffener is attached.

$$\left[{}^{11}K_{ij}^{nn} \right] = \int_{\Omega_e} \left(\frac{\partial \varphi_i}{\partial x} \frac{A_s E_s}{S_s} \frac{\partial \varphi_j}{\partial x} \right) dx\, dy$$

$$\left[{}^{12}K_{ij}^{nn} \right] = \left[{}^{21}K_{ij}^{nn} \right] = 0$$

$$\left[{}^{22}K_{ij}^{nn} \right] = \int_{\Omega_e} \left(\frac{\partial \varphi_i}{\partial y} \frac{A_r E_r}{S_r} \frac{\partial \varphi_j}{\partial y} \right) dx\, dy$$

$$\left[{}^{13}K_{ij}^{nn} \right] = \int_{\Omega_e} \left(\frac{\partial \varphi_i}{\partial x} \frac{\bar{Z}_s A_s E_s}{S_s} \frac{\partial \varphi_j}{\partial x} \frac{\partial w_n}{\partial x} \right) dx\, dy$$

$$\left[{}^{31}K_{ij}^{nn} \right] = \int_{\Omega_e} \left(\frac{\partial \varphi_i}{\partial x} \frac{\bar{Z}_s A_s E_s}{S_s} \frac{\partial \varphi_j}{\partial x} \frac{\partial w_n}{\partial x} \right) dx\, dy$$

$$\left[{}^{23}K_{ij}^{nn} \right] = \int_{\Omega_e} \left(\frac{\partial \varphi_i}{\partial y} \frac{\bar{Z}_r A_r E_r}{S_r} \frac{\partial \varphi_j}{\partial y} \frac{\partial w_n}{\partial y} \right) + \left(\frac{\partial \varphi_i}{\partial y} \frac{A_r E_r}{S_r} \frac{\varphi_j}{R} \right) dx\, dy$$

$$\left[{}^{32}K_{ij}^{nn} \right] = \int_{\Omega_e} \left(\frac{\partial \varphi_i}{\partial y} \frac{\bar{Z}_r A_r E_r}{S_r} \frac{\partial \varphi_j}{\partial y} \frac{\partial w_n}{\partial y} \right) + \left(\frac{\varphi_i}{R} \frac{A_r E_r}{S_r} \frac{\partial \varphi_j}{\partial y} \right) dx\, dy$$

$$\left[{}^{33}K_{ij}^{nn} \right] = \int_{\Omega_e} \left[\left(\frac{\varphi_i}{R^2} \frac{A_r E_r}{S_r} \varphi_j \right) + \left(\frac{\varphi_i}{R} \frac{\bar{Z}_r A_r E_r}{S_r} \frac{\partial \varphi_j}{\partial y} \frac{\partial w_n}{\partial y} \right) + \frac{\partial \varphi_i}{\partial x} \left(\frac{G_s J_s}{S_s} + \frac{G_r J_r}{S_r} \right) \right.$$
$$\times \left(\frac{\partial w_n}{\partial x} + \frac{\partial w_n}{\partial y} \right) \frac{\partial \varphi_j}{\partial x}$$
$$\left. + \frac{\partial \varphi_i}{\partial x} \frac{\partial \varphi_j}{\partial x} \frac{A_s E_s}{S_s} \left(\frac{\partial w_n}{\partial x} \right)^2 + \frac{\partial \varphi_i}{\partial y} \frac{\partial \varphi_j}{\partial y} \frac{A_r E_r}{S_r} \left(\frac{\partial w_n}{\partial y} \right)^2 \right] dx\, dy$$

APPENDIX E

The additional components of the element tangent stiffness matrix for a layerwise cylindrical shell element containing prescribed initial imperfections are given below.

$$\left[{}^{14}K_{ij}^{\alpha\beta}\right] = \int_{\Omega_e} \left[2\frac{\partial\varphi_i}{\partial x} D_{11}^{\alpha\beta\gamma} \frac{\partial\varphi_j}{\partial x}\frac{\partial w_\beta}{\partial x} + 2\frac{\partial\varphi_i}{\partial x} D_{12}^{\alpha\beta\gamma} \frac{\partial\varphi_j}{\partial y}\frac{\partial w_\beta}{\partial y} \right.$$
$$+ 2\frac{\partial\varphi_i}{\partial x} D_{16}^{\alpha\beta\gamma} \frac{\partial\varphi_j}{\partial y}\frac{\partial w_\beta}{\partial x} + 2\frac{\partial\varphi_i}{\partial y} D_{26}^{\alpha\beta\gamma} \frac{\partial\varphi_j}{\partial y}\frac{\partial w_\beta}{\partial y}$$
$$\left. + 2\frac{\partial\varphi_i}{\partial y} D_{16}^{\alpha\beta\gamma} \frac{\partial\varphi_j}{\partial x}\frac{\partial w_\beta}{\partial x} + \frac{\partial\varphi_i}{\partial y} D_{66}^{\alpha\beta\gamma} \frac{\partial\varphi_j}{\partial y}\frac{\partial w_\beta}{\partial x} \right] dx\, dy$$

$$\left[{}^{24}K_{ij}^{\alpha\beta}\right] = \int_{\Omega_e} \left[2\frac{\partial\varphi_i}{\partial y} D_{12}^{\alpha\beta\gamma} \frac{\partial\varphi_j}{\partial x}\frac{\partial w_\beta}{\partial x} + 2\frac{\partial\varphi_i}{\partial y} D_{22}^{\alpha\beta\gamma} \frac{\partial\varphi_j}{\partial y}\frac{\partial w_\beta}{\partial y} \right.$$
$$+ 2\frac{\partial\varphi_i}{\partial x} D_{16}^{\alpha\beta\gamma} \frac{\partial\varphi_j}{\partial x}\frac{\partial w_\beta}{\partial x} + 2\frac{\partial\varphi_i}{\partial y} D_{26}^{\alpha\beta\gamma} \frac{\partial\varphi_j}{\partial y}\frac{\partial w_\beta}{\partial x}$$
$$\left. + 2\frac{\partial\varphi_i}{\partial x} D_{16}^{\alpha\beta\gamma} \frac{\partial\varphi_j}{\partial y}\frac{\partial w_\beta}{\partial y} + \frac{\partial\varphi_i}{\partial x} D_{66}^{\alpha\beta\gamma} \frac{\partial\varphi_j}{\partial y}\frac{\partial w_\beta}{\partial x} \right] dx\, dy$$

$$\left[{}^{34}K_{ij}^{\alpha\beta}\right] = \int_{\Omega_e} \Bigg[\frac{1}{R}\varphi_i D_{12}^{\alpha\beta\gamma}\frac{\partial\varphi_j}{\partial x}\frac{\partial w_\beta}{\partial x} + \frac{1}{R}\varphi_i D_{22}^{\alpha\beta\gamma}\frac{\partial\varphi_j}{\partial y}\frac{\partial w_\beta}{\partial y} + \varphi_i \overline{D}_{13}^{\beta\gamma\alpha}\frac{\partial\varphi_j}{\partial x}\frac{\partial w_\beta}{\partial x}$$

$$+ \frac{1}{R}\varphi_i D_{26}^{\alpha\beta\gamma}\frac{\partial\varphi_j}{\partial y}\frac{\partial w_\beta}{\partial x} + \varphi_i \overline{D}_{23}^{\beta\gamma\alpha}\frac{\partial\varphi_j}{\partial y}\frac{\partial w_\beta}{\partial y} + \varphi_i \overline{D}_{36}^{\beta\gamma\alpha}\frac{\partial\varphi_j}{\partial y}\frac{\partial w_\beta}{\partial x}$$

$$+ 2\frac{\partial\varphi_i}{\partial x}F_{11}^{\alpha\beta\gamma\rho}\frac{\partial\varphi_j}{\partial x}\frac{\partial w_\gamma}{\partial x}\frac{\partial\hat{w}_\beta}{\partial x} + 2\frac{\partial\varphi_i}{\partial x}F_{12}^{\alpha\beta\gamma\rho}\frac{\partial\varphi_j}{\partial y}\frac{\partial w_\gamma}{\partial y}\frac{\partial\hat{w}_\beta}{\partial x}$$

$$+ 2\frac{\partial\varphi_i}{\partial x}F_{16}^{\alpha\beta\gamma\rho}\left(\frac{\partial\varphi_j}{\partial y}\frac{\partial w_\gamma}{\partial x} + \frac{\partial\varphi_j}{\partial x}\frac{\partial w_\gamma}{\partial y}\right)\frac{\partial\hat{w}_\beta}{\partial x}$$

$$+ 2\frac{\partial\varphi_i}{\partial y}F_{12}^{\alpha\beta\gamma\rho}\frac{\partial\varphi_j}{\partial x}\frac{\partial w_\gamma}{\partial x}\frac{\partial\hat{w}_\beta}{\partial y} + 2\frac{\partial\varphi_i}{\partial y}F_{22}^{\alpha\beta\gamma\rho}\frac{\partial\varphi_j}{\partial y}\frac{\partial w_\gamma}{\partial y}\frac{\partial\hat{w}_\beta}{\partial y}$$

$$+ 2\frac{\partial\varphi_i}{\partial y}F_{26}^{\alpha\beta\gamma\rho}\left(\frac{\partial\varphi_j}{\partial y}\frac{\partial w_\gamma}{\partial x} + \frac{\partial\varphi_j}{\partial x}\frac{\partial w_\gamma}{\partial y}\right)\frac{\partial\hat{w}_\beta}{\partial y}$$

$$+ 2\left(\frac{\partial\varphi_i}{\partial x}\frac{\partial\hat{w}_\beta}{\partial y} + \frac{\partial\varphi_i}{\partial y}\frac{\partial\hat{w}_\beta}{\partial x}\right)F_{16}^{\alpha\beta\gamma\rho}\frac{\partial\varphi_j}{\partial x}\frac{\partial w_\gamma}{\partial x}$$

$$+ 2\left(\frac{\partial\varphi_i}{\partial x}\frac{\partial\hat{w}_\beta}{\partial y} + \frac{\partial\varphi_i}{\partial y}\frac{\partial\hat{w}_\beta}{\partial x}\right)F_{26}^{\alpha\beta\gamma\rho}\frac{\partial\varphi_j}{\partial y}\frac{\partial w_\gamma}{\partial y}$$

$$+ 2\left(\frac{\partial\varphi_i}{\partial x}\frac{\partial\hat{w}_\beta}{\partial y} + \frac{\partial\varphi_i}{\partial y}\frac{\partial\hat{w}_\beta}{\partial x}\right)F_{66}^{\alpha\beta\gamma\rho}\left(\frac{\partial\varphi_j}{\partial y}\frac{\partial w_\gamma}{\partial x} + \frac{\partial\varphi_j}{\partial x}\frac{\partial w_\rho}{\partial y}\right)$$

$$+ \frac{1}{R}\varphi_i D_{12}^{\alpha\gamma\beta}\frac{\partial\varphi_j}{\partial x}\frac{\partial w_\beta}{\partial x} + \frac{1}{R}\varphi_i D_{22}^{\alpha\gamma\beta}\frac{\partial\varphi_j}{\partial y}\frac{\partial w_\beta}{\partial y} + \varphi_i \overline{D}_{13}^{\beta\alpha\gamma}\frac{\partial\varphi_j}{\partial x}\frac{\partial w_\beta}{\partial x}$$

$$+ \frac{1}{R}\varphi_i D_{26}^{\alpha\gamma\beta}\frac{\partial\varphi_j}{\partial y}\frac{\partial w_\beta}{\partial x} + \varphi_i \overline{D}_{23}^{\beta\alpha\gamma}\frac{\partial\varphi_j}{\partial y}\frac{\partial w_\beta}{\partial y} + \varphi_i \overline{D}_{36}^{\beta\alpha\gamma}\frac{\partial\varphi_j}{\partial y}\frac{\partial w_\beta}{\partial x}\Bigg] dx\, dy$$

Vita

Samuel Kinde Kassegne was born on June 2, 1963 in Assosa, Ethiopia. After graduating from St. Joseph School in Addis Ababa in 1980, he went to Madras, India, the same year for undergraduate studies under a Canadian International Development Agency (CIDA) scholarship program. He obtained his B. Sc. degree in Civil Engineering from Guindy Engineering College in 1984. He later went to Ankara, Turkey for graduate study in Structural Engineering at the Middle East Technical University (METU). He obtained his M. Sc. degree in June 1987 and continued working with the Structural Mechanics Group of METU until December 1988. During the same period, he also worked as a structural engineer with Kare Engineering Company in Ankara. In January 1989, he enrolled at Virginia Polytechnic Institute and State University in the Ph. D. program of the Civil Engineering Department. He transferred to the Engineering Science and Mechanics Department in the Fall of 1990.